DEVELOPMENT OF A PHOTOTHERMAL INDUCED OPTICAL SCATTERING MODULATION TECHNIQUE AND ITS APPLICATION IN MALARIA DIAGNOSIS

DANIEL MAITETHIA MEMEU (M.Sc.)
(I84/32278/2015)

A THESIS SUBMITTED IN FULFILLMENT OF THE REQUIREMENTS FOR THE AWARD OF THE DEGREE OF DOCTOR OF PHILOSOPHY (PHYSICS) IN THE SCHOOL OF PURE AND APPLIED SCIENCES OF KENYATTA UNIVERSITY

AUGUST 2023

DECLARATION

This thesis is my original work and has not been presented for the award of a degree or any other award in any other institution of higher learning

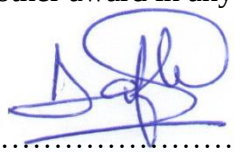

Signature…… Date ……10th June 2023

Daniel Maitethia Memeu, I84/32278/2015
Department of Physics

Supervisors

We confirm that the work reported in this thesis was carried out by the candidate under our supervision

Signature …… Date……16th June 2023

Dr. Abdallah M. Sarroney
Department of Physics
Kenyatta University

Signature……. Date… …21st, June 2023

Prof. Ciira wa Maina
Department of Electrical and Electronics Engineering
Dedan Kimathi University of Technology

ACKNOWLEDGEMENTS

I would like to acknowledge my academic advisors Dr. Abdallah Merenga and Dr. Ciira wa Maina for the tremendous effort they have put while guiding me in undertaking my research project. This work would not have been successful without their invaluable advice and mentorship.

I also wish to acknowledge Meru University of Science and Technology for granting me study leaf and partial research funds to undertake this work. I also wish to express my gratitude to Kenyatta University for granting me a PhD scholarship through the African Development Bank scholarship project. Without this support it would have been very difficult to successfully complete my doctoral studies. I am also indebted to Kenya Education Network (KENET) for granting me a travel grant to present my work in IEEE-Africon conference (2017) in Cape Town South Africa. Special Thanks also goes to Prof. Andreas Mandelis of university of Toronto, Center for Advanced Diffusion-Wave and Photoacoustic Technologies (CADIPT) and Prof. MLaden Franko of University of Nova Gorica for facilitating my travel to Sicily, Italy to attend two research workshops related to my PhD work.

I also wish to Thank Mr. Egido Mbogo, Peter Kiiria and Edison Lasoi (all of them are laboratory technologists) for the support they offered me in acquisition and processing of biological samples for my research. Special thanks and appreciation also goes to my wife - Monicah and children - Mugambi, Makena and Munene for their love, prayers and inspiration. I also would like to acknowledge and appreciate the support offered to me by my parents – my mum Evangeline and my late dad Francis.

TABLE OF CONTENTS

LIST OF FIGURES

LIST OF TABLES

LIST OF ABBREVIATIONS

ANN – Artificial Neural Network

CSV – Comma Separated Values

CT – Computed Tomography

CTCs – Circulating Tumor Cells

CW – Continuous Wave

DFT – Discrete Fourier Transform

EB – Excitation Beam

FD – Frequency Domain

FFT – Fast Fourier Transform

IDE – Integrated Development Environment

RBCs – Red Blood Cells

RBF – Radial Basis Function

RDT – Rapid Diagnostic Test

PA – Photoacoustic

PB – Probe Beam

PCA – Principal Component Analysis

PCR – Polymerase Chain Reaction

PT – Photo-Thermal

PTIOSM – Photo-Thermal Induced Optical Scattering Modulation

SNR – Signal to Noise Ratio

SVM – Support Vector Machine

TL – Thermal Lens

VHT – Vacutainer Heparin Tubes

WHO – World Health Organization

WMDPAS – Wavelength Modulated Differential Photo-Acoustic Spectroscopy

ABSTRACT

Malaria is one of the leading causes of mortality and mobility in Africa and the disease is endemic in many regions of the continent. Though curable, early diagnosis which is key to effective treatment is usually a challenge owing to lack of accurate, rapid and affordable diagnostic techniques in resource scarce settings. Therefore, there exists a need for development of an accurate, rapid, easy to operate and affordable technique for diagnosis of malaria. This work describes a novel optical based sensing and imaging technique termed as Photo-Thermal Induced Optical Scattering Modulation (PTIOSM) and its application in malaria diagnosis. The technique entails sample irradiation with two optical beams of different wavelength. One optical beam, referred to as pump beam is employed for exciting the sample chromophores to higher energy levels. What follows is chromophore transition from the excited states to lower states and subsequent photothermal processes such as photoacoustics and thermal lens effect. These processes are monitored using a second optical beam referred as probe beam. We hypothesized that application of the pump beam alters the sample optical properties and these changes can be monitored by tracking intensity modulation of the probe beam induced by the sample upon optical excitation and relaxation. The extent of the probe beam intensity modulation (referred to as PTIOSM signal) would be indicative of the molecular species present in the sample. We applied the technique for label-free detection of the presence of hemozoin (an endogenous malaria biomarker) in blood samples.Four PTIOSM setups; two for sensing and the other two for imaging were developed. The PTIOSM sensing setup employed a photodiode as the optical detector while the PTIOSM imaging setup used an image sensor for spatial-temporal PTIOSM signal from the sample. Malaria infected and non-infected blood samples as well as whole blood mixed with synthetic hemozoin at different concentrations were interrogated using the PTIOSM setups. The synthetic hemozoin was mixed with whole blood in varying concentrations to simulate different *Plasmodium* parasite load (parasitemia) in blood. The acquired signals were transformed using principal of component analysis before features extracted and used for training and classification of different sample classes using machine learning models.The technique attained an overall malaria detection accuracy of 70.6% with a sensitivity of 68.4% and specificity of 72.9%. In addition, an accuracy of 100% was attained in the classification of synthetic hemozoin concentrations in whole blood samples. A total of 4200 feature vectors were used to train and test the classifiers. The training and testing set data was split in 80% to 20% respectively. Support vector machine attained the best classification accuracy. The technique was also able to yield images of sufficiently good quality to facilitate visual identification of Plasmodium parasites in unstained blood smear samples from malaria infected human subjects. The recorded performance points to the potential of PTIOSM technique potential for adoption as an optical biosensor for rapid screen of malaria and other diseases with known endogenous light absorbing molecular biomarkers.

CHAPTER 1

INTRODUCTION

1.1 Background of Malaria disease

Malaria is a tropical disease which poses serious public health concerns. It is one of the leading causes of mortality globally with about 0.5 million deaths attributed to the disease in the year 2015 according to world malaria report (World Health Organization, 2015). Majority of these deaths comprise of children less than five years old from sub-Saharan Africa. Besides, it is estimated that approximately 200 million people are infected with the disease and 3.2 billion people are at risk of contracting the disease annually according to the report. This has created a heavy social-economic burden to the affected countries due to huge treatment costs and absenteeism from work and schools (World Health Organization, 2003).

The disease is caused by protozoan parasites of the genus *Plasmodium*. The parasites are transmitted to humans through bites by female Anopheles mosquitoes in search for blood meals. Following a mosquito bite, the parasites (sporozoites) get into the blood stream and are delivered to the liver for incubation and replication. This stage is referred as exoerythrocytic stage. Afterwards the parasites (now known as merozoites) exit the liver and enter the blood stream attacking Red blood Cells (RBCs) also known as erythrocytes. Once a merozoite enters into a RBC, it degrades the cells' hemoglobin reducing or completely inhibiting the cells' ability to carry oxygen. Hemoglobin is a complex

molecule composed of two simpler molecules – heme and a protein called globin. The parasite ingests globin for its nutritional needs while converting Heme (which is toxic to the parasite (Slater *et al.*, 1991)) into a by-product called Hemozoin. Hemozoin is an insoluble and inert crystal made of iron nano-rods (Oliveira *et al.*, 2005). Presence of hemozoin in RBCs is an indication of malaria infection and therefore hemozoin can serve as an endogeneous biomarker of malaria disease.

There are five species of *Plasmodium* parasites that affect humans namely; *Plasmodium falciparum, Plasmodium ovale, Plasmodium vivax, Plasmodium malariae,* and *Plasmodium knowlesi* (Garnham, 1966; Escalante *et al.*, 1995; Cox-Singh *et al.*, 2008). *Plasmodium falciparum* is the most fatal while other species cause mild to moderate illnesses (Kantele and Jokiranta, 2011). Each of the five species has got distinct morphological features which are used in *Plasmodium* parasite species identification using optical microscopy.

The parasites undergo three main intera-erythrocyte life stages. These are; early stage also known as ring stage, intermediate stage also called trophozoite stage and mature stage also called schizont stage (which is the reproductive stage). After the reproduction stage is complete, the infected cell raptures and the merozoites are released into the blood stream where they attack health erythrocytes and the cycle starts again (Bannister and Sherman, 2009). Figure 1.1 (a) extracted from Goldsby *et al*., 2000 shows the life cycle of *Plasmodium* parasites.

1.2 Malaria diagnostic techniques

Malaria diagnosis entails detection of the presence of the *Plasmodium* parasites in the patient blood, determination of the parasite species, life stage, and parasite load in blood (parasitemia estimation – an indicator of disease severity). A number of techniques for diagnosis of malaria exist while others are under development. The gold standard method is optical microscopy (Wongsrichanalai *et al.*, 2007). The technique involves drawing peripheral blood from a patient, preparing a stained blood smear slide and examining the slide using an optical microscope to detect the presence of *Plasmodium* parasites as well as determine the parasite life stages, species and parasitemia. Labeling (staining) of the blood smear sample highlights the parasite pigment (hemozoin) which makes the parasites visible. The technique is time consuming and labor intensive due to the need for sample preparation and counting of detected parasites in each microscope field of view. World Health Organization (WHO) recommends counting at least 100 microscopic fields of view before a smear is declared negative and therefore a single malaria test can take between 30 to 60 minutes. Figure 1.1b-c shows microscopic images of *Plasmodium* infected erythrocytes.

Other methods include; Polymerase Chain Reaction (PCR) based technique (Berry *et al.*, 2008), *Plasmodium* parasite antigen detection based techniques also referred as Rapid Diagnostic Tests (RDTs) and Flourescent microscopy based techniques (Makler *et al.*, 1998). PCR technique involves amplification of *Plasmodium* parasites DNA present in the patient's blood sample to improve

detection sensitivity. This technique is very sensitive with the limit of detection reported as one parasite per microliter. Drawbacks of the technique include need for sophisticated equipments, expensive reagents and skilled manpower.

RDT on the other hand uses antibodies to bind on antigen produced by the *Plasmodium* parasites. A color change in a RDT test kit indicates presence of the parasite. The technique uses lateral flow assay technique where whole blood is loaded onto the kit and travels along a nitrocellulose membrane to react with a conjugated matrix comprising of an optical contrast agent and antibodies which are supposed to bind to target analyte if present in the sample. The complex is then transported along the membrane (strip) and binds at the test line to another set of immobilized antibodies in case the analytes are present. Otherwise, the complex will flow past the test line and get immobilized at the control line. The excess sample is deposited at the the sample absorbent pad. A visible color band appears at the test line position if the test turns positive and another band at the control line is expected form to indicate the test sample was valid. Technique takes about 15 minutes but suffers from low sensitivity with the limit of detection of this technique being 50 – 100 parasites per micro-litre of blood. Flourescent microscopy is a variant of optical microscopy that uses fluorochrome such as acridine orange nucleic acid to label *Plasmodium* parasites in the blood sample. Limitations of this technique include the need to use specialized microscope (fluorescent microscope), toxic and expensive reagents, is time-consuming and low detection sensitivity. Fluorescent-based flow cytometry technique has also be

reported as an alternative malaria diagnostic method (Shapiro and Perlmutter, 2008) with its main drawback being need for use of a flow cytometer which is a sophisticated equipment requiring use of special reagents, multiwavength laser source and highly skilled expertise to operate.

Generally the mainstream malaria diagnostic techniques suffer from a number of short comings (Makler *et al*., 1998) which include low detection sensitivity and specificity, time consuming – as is the case optical microscopy and PCR techniques. Besides, the techniques are invasive and demand use of reagents which add the cost of diagnosis. They also demand special storage requirements for the reagents and some reagents have a short shelf life. Limited studies have reported emergence of new optical based malaria diagnostic techniques that have potential of either substituting or complimenting the conventional methods for malaria diagnosis. The following section briefly describes the working principles of these techniques.

1.3 Photoacoustic effect and its application in biomedical imaging

Photoacoustic (PA) effect is a process in which acoustic waves in Ultra-Sound (US) frequency range are emitted upon absorption of optical radiation by a molecule (Xia *et al.*, 2014). When an object absorbs light, part of the optical energy is converted to thermal energy which results to a temperature raise and thermo-elastic expansion. Consequently, a transient pressure (acoustic) wave is generated and propagates through the sample. Generation, detection and processing of these waves can be used for both structural (anatomical) and

functional imaging of biological tissue (Wang *et al*., 2006; Zhang *et al.*, 2006; Yang *et al.*, 2009; Dima and Ntziachristos, 2012; Wang and Hu, 2012; Wang *et al.*, 2013; Xia *et al.*, 2014) as well as tissue sensing (Pramanik and Wang, 2009). Efficient generation of PA signals demands two conditions to be satisfied namely; thermal and stress confinement (Wang and Wu, 2007). This means that heat conduction and thermo-elastic expansion in the illuminated region are negligible. This calls for use of sample optical excitation using either a narrow optical pulse with a pulse-width in the order of nanoseconds (Xia *et al*., 2014; Yao and Wang, 2014) or high frequency modulated Continuous Wave (CW) laser light (Maslov and Wang, 2008; Winkler *et al.*, 2013). Generation of PA signal using optical pulses is more efficient than use of modulated CW optical excitation (Yao and Wang, 2014).

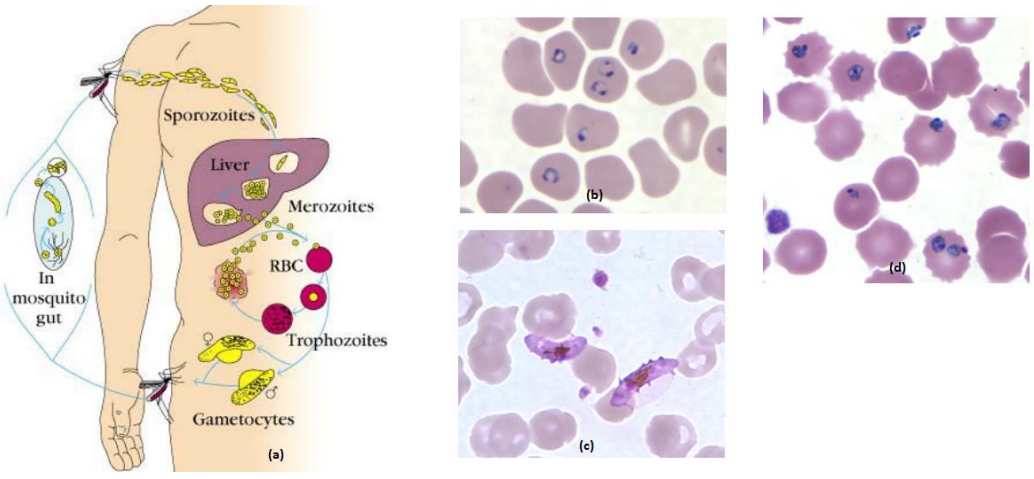

Figure 1.1: Plasmodium parasites intra-erythocytic life cycle and microscopic images of the parasites in blood smears (Images from (Goldsby et al., 2000) figure 17.11 and CDC malaria image gallery: https://www.cdc.gov/dpdx/malaria/index.html)). Panel (a) shows the life cycle of the *Plasmodium* parasite inside the human host and in the mosquito host. Panels (b) to (d) show microscopic images of red blood cells infected with the parasites. Panels (b) and (d) show cells infected with parasites at ring stage while panel (c) show the gametocyte stage of the parasite.

The intensity of the generated PA waves is a measure of the following tissue properties: optical absorption coefficient, , mechanical elasticity and thermal compressibility. To make a photoacoustic measurement, the sample is irradiated with an optical beam while an ultrasonic transducer is placed in proximity to the sample being probed to detect the emitted acoustic waves. The signal is then amplified and processed to obtain the time evolution of the PA signal. Using appropriate signal inversion models it is possible to obtain the sample μ_a and its depth profile. When multiple optical wavelengths are used to irradiate the sample, molecular composition, and concentration of chromophores present in the sample can be determined. The technique boasts of a number of advantages over other imaging and sensing modalities including; high spatial resolution and image contrast, multi-scale imaging depths – from cell organelles to organs (L. V. Wang and Hu, 2012), use of safe (non-ionizing) optical radiation for probing the sample, non-invasive operation and ability to perform both functional and anatomical imaging. The technique is also relatively cheap compared to other medical imaging modalities such as Nuclear Magnetic Resonance Imaging (NMRI) and X-Ray Computed Tomography (X-Ray CT). Recently, Photoacoustic Flow Cytometry (PAFC) has be proposed for detection of Ciculating Tumor Cells (CTC) among other diseases (Galanzha and Zharov, 2013). It has also been employed in malaria diagnosis (Cai *et al*., 2016).

1.4 Principle of malaria diagnosis using photoacoustic technique

The dominant optical absorbers in a malaria infected blood are hemoglobin (Hb)

and hemozoin (Hz). Hemoglobin comes in two forms; oxy-hemoglobin (HbO_2) and deoxy-hemoglobin (HbR). Figure 1.2 gives the optical absorption spectra of HbO_2, HbR and Hz and Table 1 gives values of the optical absorption coefficient and molar concentration of hemozoin in an infected erythrocyte as extracted from the work of Saha *et al*. (Saha *et al*., 2012). Based on the values of molar concentration of hemozoin present in the cell, it is possible to differentiate various parasite life stages present. Previous studies have demonstrated the possibility of *in vivo* imaging of oxygen saturation in blood microvasculature and oxygen release rate in individual erythrocytes using sub-wavelength Optical Resolution Photoacoustic Microscope (OR-PAM) (L. Wang *et al*., 2013). This suggests that a similar technique can be used to test the presence of other dominant optical absorbers in the cell such as hemozoin in case of a malaria infection.

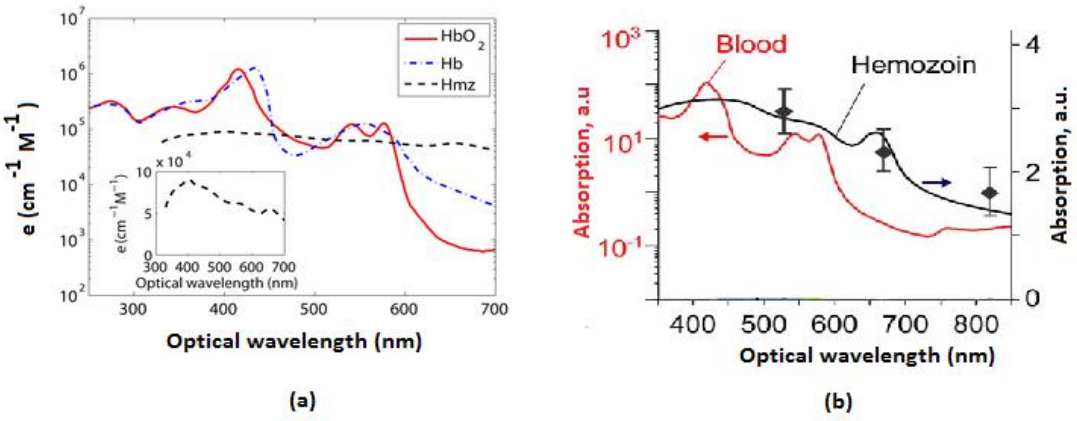

Figure 1.2: Optical absorption spectra of hemoglobin and hemozoin (a) molar extinction spectra of oxyhemoglobin, deoxyhemoglobin, and hemozoin (Saha *et al.*, 2012), the inset plot is an expanded view of hemozoin spectrum (b) 70% oxygenated blood and hemozoin (Cai et al., 2016b)

Table 1.1: Optical absorption coefficients μ_a, and molar concentration of hemozoin in both single healthy and *Plasmodium* infected erythrocytes. Values of μ_a were extracted from (Saha *et al.*, 2012)

	Optical Absorption Coefficients μ_a (cm^{-1})		Hemozoin Molar concentration (M)
	λ = 434nm	λ = 700nm	
Healthy erythrocyte	6351.59	20.47	0
Ring stage infected erythrocyte	6075.31	40.22	5.3×10^{-13}
Trophozoite infected erythrocyte	4239.99	171.41	6.2×10^{-12}
Schizoint infected erythrocyte	2858.57	270.15	1.7×10^{-11}

The following is a brief analysis of the problem. Optical absorption coefficient due to a malaria infected erythrocyte can be described by equation (1) (Memeu et al., 2019)

$$\mu_a^{\lambda_i} = \varepsilon_{Hz}^{\lambda_i}[c_{Hz}] + \varepsilon_{HbO_2}^{\lambda_i}[c_{HbO_2}] + \varepsilon_{HbR}^{\lambda_i}[c_{HbR}] \quad (1.1)$$

$\varepsilon_i^{\lambda_i}$ is the molar extinction coefficient of the i^{th} chromophore present in the blood sample. Both ε and μ_a are wavelength dependent hence the superscript λ_i. $[c_i]$ is the molar concentration of the i^{th} bio-molecule in the sample. Hz, HbO_2, and HbR represents hemozoin, oxy-hemoglobin and deoxy-hemoglobin molecules respectively.

The initial photoacoustic signal generated in the sample following absorption of

an optical pulse is proportional to the deposited optical energy $A_e = \mu_a^{\lambda_i} \Phi^{\lambda_i}$ where Φ is the optical fluence (light intensity in the irradiated region given in J/cm^2). Therefore, the induced PA pressure is given by equation (1.2) (L. V. Wang and Wu, 2007).

$$P_0^{\lambda_i} = \Gamma H \tag{1.2}$$

With

$$H = n_{th} A_e \tag{1.3}$$

H is the thermal energy density gained by tissue due to non-radiative relaxation of chromophores' electrons following photon absorption. The parameter is a function of the tissue's optical absorption coefficient and the optical fluence distribution in the tissue. n_{th} is the fraction of optical energy converted to heat energy ($n_{th} = 1$ for non-fluorescent and non-photoluminescent chromophores (Yao and Wang, 2014)). Γ is the tissue grueneisen parameter - a thermodynamic quantity which gives the photoacoustic efficiency of the tissue, i.e., the fraction of the thermal energy converted to acoustic waves.

The induced acoustic signal P_o (also referred as initial PA pressure) propagates through the tissue and is detected by an ultrasonic transducer placed at the tissue surface, a distance r from the target absorber (in this case infected erythrocyte).

The detected acoustic signal, P_d differs from the initials signal as a result of acoustic attenuation through the tissue, partial detection geometry of the transducer and the detector efficiency $\eta(f)$. The transducer output signal, P_d can therefore be expressed as a product of the initial signal, P_o and a scaling factor, T_d that accounts for acoustic signal attenuation i.e.,

$$P_d(f) = T_d(f)P_o \tag{1.4}$$

with

$$T_d(f) = \sqrt{\eta(f)}\frac{NA}{2}e^{-\alpha_o f^2 l} \tag{1.5}$$

NA is the traducers' numerical aperture, l is its focal length and α_o is the tissue attenuation coefficient. T_d is frequency dependent and increases with frequency. Numerical values for the parameters in equation (1.4) for some commercially ultrasonic transducers can be found in literature (Winkler *et al*., 2013).

Equations (1.5 and 1.4) indicate that the generated photoacoustic signal undergoes an exponential decay as it propagates through the tissue before detection by the transducer. The exponential decay constant is given by the product of α_o, f^2, and l. This means the greater the distance traveled by PA signal before detection the more the signal is attenuated. In addition higher frequency signal components are attenuated more rapidly than the lower frequency components. To prevent excessive loss of signal energy at the tissue transducer interface, an acoustic coupling gel whose acoustic impedance is similar to that of the tissue is usually

applied. The rapid attenuation of higher frequency components of the tissue implies that information regarding finer tissue structures such as erythrocytes is rapidly lost with increasing detector distance from the target object. In addition, signal transduction from acoustic to electrical energy by the transducer induces further losses since practical transducer efficiencies is less than 100%. The above mentioned drawbacks of PA signal detection coupled with the need for use of complex instrumentation such as lock-in amplifier and high power laser systems which are bulky and expensive and challenges in PA signal calibration are among factors that have hindered the translation of the technique to clinical use.

The reported work was aimed at development of a variant technique termed as PTIOSM having simpler instrumentation complexity and capable of detecting hemozoin from blood samples. The technique employed optical rather than acoustic detection for sensing and imaging of photothermally generated signals from blood samples following optical excitation. Machine Learning (ML) models were incorporated for automation of blood sample classification. In addition, an analytical model for describing the physical significance of the detected PTIOSM signals was developed.

1.5 Statement of the research problem

Reported studies show that photoacoustics has potential for detecting *Plasmodium* parasites in malaria infected blood samples. It has also been demonstrated that the technique is more sensitive than the optical microscopy (Samson *et al*., 2012; E. Y. Lukianova-Hleb *et al*., 2014; E. Lukianova-Hleb *et al*., 2015; Cai *et al*.,

2016a). However, the technique has not yet been adopted clinically as routine malaria screening method. Some of the limitations hampering its adoption include the demand for highly sophisticated instrumentation such as high power pulsed multi-wavelength laser source, high frequency ultrasonic transducer, lock-in signal processing, high frequency and bandwidth signal acquisition and processing hardware which makes the setup bulky, complex to handle and expensive. This has slowed down the process of translating the technology from research laboratories to clinics.

The present work was aimed at development of photo-thermal based technique for detection and imaging of hemozoin present in unstained malaria infected blood samples. To simplify the hardware, high power laser light was replaced with multi-color Light Emitting Diode (LED) that served as sample excitation and probing optical source. A custom-made hardware was used for driving the LED. An analytical model was developed that guided the signal processing algorithms implemented for image analysis.

1.6 Hypothesis

If a light absorbing sample is momentarily irradiated by an optical source (excitation beam) of sufficient energy, it would undergo four photo-thermal transitions which can temporary alter its thermal and optical properties provided that relaxation of the molecules from the excited is non-radiative. The first phase is optical excitation where molecules move to elevated energy states. As the number of molecules in the excited state increase, the sample becomes more

optically transparent (less photon absorbing) since molecules would be approaching optical absorption saturation. Under this condition, the depth of penetration by a secondary light beam (probe beam) would increase. Consequently, the transmitted intensity value of the probe beam would fluctuate from its steady state value due to perturbation of the sample's optical properties caused by irradiation by the excitation beam.

Return of molecules to ground state through conversion of absorbed optical energy to heat marks the second phase. Here heat energy is initially deposited and locally confined in the formerly irradiated region. Temperature variation has the effect of modifying the sample's refractive index which results to change of path and intensity of light propagating in the irradiated sample through a process called thermal lens deflection effect.

The next phase is generation and propagation of photoacoustic waves due to transient thermoelastic expansion following heating of the sample, a process that takes place in a couple of microseconds after sample optical excitation. Photoacoustic wave propagation in the sample can lead to spatial displacement of optical scatters and creation of alternating regions of compression and rarefaction in the specimen thus further modulating the intensity of the probe beam in time through a process known as acousto-optic modulation. When this probe beam modulation is detected and analyzed it can give information regarding optical absorption of chromophores present in the sample.

Finally, heat diffusion from the initial region of heat deposition follows. This is a slow process and its net effect is to restore the perturbed sample optical properties back to the steady state. Monitoring changes in the detected probe beam intensity during this phase can yield the sample's thermal properties. Figure 1.3 gives the schematic diagram of the proposed model of Photothermal Induced Optical Scattering Modulation in a tissue sample. This model will be employed to differentiate hemozoin-positive from hemozoin-free blood samples and therefore form the basis for development of photo-thermal based malaria sensor with potential for non-invasive operation.

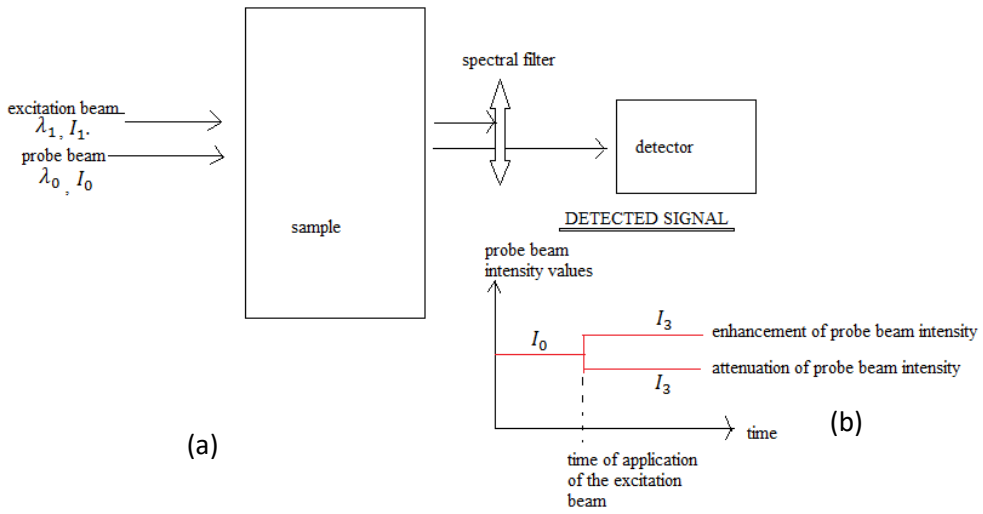

Figure 1.3: Photothermal Induced Optical Scattering Modulation model. (a) Setup, (b) Expected PTIOSM signal – the intensity of PTIOSM signal can be either enhance or attenuated as indicated by I_3

1.7 Objectives

1.7.1 General objective

To develop a Photo-Thermal Induced Optical Scattering Modulation (PTIOSM) technique and apply it for detection of hemozoin in blood samples.

1.7.2 Specific Objective

i. To develop model for analytically describing the PTIOSM phenomenon

ii. To design and fabricate setups for acquisition of one dimensional PTIOSM signals from whole blood samples.

iii. To fabricate a setup for acquisition of PTIOSM images from blood smear samples.

iv. To determine suitable features for classifying detected PTIOSM signals as hemozoin positive or hemozoin negative.

v. To develop machine learning models for automating the classification of PTIOSM signals into respective malaria infection status and determine the sensitivity and specificity of the technique in malaria diagnosis.

1.8 Significance and justification

Malaria is a life-threatening disease which results in high number illnesses and deaths in Africa annually. The disease also poses huge social-economic burden to countries where it is endemic. Current diagnostic techniques lack high detection sensitivity and are not optimized for rapid, in-the-field, mass screening campaigns. A suitable diagnostic technique is one that is accurate, fast, and simple to administer with minimal infrastructural and expertise demands.

This work was aimed at developing a simple, rapid, accurate, label-free hemozoin sensor that leverages on sensing and imaging of PTIOSM signals in un-stained

blood samples. Through an analytical derivation, it was deduced that PTIOSM signal contains information regarding molecular composition of the sample. Principal of Component Analysis (PCA) and Discrete Fourier Transform (DFT) were used to extract PTIOSM signal features that aided in differentiation of sample classes. In order to automate the process of PTIOSM signal classification, Support Vector Machine (SVM) was trained using the extracted signal features and its classification accuracy assessed. An overall malaria diagnostic accuracy of 70% was achieved.

The technique holds potential for diagnosis of other blood related diseases such as anemia, diabetes, melanoma and CTCs. The PTIOSM analytical model developed and experimentally verified in this work will provide new insights to the scientific community regarding mechanisms guiding photon-matter interactions and possibly lead to further research and innovation in development of other PTIOSM imaging and sensing technologies.

CHAPTER 2

LITERATURE REVIEW

2.1 Emerging optical based malaria diagnostic techniques

(Lawrence and Olson, 1986) reported for the first time that hemozoin was birefringent. The authors observed that when Wright's-stained malaria blood smear was examined under optical microscope using polarized light, bright birefringent granules of *Plasmodium* pigment (hemozoin) were detected. This enabled localization and quantification parasites. To characterize the techniques sensitivity, serial dilution of infected blood samples was performed while examining the birefringent granules produced by hemozoin. Parasitemia detection limit of 0.01% was attained. Following on this lead, (Mendelow *et al*., 1999) reported a method for diagnosing malaria by analyzing polarized light scattered by white blood cells. The authors observed that light scattered by white blood cells containing hemozoin had a distinct pattern that was different from scattered light by white blood cells that did not contain hemozoin pigments. The equipment used for the study was an automated hematology analyzer (Abbott CELL-DYN 3500 cell counter). Malaria diagnostic sensitivity of 72% and specificity of 96% were attained.

(Newman *et al*., 2008) reported a magneto-optic technique for detection of hemozoin in blood. The technique is premised on the fact that hemozoin crystals are paramagnetic but their magnetic axes are randomly oriented in absence of an external magnetic field. However, when an external magnet field is applied, the

axes are aligned towards the field. Optically, this has an effect of inducing dichroism in the sample. The authors of the paper applied an alternating magnetic field through the sample and measured the extent of optical modulation detected after optically polarized light traversed the sample. A linear correlation between the intensity of modulation and hemozoin concentration was observed. The technique was applied in diagnosis of malaria in human subjects and the results obtained were in agreement with conventional diagnostic techniques. The authors were not able to directly determine parasitemia from the concentration of hemozoin present in the blood. Besides, *Plasmodium* speciation and parasite life stage determination is obviously not possible using this technique. Hemozoin is also known to persist in blood plasma after the disease has been treated. The technique can misinterpret this to mean an active infection.

Davidson *et al*. (2021) reported their work on the use of deep machine learning for diagnosis of malaria using stained thin blood smears microscope images. The technique employed three stage classifiers for erythrocyte identification, differentiation of infected and uninfected cells and categorization of intraerythrocyte life stages. Convolution Neural Network (CNN) was used for erythrocyte identification and detection of infected cells whereas a regression model was trained to categories different Plasmodium parasite life stages present in the image. An average precision score of 0.99 at an intersection-over-union threshold of 0.5 was attained for the model performing erythrocyte identification. The model trained for classification of cells as infected or uninfected attained a classification accuracy of 0.998 with a sensitivity of 0.995, specificity of 0.998 and an area under the receiver

operating characteristic curve of 0.979. Additionally, the co-workers developed a web-based platform to facilitate remote access of the classification service through uploading the images captured from a microscope whether using microscope camera or mobile phone camera. A cloud server was setup to perform the described imaging processing and classification, serving of the re\

sults to remote users and archiving of the raw images and predicted results.

Collins *et al*. (2022) reported the development of a low cost, open source 3D printed optical microscope termed as the Open Flexture Microscope (OFM). The device has got a modular design allowing for incorporation of custom optical components that enable both epi- and trans-illumination of the sample as well as different sample imaging modalities such as bright field, dark field, fluorescence and phase contrast imaging. The microscope light source is comprised of light emitting diode(s). The light from the sample passes through a Royal Microscope Society (RMS) objective and a tube lens before the image is formed and registered by an image sensor. The OFM uses a raspberry pi for imaging and sample stage positioning and auto-focus operations. The stage translation is achieved by flexture mechanism occasioned by elastic stretching of the 3D printed microscope parts when put under mechanical pressure either through rotational motion of geared motors or manual rotation of the actuator gears. The study established that the lateral resolution of the microscope is about 480nm. The raspberry pi also runs a server that facilitates remote access of the OFM through the network.

Knapper *et al*. (2021) assessed the performance of two auto-focusing algorithms implemented in the OFM software. When a microscope is automatically scanning and imaging different positions of the sample, the image plane often shifts as a result of manufacturing detects of the sample stage and actuator gear backlash. This results to defocusing of the image. The situation is more pronounced when using a high magnification objective lens due to its narrow field. Implementation of auto-focusing in OFM is particularly challenging due to the low computational resources of the Raspberry pi. The auto-focusing algorithms implemented by the microscope are; a modified 2D laplacian filtering and monitoring of the JPEG image file size. The performance of a third method termed as "smart-stack algorithm" developed by the authors was also investigated. They noted that JPEG file size method performed better while imaging malaria blood samples since it was faster, less prone to errors and less computationally intensive. It was however found not suitable for imaging sparse and plane samples.

2.2 Photoacoustic Malaria Detection

A limited number of studies have so far been carried out regarding *in vivo* photoacoustic diagnosis of malaria. Generally, the principle of *in vivo* Photoacoustic Flow Cytometry (PAFC) (Tuchin, 2011)) has been adopted. The technique entails use of a focused ultrasonic transducer for detection of PA signals emitted due to optical excitation of the flowing erythrocytes in blood vessels located below the skin surface. The signal peak intensity is monitored in time to keep track of the flowing erythrocytes (infected and non-infected).

Healthy erythrocytes produce signals with distinct amplitude levels in comparison to *Plasmodium* infected erythrocytes. The following is a brief review of a few reported publications.

(Cai *et al*., 2016c) proposed an *in vivo* (PAFC) technique for early diagnosis of malaria. They used a focused US transducer for detection of PA signal from flowing erythrocytes irradiated by three pulsed laser lights of wavelengths 532nm, 671nm, and 820nm. The signal was then amplified, digitized and loaded to a PC for processing. The system's spatial resolution was reported to be between 1 – 6 µm. Both *in vitro* and *in vivo* experiments using mice as the animal model were conducted to determine the sensitivity of the device. The authors reported that their technique was 1000 times more sensitive than optical microscopy method and could detect an infected erythrocyte 3 hours after inoculation of *Plasmodium* parasites into a healthy mouse compared to 3 days taken before detection using optical microscopy. They observed that when the optical energy used was increased beyond a certain threshold, hemozoin vapor nano-bubble formation occurred in the infected cells and this produced PA signal of increased intensity – a process termed as non-linear photoacoustics. They also used the process to perform real time destruction of infected cells (photo-thermal malaria therapy) while photoacoustically monitoring the efficiency of the therapy. They observed that PA signal ratio of infected cells to non-infected cells was highest at 671nm optical excitation wavelength.

Lukianova-Hleb *et al.* (2014) described a picosecond pulsed laser technique for generation and detection of hemozoin induced vapor nano-bubbles. The authors argued that when hemozoin crystals in infected RBCs absorbs the ultra-short pulsed radiation (having picoseconds range pulse width) of sufficient energy, nano-volume liquid around the hemozoin crystals was overheated and vaporized resulting in generation of transient vapor bubbles leading to explosive expansion and collapsing. This process resulted to emission of high intensity acoustic waves. Both *in vitro* and *in vivo* sets of hemozoin positive and hemozoin negative samples comprising of blood smears, whole blood and live mice were studied. Laser pulses were shone on samples and the emitted acoustic waves detected by an ultrasonic transducer. The transducer output was coupled to a digital oscilloscope. The detected signal was then analyzed in time domain. It was found that samples containing hemozoin produced acoustic signal of higher amplitudes than hemozoin negative samples. The technique yielded better results in differentiating *Plasmodium* parasite life stages and parasitemia estimation in comparison to optical microscopy. The optical wavelength used for exicitation of PA signals was 672nm – an optical absorption peak for hemozoin. The optical energies per pulse used for *in vitro* and *in vivo* experiments were $10\mu J$ and $15\mu J$ respectively. (E. Y. Lukianova-Hleb *et al*., 2014 and E. Lukianova-Hleb *et al*., 2015) used the technique for *in vivo* detection of $Plasmodium$ parasites in humans and infected mosquitoes. Similar results were obtained.

In general, photoacoustic based malaria diagnosis boasts of salient advantages over other diagnostic methods which includes; use of endogenous contrast agent

(hemozoin) for parasite detection as opposed to exogenous contrast agents as is the case in optical and fluorescent microscopy, potential for *in vivo* diagnosis, use of non-ionizing radiation which makes it safe, real time monitoring and capability for early detection of the disease hence making treatment more effective. In addition, it is possible to use the technique for diagnosis of other blood related disease.

However, the reported photoacoustic diagnostic systems suffer from a number of challenges which must be addressed before the technology can be clinically adopted. One of the major drawback of photoacoustic based disease diagnostic technique is difficulty in performing quantitative measurement of chromophore molar concentration in absolute units. In most of the reported work (Lukianova-Hleb *et al*., 2014; Lukianova-Hleb *et al*., 2015 and Cai *et al*., 2016), the distinction between healthy and diseased samples was made based on their relative differences in amplitudes values. The disadvantage of this approach is the wide signal amplitudes variability within subjects of the same class (either infected or non-infected subjects) which makes system difficult to calibrate.

Secondly, the reported PA systems are bulky and expensive due to the demand for high energy nanosecond pulsed multispectral laser sources, high frequency sensitive ultrasonic transducers and lock-in amplifiers. Use of fluence estimation models for quantitative PA spectroscopy makes the technique computational intensive and quasi real time. Their accuracy also depends on whether the tissue geometry is known a priori.

There is a promising trend in addressing of the above-mentioned challenges going by the number of publications and research groups working on the problem. Simplification of PA hardware has been attempted by substitution of the bulky and expensive Optical Parametric Oscillator (OPO) tuned laser sources with much smaller and cheap diode laser sources (Kolkman, *et al.*, 2006; Allen and Beard, 2007; Wang, *et al.*, 2014) and Light Emitting Diodes (LEDs) (Allen and Beard, 2013) that have a wide range of optical wavelengths commercially available. Quantel laser^{TM} has developed a compact high energy multispectral pulsed diode laser module operating in four different wavelengths (808, 915, 940 or 980 nm) in the NIR region customized for PA applications. Its high optical pulse energy (1mJ per wavelength per 80nS pulse width) is achieved by stacking of multiple diode lasers of same wavelength. Attempts to develop a compact hand held photoacoustic probe for *in vivo* imaging have also been reported *(* Deán-Ben and Razansky, 2013; *Daoudi et al.*, 2014; Zhou *et al*., 2015; Kuniyil *et al.*, 2016).

Use of chirped Frequency Domain (FD) techniques in photoacoustic spectroscopy applications (Fan, *et al.*, 2004; Sergey and Andreas, 2006) has the potential of minimizing the instrumentation complexity of the PA systems by enabling use of cheap and portable CW diode lasers as PA optical sources and simplify the numerical algorithms for fluence estimation. The authors applied FD photoacoustics in development of a sensitive technique for hypoxia monitoring and early cancer detection. The technique is termed as Wavelength Modulated Differential Photacoustic Spectroscopy (WM-DPAS). The technique uses two

optical wavelengths (680nm and 808nm) to monitor variations in oxyhemoglobin concentration in tissue. One wavelength (680nm in this case) should have maximum variation in extinction coefficients for oxyhemoglobin and de-oxyhemoglobin while the other wavelength (808nm which is the isosbetic wavelength) should ideally have the extinction coefficients coinciding. Two CW laser sources are intensity modulated out of phase (differentially) and their output coupled to the sample for photoacoustic excitation. The emitted PA signal is detected by an ultrasonic traducer. Upon signal preprocessing, the Fourier transform of the signal is performed to obtain both amplitude and phase signals of the differential PA time domain signal. The phase signal is said to be independent of the optical fluence and its variation is only due to variations in the molar concentration of the probed chromophore. Judging from the reported features and performance of WM-DPAS, this technique is likely to find application in *in-vivo* detection of malaria.

2.3 Research gap

The gold standard method for malaria diagnosis is optical microscopy. However, the technique suffers from a number of short comings with the most severe ones being that the method is slow and labor intensive. The demand for use of high optical magnification microscopes implies that screening of the disease is only limited to laboratory settings and not suitable for on-field testing. Many optical based malaria diagnostic techniques reported in literature have not moved past the proof of concept stage. There are two main challenges that render the reported

methods not practical for clinical use in malaria diagnosis. One is calibration difficulties. Due to the high variability in body physiology between human subjects, optical signals acquired from human samples vary significantly even between subjects having similar infection status. This poses a challenge of setting a threshold value for categorizing samples as infected or non-infected based on the acquired optical signal intensities. In other words, it's impossible to have a universal standard reference for calibrating the diagnostic systems. The second challenge is demand for complex instrumentation in designing the reported malaria diagnostic systems. For instance, photoacoustic based malaria diagnostic technique requires use of high power pulsed laser source and sophisticated signal detection instruments which makes the diagnostic instrument bulky, complex to operate and expensive. The present work attempted to address these two problems. Two portable and compact prototypes with capability of PTIOSM signal sensing and imaging were fabricated and tested for malaria diagnosis using un-stained blood samples. The light source used for sample excitation and probing was a RGB LED. A photodiode was use to detect PTIOSM signals in the case of PTIOSM sensing setup while an image sensor was used as the signal detector in the PTIOSM imaging setup. An analytical model was developed that yielded an absolute calibration procedure for the PTIOSM imaging system. In the case of PTIOSM sensing setup, Machine learning model were employed for sample classification. The use of ML also cured the problem of relative calibration of the acquired PTIOSM signals from different human blood samples.

CHAPTER 3

THEORETICAL BACKGROUND

3.1 Light tissue interactions

Optical absorption and scattering are the primary processes that characterize photon matter interaction (Lihong V. Wang and Wu, 2007). When a molecule is excited with EM radiation, its electrons move from ground state to higher energy levels provided the radiation energy corresponds to the molecules' real or virtual energy states. After the electron has been raised to excited state, it tends to lose energy (relax) and get back to the ground state level where electrons are more stable. This process of molecule relaxation is attained through energy release either in form of photons (radiative relaxation) or heat (non-radiative relaxation). The Jabloski's energy diagram given in figure 3.1 illustrates some of the different photon matter interaction processes involved.

Fluorescence and phosphorescence are two processes that result from radiative relaxation of an excited molecule (Richards-Kortum and Sevick-Muraca, 1996). Fluorescence occurs after an initially excited electron transitions from lowest vibrational energy level of an excited electronic state to ground state (see figure 3.1). Its lifetime (time an electron stays in excited state) is in the order of nanosecond. Flouresence can reveal the composition, dynamics and structure of a biomolecule. Phosphorescence on the other hand involves an additional intermediate transition of electron from excited state to a metastable state before eventually decaying to ground state. Its lifetime is in the range of milliseconds or longer.

When a molecule is excited and electrons move to a virtual stationary state instead of a real stationary energy level, scattering occurs. There are two types of scattering namely; elastic and inelastic scattering. In elastic scattering an excited electron releases a photon of equal energy as the initial photon that excited it. In other words the molecule does not loss or gain energy following elastic scattering. In inelastic scattering on the other hand, the emitted photon is either less energetic than the excitation photon (stoke emission) or more energetic than the initial excitation photon (anti-stoke emission). Inelastic scattering is also referred as Raman scattering.

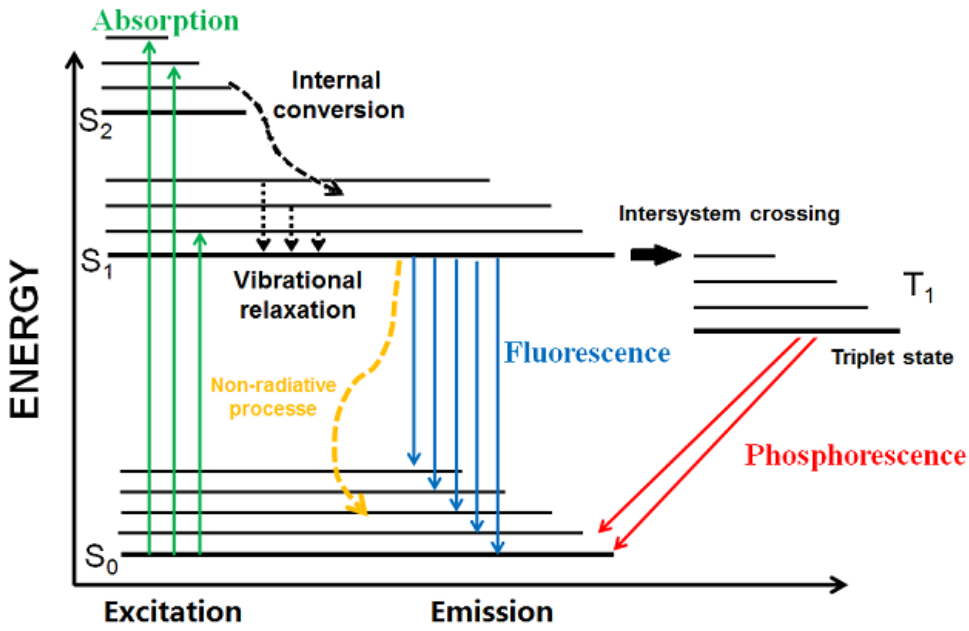

Figure 3.1: Jabloski's Diagram illustrating different photon interaction processes with matter. Sources: https://www.researchgate.net/publication/355485633_Investigations_to characterize_the_interactions_of_light_radiation_engine_operating_media_and_fluorescence_tracers_for_the_use_of_qualitative_lightinduced_fluorescence_in_engine_systems/figures?lo=1, May, 2022)

Another important phenomenon that is a consequence of light tissue interaction is birefringence (Lihong V. Wang and Wu, 2007). This is a material property that involves rotation of the axis of polarization of light as it traverses through the material. Some of the biomaterials known to be birefringent include muscle fiber, retina, amino acid and glucose. The amount of rotation of the axis of polarization by the material is a function of optical wavelength, path length and concentration of the active sample.

3.2 Tissue optical scattering

When light travel in a medium whose spatial distribution of refractive indices is non-uniform, it takes a tortuous path of propagation. This results in photon diffusion and the phenomenon is referred to as scattering. Scattering in a medium can be characterized by an optical property called optical scattering coefficient μ_s $[cm^{-1}]$. This is the probability of a photon undergoing a scattering event per unit path length. In case of a single scatter, scattering is described by optical scattering cross-section σ_s. σ_s is related to geometrical cross-sectional area and the scattering efficiency Q_s as shown in equation 3.1. μ_s is related to σ_s through N_s which is the number of scatterers per unit volume of a medium as shown in equation 3.2 (Jacques, 2013).

$$\sigma_s = Q_s \sigma_s \tag{3.1}$$

$$\mu_s = N_s \sigma_s \tag{3.2}$$

The major scatterers in a biological tissue include cells and cell organelles such as nuclei, cell membrane, mitochondria and lybosomes.

3.3 Tissue optical absorption

Optical absorption in tissue is characterized by the tissue's optical property called optical absorption coefficient μ_a $[cm^{-1}]$. μ_a is the probability of a photon being absorbed per unit path length. A single absorber is characterized by absorption cross-section σ_a which in turn is related to the geometrical cross-sectional area σ_a of the absorber through absorption efficiency Q_a as shown in Equation 3.3. Equation 3.4 (Jacques, 2013) gives the relationship between μ_a and σ_a where N_a is the number of absorbers per unit volume of the media.

$$\sigma_a = Q_a \sigma_a \tag{3.3}$$

$$\mu_a = N_a \sigma_a \tag{3.4}$$

The ratio of μ_a to molar concentration of the optical absorber is referred to as the specific absorption coefficient or extinction coefficient ε. Extinction coefficient is a function of the excitation wavelength and its values are unique for different chromophores. Equation 3.5 (Jacques, 2013) gives the expression for μ_a in terms of molar concentration, $[C]$ of the chromophores and ε.The summation is taken over the number of absorbers present in a sample.

$$\mu_a = \sum_i \varepsilon_i [C_i] \tag{3.5}$$

The major biological absorbers in a human tissue include hemoglobin, melanin, proteins, fats and water.

3.4 Light transport in tissue

Optically, biological tissues can be categorized as highly scattering (turbid) media. A collimated light beam launched on the tissue surface quickly losses its direction after propagating a short distance into the tissue due to optical diffusion.

The major tissue properties that affect photon propagation include μ_a, μ_s, n and g. n is the tissues' refractive index and g is scattering anisotropic factor which determines the direction light is scattered. Values of g range from -1 to 1 where values close to -1 signifies backward scattering, values close to zero imply isotropic scattering, and values close to +1 imply forward scattering.

Photon propagation in tissue can be modeled analytically or numerically. The Boltzmann's Radiative Transport Equation (RTE) given in Equation 3.6 (Richards-Kortum and Sevick-Muraca, 1996) is an analytical approach for describing photon propagation traveling in given direction in a small region in a sample.

$$\frac{1}{c}.\frac{\partial}{\partial t}\emptyset(\boldsymbol{r},\hat{\boldsymbol{s}},t) = q(\boldsymbol{r},\hat{\boldsymbol{s}},t) - [\mu_a + \mu_s + \nabla\cdot\hat{s}]\emptyset(\boldsymbol{r},\hat{\boldsymbol{s}},t) + \mu_s \int \Theta(\hat{\boldsymbol{s}},\hat{\boldsymbol{s}}')\,\emptyset(\boldsymbol{r},\hat{\boldsymbol{s}}',t)d\hat{s}' \quad (3.6)$$

where: $\emptyset(\boldsymbol{r},\hat{\boldsymbol{s}},t)$ is the light radiance, $q(\boldsymbol{r},\hat{\boldsymbol{s}},t)$ is the source term, and $\Theta(\hat{\boldsymbol{s}},\hat{\boldsymbol{s}}')$ is the scattering phase function which gives the probability of a photon originally traveling in direction $\hat{\boldsymbol{s}}'$ being scattered to direction $\hat{\boldsymbol{s}}$. Equation 3.6 states that the time rate change of photons in a small region **r** traveling in direction $\hat{\boldsymbol{s}}$ is given by adding the radiance from the source (given by $q(\boldsymbol{r},\hat{\boldsymbol{s}},t)$) to the radiance due to photons scattered towards $\hat{\boldsymbol{s}}$ from $\hat{\boldsymbol{s}}'$ (given by the phase integral) and subtracting radiance lost by; photon absorption (given by $\mu_a \cdot \emptyset(\boldsymbol{r},\hat{\boldsymbol{s}},t)$), photons scattered away from direction $\hat{\boldsymbol{s}}$ (given by $\mu_s \cdot \emptyset(\boldsymbol{r},\hat{\boldsymbol{s}},t)$) and photon outflow due to

radiance gradient (given by $\nabla \cdot \{\hat{s} \cdot \emptyset(\boldsymbol{r}, \hat{\boldsymbol{s}}, t)\}$). Approximate solutions of Equation 3.6 are given in Equation 3.7 and Equation 3.8.

$$\Phi(x) = \Phi_o \exp(-\mu_a z) \tag{3.7}$$

$$\Phi(x) = \Phi_o \exp\left(-\mu_{eff} z\right) \tag{3.8}$$

Where Φ is optical fluence which is the radiance intensity in a point coming from all angle and is given by:

$$\Phi = \int_{4\pi} \emptyset(\boldsymbol{r}, \hat{\boldsymbol{s}}', t) d\hat{s}'$$

and μ_{eff} is the effective attenuation coefficient given by:

$$\mu_{eff} = \sqrt{3\mu_a(\mu_a + \mu_s')}$$

where μ_s' is the reduced scattering coefficient given by:

$$\mu_s' = (1 - g)\mu_s$$

A commonly used technique for numerical modeling of photon propagation in tissue is Monte Carlo (MC) simulation (Prahl, 1989). This method assumes that the tissue is made of discrete ensembles of optical absorbers and scatterers. Photon packets of unity weight are launched into the medium and propagated in discrete steps of random sizes and in random direction (this is known as the random photon walk). After each step taken by the photon, a fraction of the

photon weight is deducted from the initial weight to account for probable photon absorption. The direction taken by a photon packet at each step is determined by the scattering phase function which is a probability density function that gives the probably of a photon being scattered in a given angle. When a photon packet reaches at the tissue boundary, the probability of exit or total internal reflection is determined using the Fresnel equation of reflection given in equation 3.9 (Tuchin (2015)). If the photon is exited, the photon walk is terminated and another photon packet is launched. In case the photon walk is internally reflected, the direction of propagation is reversed and the process is repeated. At each interaction site, the photon weight is updated by subtracting the contribution of absorption from the initial photon weight and the new value is recorded. At the tissue interface the number of photon exited at each point is also recorded. In order to approximate the practical situation, a near infinite number of photon packets is launched and propagated. This technique gives results that are in close agreement with practical measurements provided high number of photon packets are used. A major drawback of this technique is that the algorithm is computation intensive and takes several hours to simulate a non-trivial problem. Also it is difficult to model photon propagation in optically heterogeneous tissue samples.

$$R(\alpha_i) = \frac{1}{2}\left[\frac{sin^2(a_i - a_t)}{sin^2(a_i + a_t)} + \frac{tan^2(a_i - a_t)}{tan^2(a_i + a_t)}\right] \tag{3.9}$$

where: a_i is the angle of incidence whereas a_t is the angle of transmittance. Snell's law of refraction gives the relationship between the two angles

i.e. $n_i sin\alpha_i = n_t sin\alpha_t$, with n_i being refractive index at the medium where light is incident and n_t is the refractive index at the medium where light is being transmitted.

3.5 Photothermal processes and detection techniques

If chromophore relaxation is non-radiative after photon absoption, the deposited heat in the irradiated region in the specimen can trigger a number of thermal processes. These processes include; photoacoustic effect, thermal lens effect, thermal wave generation among others (Tuchin and Tuchin, 2007). A description of photoacoustic and thermal lens effect is given in the sections that follow.

3.5.1 Photoacoustic effect

When a sample undergoes a non-radiative electron decay following optical absorption, the heat deposited causes thermal elastic expansion in the irradiated sample volume. This leads to induction of pressure (acoustic) waves which propagate through the sample and can be detected using a broadband ultrasonic sensor. Figure 3.1 illustrates the energy conversions and detection scheme involved in photoacoustic effect. The intensity of the induced pressure wave P_o is proportional to the sample's optical absorption coefficient and the optical energy induced. Equation 3.10 gives the expression for P_o induced following a pulsed optical excitation (Xia *et al*., 2014).

$$P_o = \Gamma H \qquad (3.10)$$

$$H = \eta \mu_a \Phi.$$

With where Γ is the sample's Grueneisen parameter which is dimensionless and represents the percentage of heat energy converted to sound energy. H is the amount of optical energy per unit volume converted to heat (measured in Joules per cubic meter) and Φ is the optical fluence which is the light intensity absorbed by the sample (its units are Joules per square meter). Γ is a thermodynamic property of the sample and is related to the sample specific heat capacities C_v and C_p, thermal coefficient of volume expansion β and velocity of sound in the sample v_s according to equation 3.11.

$$\Gamma = \frac{\beta}{k\rho C_v} = \frac{\beta v_s^2}{C_p} \qquad (3.11)$$

where k is the samples thermal conductivity whereas ρ is the mass density.

3.5.2 Thermal lens effect

This phenomenon occurs when a optically thin sample is irradiated with laser light having Gaussian beam profile (Sell, 2012). The illuminated sample region acquires a temperature gradient. This heating pattern induces a change in the sample's refractive index resulting in formation of a lens-like element in the illuminated sample region. Depending on the nature of the sample under illumination, the resultant lens-like element can converging (positive lens) or diverging (negative lens). The optical beam that causes heating in the sample is referred as the Excitation Beam (EB). If a secondary optical beam know as the Probe Beam (PB) passes through the induced thermal lens, it can either be diverged or converged and its incident intensity is altered.

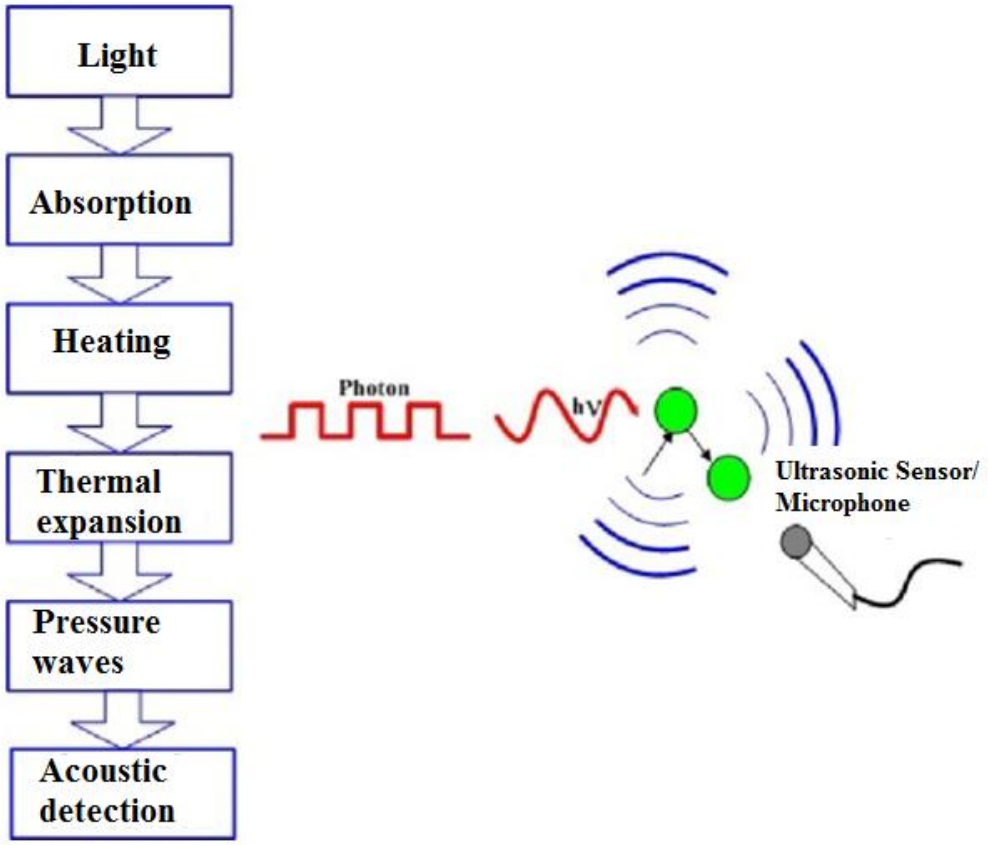

Figure 3.2: Illustration of photoacoustic effect of Production and detection of photoacoustic waves. On the left is the schematic diagram showing processes leading to generation of PA signal and on the right a graphical illustration of the phenomenon.

Equation 3.12 gives an expression of a Thermal Lens (TL) signal S which is defined as the fraction change of the probe beam intensity as detected in far field following the development of a thermal lens in a sample. It is a function of both time, t and lateral position, z. When the excitation beam is applied in the sample, the heating and temperature rise increases up to a point when the steady state temperature distribution is reached.

$$S(t,z) = \frac{I(t,z) - I(0,z)}{I(0,z)} \qquad (3.12)$$

$I(t,z)$ is the TL signal intensity after application of the EB, $I(0,z)$ is the TL signal intensity before application of EB. Under some TL configurations, the TL signal can be expressed as follows.

$$S = \frac{\pi P_e \mu_a l}{2k\lambda_p} . \frac{dn}{dT} \tag{3.13}$$

where P_e, l, λ_p and $\frac{dn}{dT}$ are excitation beam power, optical interaction length, probe beam wavelength and temperature coefficient of refractive index gradient respectively. Other parameters have been defined above.

There are two major implementation geometries of thermal lens setup as shown in Figure 3.3. One geometric configuration involves aligning both the probe beam and the excitation beam in the same direction with respect to the sample (coaxial configuration). An optical filter is then placed after the sample to block the excitation beam and allow the probe beam to be transmitted and detected as the TL signal. In this configuration (shown in Figure 3.3(a)) the focal points for the two beams could be matched or mismatched. The second implementation (transverse configuration) is where the probe beam and excitation beam are perpendicular to each other and intersect in the sample region as shown in Figure 3.3(b).

The focal length F of the induced TL is given by the following expression.

$$F = -\left[l\left(\frac{dn}{dT}\right)\left(\frac{\partial^2 T}{\partial r^2}\right)_{r=0} \right]^{-1} \tag{3.14}$$

with $\frac{\partial^2 T}{\partial r^2}$ being the second partial derivative of induced temperature with respect to radial distance of the EB.

Thermal lens has found application in diverse fields including detection and quantification of toxins in foodstuffs and water as well as analysis of trace gases (Franko, 2001) . Some of the salient features of the technique are the ability to use small sample quantities and high detection sensitivity. The drawbacks of the technique include difficulty in optical alignment and the need to use thin transparent samples.

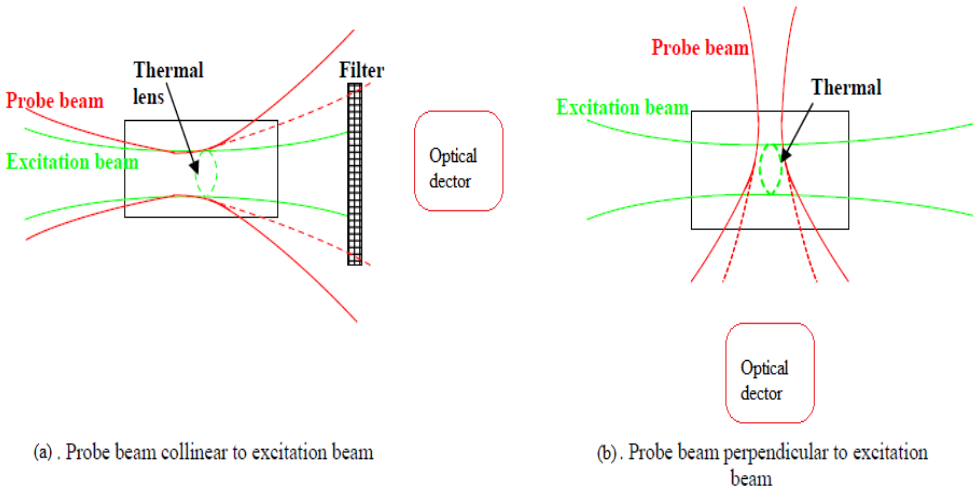

Figure 3. 3: Thermal Lens implementation geometries (Canto *et al.*, 2008)

CHAPTER 4

METHODOLOGY

The goal of this work was to develop an optical pump probe device (referred to as PTIOSM hemozoin sensor) capable of performing label-free *in-vitro* detection of *Plasmodium* parasites pigment present in malaria infected blood samples. The working principle of the sensor is based on the PTIOSM hypothesis. In this chapter, an analytical model of describing the PTIOSM hypothesis is developed and a methodology for testing the hypothesis and validating the technique's efficiency in detection of hemozoin is described. The chapter is organized into four sections. In section 4.1, a derivation of the PTIOSM model describing the origin and characteristics of the optical scattering modulation as a result of the sample excitation by the pump beam is given. Section 4.2 describes the hardware design of PTIOSM setup (sensor). Two different optical detection approaches were employed in the development of the PTIOSM setups. In one setup, a photodiode was used as the photon detector that yielded a one dimensional PTIOSM signals while the second setup (PTIOSM hemozoin imaging setup) an image sensor for acquisition of 2D PTIOSM signals from the sample was used. Section 4.3 describes the samples and sample preparation steps employed. Section 4.4 gives the algorithmic steps used in processing the acquired raw PTIOSM signals. Details of the computational methods used for feature extraction, signal processing and classification are explained. Results obtained from implementation of this chapter are given in Chapter 5.

4.1 Derivation of the PTIOSM model

Suppose an incident probe beam interacts with the sample and then the transmitted portion is measured with a photo detector as shown in figure 4.1. An optical filter is incorporated in the setup to allow only the probe beam light to pass through it but block any other light wavelength. x is the optical path length.

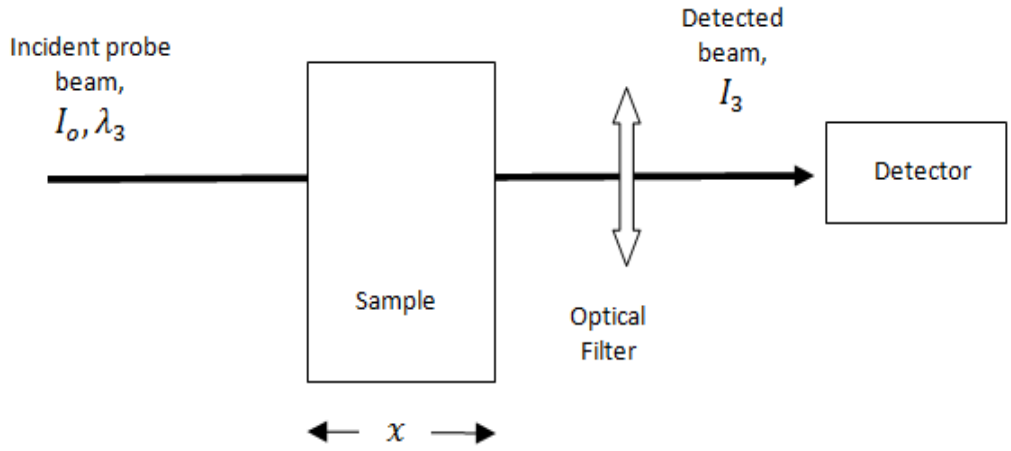

Figure 4.1: Sample irradiated with only probe beam light, x is the sample optical path length, I_o is the incident intensity while I_1 is the transmitted intensity of the probe beam light whose wavelength is λ_3. An optical filter is placed between the sample and the detector to block any other light except the probe beam wavelength.

A fraction of the incident light will be attenuated due to sample absorption and scattering. Ignoring scattering and following the Beer Lambert law, the detected light intensity is given by Equation 4.1:

$$I_1 = I_o e^{-\mu_a x} \tag{4.1}$$

If an Excitation Beam (EB) having wavelength λ_2 is introduced with the probe beam still ON as shown in Figure 4.2, the sample undergoes Photo-Thermal (PT)

processes that causes its optical extinction coefficient to change and therefore the detected probe beam signal will now be given by Equation 4.2. The excitation beam after interacting with the sample, the transmitted part is blocked by the optical filter therefore it does not reach the detector. The parameter μ_a' gives the modified value of μ_a caused by alteration of the sample optical properties due to application of the EB of wavelength λ_2 .

$$I_2 = I_o e^{-\mu_a' x} \qquad (4.2)$$

By repeating the above process using an EB of different wavelength (say λ_3), detected PB signal changes is intensity and can be expressed by Equation 4.3:

$$I_3 = I_o e^{-\mu_a'' x} \qquad (3)$$

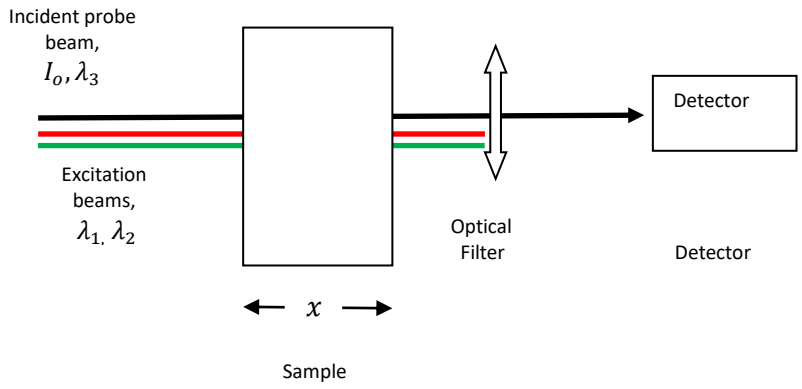

Figure 4.2: Sample irradiated with both probe and excitation beams. The optical filter blocks the excitation beams from reaching the detector only allowing the probe to reach the detector.

The parameter μ_a'' is the perturbed value of optical absorption coefficient of the sample due to application of EB of wavelength λ_3. Subtracting Equation 4.1 from Equation 4.2 and dividing the difference with Equation 4.1 gives Equation 4.4:

$$\frac{I_2 - I_1}{I_1} = \frac{e^{-\mu_a' x} - e^{-\mu_a x}}{e^{-\mu_a x}} = e^{(\mu_a - \mu_a')x} - 1 \tag{4.4}$$

Rearranging Equation 4.4 gives rise to equation 4.5

$$\frac{I_2}{I_1} = e^{(\mu_a - \mu_a')x} \tag{4.5}$$

Replacing Equation 4.2 with Equation 4.3 in Equation 4.4 and repeating the same procedure we arrive at Equation 4.6.

$$\frac{I_3}{I_1} = e^{(\mu_a - \mu_a'')x} \tag{4.6}$$

Taking natural logarithms of Equation 4.5 and 4.6 gives Equations 4.7 and 4.8

$$\ln\left(\frac{I_2}{I_1}\right) = (\mu_a - \mu_a')x \tag{4.7}$$

$$\ln\left(\frac{I_3}{I_1}\right) = (\mu_a - \mu_a'')x \tag{4.8}$$

Dividing Equations 4.7 by Equation 4.8 we get Equation 4.9

$$\frac{\ln\left(\frac{I_2}{I_1}\right)}{\ln\left(\frac{I_3}{I_1}\right)} = \frac{(\mu_a - \mu_a')}{(\mu_a - \mu_a'')} = \frac{\Delta\mu_{a,\lambda 2}}{\Delta\mu_{a,\lambda 1}} \tag{4.9}$$

$\Delta\mu_{a,\lambda1}$ and $\Delta\mu_{a,\lambda2}$ give the change of optical absorption coefficients due to application of EB radiations having wavelengths λ1 and λ2 respectively. Optical absorption coefficient μ_a of a material is a derived quantity and is equivalent to the product of the materials' specific molar extinction coefficient $\varepsilon_{\lambda i}$ (an optical property of molecules that indicates how strongly the molecule absorbs light of a given wavelength) and the molar concentration $[C]$ of the light absorbing molecules (chromophores) present in the sample. Equation 4.10 gives the expression of μ_a in terms of $\varepsilon_{\lambda i}$ and $[C]$.

$$\mu_a = \varepsilon_{\lambda i}[C] \tag{4.10}$$

For a given sample with fixed molar concentration of chromophores, the changes in μ_a are only due to the variations of $\varepsilon_{\lambda i}$ as a result of the sample undergoing PT processes due optical excitation by the EB ($[C]$ is constant). Therefore Equation 4.9 can be expressed in terms of changes of specific molar extinction coefficient $\Delta\varepsilon_{\lambda i}$ as shown in Equation 4.11.

$$\frac{\ln\left(\frac{I_2}{I_1}\right)}{\ln\left(\frac{I_3}{I_1}\right)} = \frac{\Delta\varepsilon_{\lambda 1}}{\Delta\varepsilon_{\lambda 2}} \tag{4.11}$$

From Equation 4.11 it can be deduced that by optically pumping (exciting) the sample with two distinct EB wavelengths λ_2 and λ_3 and measuring the intensities of the transmitted probe beam signal I_1, I_2 and I_3, and performing the operation $\frac{\ln\left(\frac{I_2}{I_1}\right)}{\ln\left(\frac{I_3}{I_1}\right)}$ yields the fraction change in the sample's extinction coefficient $\frac{\Delta\varepsilon_{\lambda 1}}{\Delta\varepsilon_{\lambda 2}}$. We

expect that this parameter can be used for differentiation of different molecule species present in the sample. For instance, we expect the values of the parameter to be distinct for malaria infected and non-infected blood samples.

4.2 PTIOSM sensor setup

Four designs of PTIOSM sensor for detection of *Plasmodium* parasite pigment (hemozoin) in blood were investigated. Their working principle was similar in the sense that in all setups a RGB LED light source provided both the probe and excitation optical beams. However, the key difference was the type of optical detectors used and the signal processing algorithms employed. One setup employed a photodiode for detection of probe beam light from the sample. In order to block the excitation beam from reaching the detector, an optical spectral filter was used. The transduced photodiode current was converted to a voltage signal and amplified by a trans-impedance amplifier. The signal was then coupled to a digital oscilloscope for digitization. The digitized oscilloscope signals were loaded to a PC for processing and classification. The second hemozoin probe still employed a photodiode detector but allowed both the excitation and probe beam light to reach the detector. To separate the probe beam and excitation beam a computation approach was used. The third and fourth setup used an image sensor for capturing short video clips of the diffuse reflected probe beam light passing through the sample following sample optical excitation. The distinction between the third and the fourth setups was that, whereas one setup employed optical filter to separate the probe and excitation beams from reaching the optical detector, the

other setup used a computational technique similar to the one used in the second setup. The images were then preprocessed and classified according to their infection status. The following is a description of each setup in details.

4.2.1 Photodiode PTIOSM setup using optical spectral filtering

Figure 4.3 show a block diagram and photo of setup while Figure 4.4 give the electronic schematic diagram of the RGB LED driver circuit used for sample illumination in both the photodiode detector and image sensor setups. The working principle of the setup is as follows: Blood samples (both Thick blood smears and whole blood in petri-dishes) were placed on the sample stage and illuminated by two types of optical beams produced by a common anode 3W Red, Green, and Blue Light Emitting Diode (RGB LED) [https://cdn-shop.adafruit.com/product-files/2524/FD-9RGB-Y2.pdf]. The two beams were termed as Excitation Beam (EB) and Probe Beam (PB) respectively. The function of the EB was to raise the sample chromophores to excited state and consequently generate transient photothermal changes that would be detected using the PB. The red (625nm) and green (525nm) wavelengths of the RGB LED were used as the excitation beam and their intensities were modulated using a driver circuit. The blue wavelength (465nm) was used as the probe beam. The driver circuit comprised of a custom made electronic circuit for forward biasing RGB LEDs using two Bipolar Junction Transistors (BJT - package number 2N3904). The transistors were driven ON and OFF by a signal from a function generator that was set to produce 50nS pulse train at a repetition frequency of 1 MHz. The signal

generator signal was applied at the base terminal of BJT transistors. The blue light (465nm) from the RGB LED was used as the probe beam and was connected to the driver circuit such that a constant intensity light was produced. The two beams passed through the sample before reaching an optical filter (Omega Optical, Inc. 450 nm SP Rapid Edge 25 mm Optical Short pass Filter) that blocked the excitation beam coming from the sample while passing through the probe beam. The probe beam was then directed to a photo-detector (BPW34 pin photodiode module) that converted the received probe beam light intensity into electrical current. The voltage signal across the photodiode terminals was then coupled to a digital oscilloscope (OWON SDS1052, 2 channel, 500 MS/s, 10 KB recording length) for digitization.

The oscilloscope signal sampling rate was set at 250 Mega Samples per Second (MSa/S) and its second input channel was connected to receive excitation beam trigger signal from the function generator. A laptop computer pre-installed with OWON SDS1052 oscilloscope software was connected to the scope using a Universal Serial Bus (USB) cable to log in the digitized oscilloscope signals. The data was automatically loaded and stored in the computer in Comma Separated Value (CSV) format. A select switch at the driver circuit was used to manually switch between the red and green optical excitation beams before data acquisition began. At least ten PTIOSM signal from each sample were acquired and stored for each sample. Time Domain (TD) signal analysis and visualization was performed with a view to determine the degree of PB signal modulation due to

sample irradiation by the EB.

4.2.2 Photodiode PTIOSM Setup using computational spectral filtering

A variant setup from the one described in section 4.2.1 employing a different technique for separating EB and PB signals after signal acquisition was also developed. The intensity of the EB beam was kept constant while modulating the frequency of the PB at a fixed frequency of 1MHz. Instead of blocking the EB from reaching the detector using an optical filter, the two optical signals were allowed to reach the detector, and were detected and converted to 1D electrical signal which was digitized and loaded to a computer. The acquired TD signal was converted to Frequency Domain (FD) using Discrete Fourier Transform (DFT). The magnitude and phase values of the FD signal at the oscillating frequency of the PB were then obtained and used for sample analysis. Figure 4.3 and Figure 4.4 show the setup diagrams including the block diagram and its photo as well as the schematic diagram of the LED driver circuit. Whole blood in culture glass slides was probed and FD PTIOSM signal analyzed and visualized to determine the degree of signal modulation.

4.2.3 Image sensor PTIOSM setup using optical spectral filtering

In this case, similar sample irradiation pattern as the one described in section 4.2.1 was employed. However, a Charge Coupled Device (CCD) image sensor was used for acquisition of short video clips of the samples as they were irradiated by pulsed EB and constant intensity PB. The CCD image sensor was extracted from a webcam (Logitech C525). The webcam image sensor was exposed by removing its focusing lens module. The exposed CCD was used to capture video clips of the blood smear samples under photo-thermal excitation by plugging its USB cable to

a computer and using the webcam driver software installed in the computer for video acquisition. The captured video clips were two minutes long.

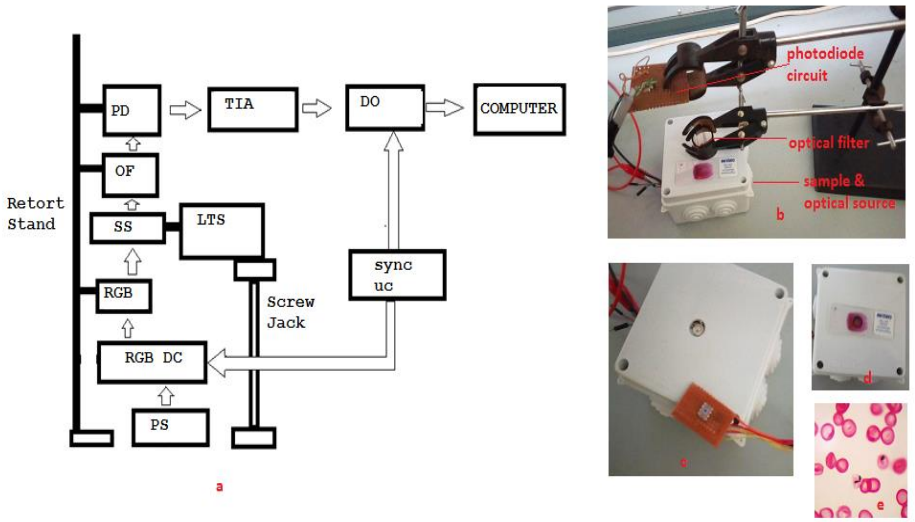

Figure 4.3: (a) Setup diagram and images of the photodiode PTIOSM setup with optical filter. PS is the power supply, RGB DC is the RGB LED Driver Circuit, RGB is the RGB LED, SS is the Sample Stage, OF is the Optical Filter, PD is the Photo-Diode, TIA is the Trans-impedance amplifier, DO is the Digital Oscilloscope, LTS is the manually controlled Linear Translational Stage, sync uC is the synchronization microcontroller. (b,c,d) images of sections of the setup, (e) is a microscopic image of a sample of blood smear specimen used.

Figure 4.5 gives both the block diagram and a photo of the setup. A Python code was written to read the captured video clips, split the video clip into separate images and preprocess the images. The EB was pulsed at a frequency of 2Hz with the pulse width duration of 500mS to accommodate the slow image acquisition process by the image sensor module. The PB was biased to produce constant intensity beam. Whole blood in culture glass slides was used as the sample for testing the operation of the setup. The acquired images were analyzed

in TD and the resultant PTIOSM signals visualized. Table 4.3 gives the image processing algorithm implemented.

4.2.4 Image sensor PTIOSM setup using computational spectral filtering

A variant of the setup from the one described in section 4.2.3 but employing a computational technique (similar to the one described in section 4.2.2) for separating EB and PB signals after

signal acquisition was developed. The intensity of the EB beam was kept constant while the intensity of the PB was modulated at a fixed frequency of 2 Hz. Instead of blocking the EB from reaching the image sensor using an optical filter, the two optical beams passed through a microscope objective before reaching the image sensor for sample image formation. A five minute video was acquired and uploaded to a computer for further processing. Figure 4.7 shows a photo of the setup. Open Flexture Microscope (OFM), which is a open source 3D printed robotic microscope (Collins *et al*., 2020) was modified to realize the setup described above. By using the OFM platform to build the setup, it was possible to automatically scan the sample, perform auto focusing and automate image acquisition.

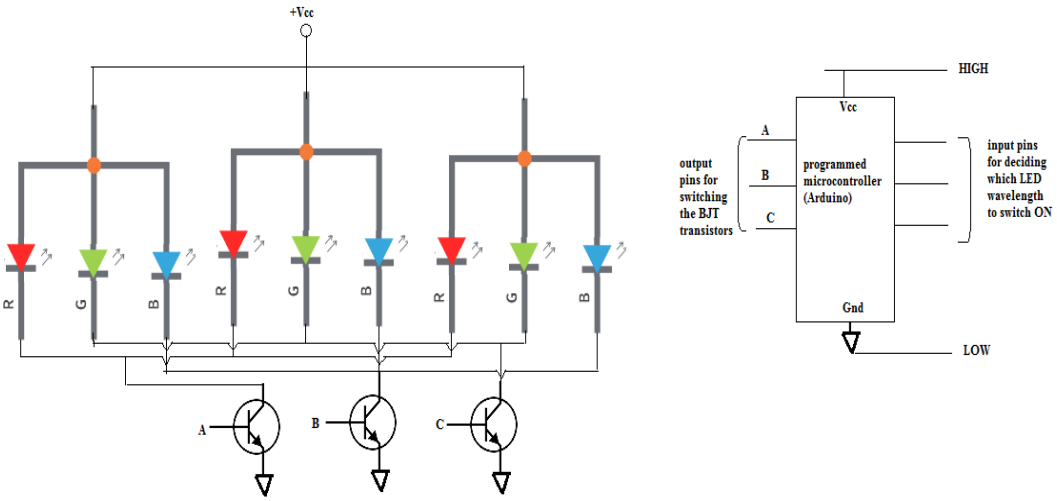

Figure 4.4: Schematic diagram of custom made RGB LED driver circuit for the PTIOSM setups

4.3 Description of specimen and experiments performed

Whole blood and blood smears from healthy and malaria infected subjects were used as samples for testing the performance of the developed PTIOSM setups. Ethical approval from Meru University Institutional Research Ethical Review Committee (MIRERC) was sought before undertaking experiments involving human samples. Besides, synthetic hemozoin acquired commercially was mixed with whole blood to simulate *Plasmodium* parasite pigment in blood. A total of twenty four human subjects participated in this study. Blood samples of participants were tested for malaria using microscopy method. Thick blood smears, thin blood smears and whole blood samples were prepared and passed to the PTIOSM hemozoin sensor setups for signal acquisition. Blood smears were then stained and examined under an optical microscope for presence of

Plasmodium parasites. Four of the participants tested positive while the rest were negative. The malaria positive participants had their venous blood drawn to make more sample aliquots. From each participant, a total of ten blood smear aliquots were made and their video signals acquired. A total of forty malaria positive smears were made and their PTIOSM video signals acquired. The total number of samples used for the experiment therefore was sixty (40 malaria positive and 20 malaria negative).

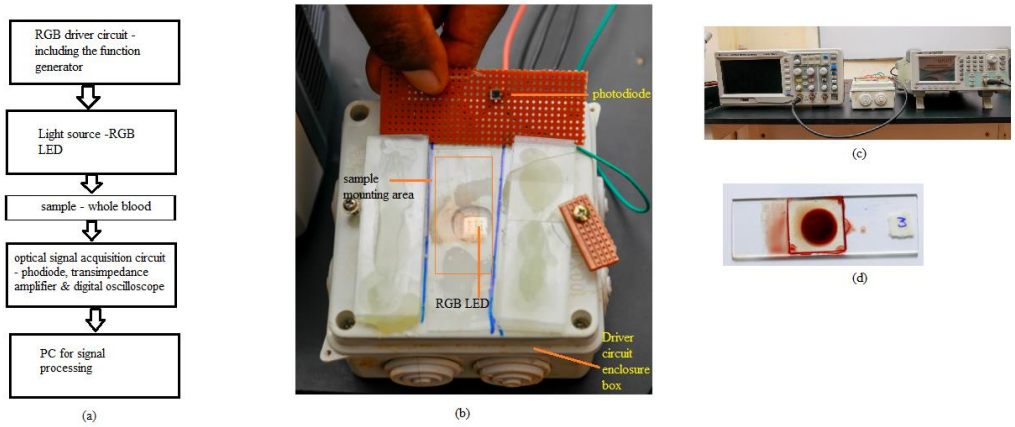

Figure 4.5: Setup diagram and images of the photodiode PTIOSM setup employing computational spectral filtering. (a) setup diagram, (b and c) photos of the setup with labeled parts, (d) sample whole blood in a special glass slide containg a sample well.

4.4 Description of PTIOSM Signal Processing Algorithms

4.4.1 Testing of PTIOSM hypothesis

From the derivation done in section 4.1, we expect the application of the EB into the sample to either lead to enhancement or attenuation in intensity of the detected PB signals. For the setups employing optical filtering technique to separate EB and PB, EB intensity was pulsed while PB intensity from the source was kept

constant. Any modulation observed from the detected PB that was above the Signal to Nose Ratio (SNR) of the detector was considered to be due to effects emanating from interactions of the EB with the sample.

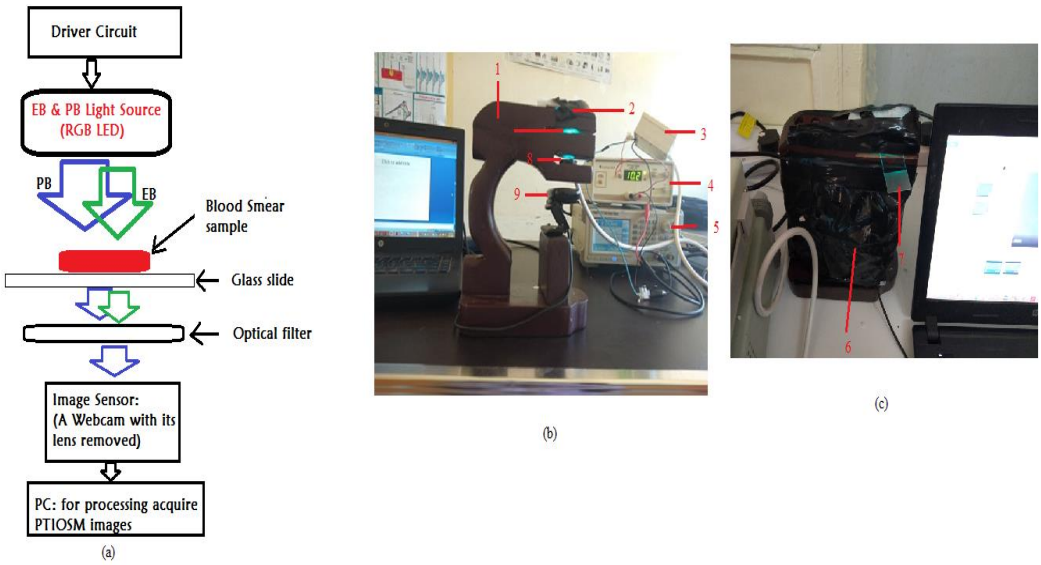

Figure 4.6: The image sensor PTIOSM sensor employing optical spectral filtering. Panel (a) gives the block diagram of the setup, panel (b and c) are the photos of the setup with the parts labeled numerically. 1 – wood body, 2- RGB LED light source, 3 - Driver circuit, 4 – power supply, 5-function generator, 6 – black polythene sheet for shielding the image sensor from stray light. 7 – blood smear sample, 8 optical filter

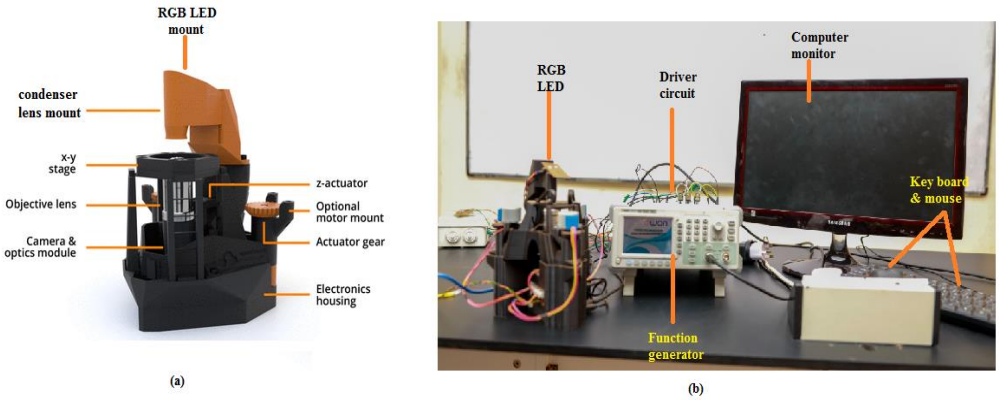

Figure 4.7: OFM PTIOSM setup. (a) OFM with parts labeled, diagram adopted from (Collins *et al.*, 2020). (b) parts of the OFM PTIOSM setup

Both Time Domain (TD) and Frequency Domain (FD) of the acquired signals were analyzed to determine and quantify differences in detected PB signals with and without the sample being irradiated by the EB. Table 4.1 gives the steps for processing the signal acquired by the photo-diode PTIOSM setup employing optical filtering while the algorithm for the image sensor PTIOSM setup employing the same scheme of spectral separation are given in table 4.2.

Computational filtering involved acquisition both PB and EB optical signals reaching the detector and performing digital signal filtering to separate the two signals. In this case, the EB source was operated under constant intensity while the PB intensity was modulated in intensity using a fixed frequency. Table 4.3 and Table 4.4 give the algorithmic steps used to process signals acquired by the photodiode and image sensor setups respectively.

4.4.2 Application of PTIOSM technique in label-free detection of hemozoin in blood samples

The Principal Component Analysis (PCA – describe in detail in sub-section 4.4.3) of 100 consecutive video frames captured by image sensor setup employing optical spectral filtering was performed and the first few principal component images averaged to form the feature vectors for training machine learning classifiers to distinguish between malaria positive and malaria negative samples from their PTIOSM video signals. Both Support Vector Machine (SVM) and Logistic Regression classifiers were trained and their performance evaluated. The working Principle of SVM is given in section 4.4.3. Table 4.5 and Table 4.6 gives

the algorithmic steps used in processing and classifying the acquired PTIOSM video signals into their respective malaria infection status.

4.4 Description of signal processing and classification algorithms used to process PTIOSM signals

The algorithms described above were implemented using Python programming language. Jupyter notebook (which comes with Anaconda Integrated Development Environment (IDE) for python) was used in editing and executing Python programs. Python codes used for implementation the algorithms described in Tables 4.1– 4.5 are given in Appendix A. Table 4.6 summarizes the role of the main python packages (libraries) used to implement the algorithm.

Table 4. 1: Algorithmic steps for verifying PTIOSM hypothesis using the photodiode type PTIOSM setup using optical spectral filtering

1.	*Load the computer with the oscilloscope signals acquired from samples irradiated only by the PB light – signal processing was implemented using Python programming language executed using Anaconda's Jupiter Notebook platform*
2.	*Compute the following TD signal properties; peak to peak amplitude, maximum intensity, mean intensity, standard deviations of the mentioned parameters for different samples.*
3.	*Plot graphs for visualization of the parameters stated in step 2 above*
4.	*Perform Fast Fourier Transform (FFT) of the detected signal and plot both the magnitudes and phases of the signals acquired from different samples*
5.	*Compute the power density spectrum from the FFT results obtained in step 4*
6.	*Repeat steps 2 to 4 using acquired oscilloscope signals acquired from samples irradiated by both EB and PB as described in section 4.1.1*

Table 4.2: Algorithmic steps for verifying PTIOSM hypothesis using image sensor and optical filter PTIOSM setup

1. *Acquire video clip from samples irradiated only by the PB light*
2. *Split the acquired video clips into separate time series RGB images*
3. *Crop the region of interest*
4. *Covert the RGB sub-images to Gray scale images using Otsu's algorithm*
5. *Compute the mean intensity of each gray scale time series images*
6. *Plot a graph of these time series averaged image intensities*
7. *Compute statistical metrics of the mean intensities of images i.e. mean, standard deviation, maximum peak intensity, minimum peak intensity, magnitudes and phases of Fourier Transform signal*
8. *Repeat steps 2 to 7 using video clips acquired from samples irradiated with both EB and PB light.*

Besides computation of basic statistical metrics, the PTIOSM Signal to Noise Ratio (SNR) was also computed. SNR is defined as the ratio of signal power to noise power and is given in equation 4.12.

$$SNR = \frac{<s^2>}{<n^2>} \quad (4.12)$$

where s is the acquired PTIOSM signal from a blood sample while n is the PTIOSM signal from a blank sample. Parseval's signal energy theorem (Yu, 2014) gives the energy of a signal in time and is given by the formula given in equation 4.13.

$$E = < f^2(t) > = \int_{-\infty}^{\infty} f^2(t)dt \quad (4.13)$$

4.5 Feature extraction

The aim of this task was to explore the structure of the preprocessed PTIOSM data and obtain suitable features to be used for automatic classification of samples as hemozoin positive or negative and also categorize samples based on hemozoin concentrations present. Two techniques namely Discrete Fourier Transform and Principal Component Analysis were used to analyze relevant features in the PTIOSM data and aid in classification of various types (classes) of samples used. The following is a brief description of the two techniques and how they were used in the analysis of PTIOSM data.

4.5.1 Discrete Fourier Transform (DFT)

Fourier transform is a popular signal processing technique used for converting signals from time domain to frequency domain and verse versa. Equation 4.14 gives the Fourier transform and its inverse transform counterpart in complex notation form. $F(j\omega)$ is the frequency domain signal components whereas $f(t)$ is the time domain signal. ω is the continuous frequency variable.

Table 4. 3: Algorithmic steps for verifying PTIOSM hypothesis using the photodiode type PTIOSM setup using computational spectral filtering

1. *Load the computer with the oscilloscope signals acquired from samples irradiated only by the PB*
2. *Perform Fast Fourier Transform (FFT) of the detected signal and plot both the magnitudes and phases of the signals acquired from different samplesDetermine the magnitude and the phase values of the FFT signal at the oscillating frequency of the PB*
3. *Repeat steps 2 and 3 using acquired oscilloscope signals acquired from samples irradiated by both EB and PB as described in section 4.1.2*
4. *Plot bar graphs to aid comparison of the detected PB beam (also referred as PTIOSM signal) magnitude and phase when the sample is irradiated with EB and without sample irradiation with the EB*
5. *Compute the PTIOSM signal enhancement/attenuation factor i.e.*

$$\frac{I_3}{I_1} = e^{(\mu_a - \mu_a'')x}$$

Table 4.4: Algorithmic steps for verifying PTIOSM hypothesis using image sensor PTIOSM setup that employed computational spectral filtering

1. *Acquire video clip from samples irradiated only using PB*
2. *Compute FFT of the video in the time axes*
3. *Extract the Fourier image frame corresponding to the oscillating frequency of the PB ie 2Hz*
4. *Compute the magnitude and Phase images from the resultant Fourier image*
5. *Repeat steps 2 to 4 using video clips acquired when the sample is simultaneously irradiated by the PB and EB*
6. *Compute the fractional change in intensity from magnitude images obtained in step 5 and 4 i.e.,*

$$I_{mag} = \frac{|mag\_I_{PB+EB}|}{mag\_I_{PB}}$$

Where mag_I_{PB+EB} *is the magnitude image acquired under both EB and PB sample irradiation*

mag_I_{PB} *is the magnitude image acquired under only PB sample irradiation*

Table 4.5: Python libraries used to implement signal processing algorithms

	Python Library	Function
1.	Numpy	For performing computations using the acquired PTIOSM signals
2.	Matplotlib	For visualization of data using graphs
3.	Pandas	For manipulation and visualization of tabular data
4.	FFT	For implementation of Fast Fourier Transform Algorithm
5.	Sklean	For performing machine learning tasks such as scaling data, implementing PCA, and design and implementation of Support Vector Machine (SVM)

$$F(j\omega) = \int_{-\infty}^{\infty} f(t)e^{-j\omega t}dt \quad (4.14a)$$

$$f(t) = \frac{1}{\sqrt{\pi}}\int_{-\infty}^{\infty} F(jw)e^{j\omega t}dt \quad (4.14b)$$

DFT is an equivalent Fourier Transform technique that operates on discrete (digital) signals rather than continuous input variables. Equation 4.15 gives expressions for computing the forward DFT and inverse DFT respectively.

$$F[n] = \sum_{k=0}^{N-1} f[k]e^{-j\frac{2\pi}{N}nk} \quad (4.15a)$$

$$\text{for } : n = 1,2,3, \ldots \ldots . N-1$$

$$f[n] = \frac{1}{N}\sum_{k}^{N-1} F[k]e^{j\frac{2\pi}{N}nk} \quad (4.15b)$$

F[n] is the DFT also know as Fourier coefficients of the time domain discrete signal f[n]and is assumed to be periodic over N samples such that

$$F[n+N] = F[n] \quad (4.15c)$$

Equation 4.15c implies that:

$$e^{-j\frac{2\pi}{N}(n+N)k} = e^{-j\frac{2\pi}{N}(n)k}e^{j2\pi k} = e^{-j\frac{2\pi}{N}(n)k} \quad (4.15d)$$

which further implies that

$$N = 2\pi \quad (4.15e)$$

One way of computing DFT is using matrix method given in Equation (4.16)

$$\begin{bmatrix} F[0] \\ F[1] \\ F[2] \\ \vdots \\ F[N-1] \end{bmatrix} = \begin{bmatrix} 1 & 1 & 1 & \dots & 1 \\ 1 & W & W^2 & \dots & W^{N-1} \\ 1 & W^2 & W^4 & \dots & W^{N-2} \\ 1 & W^3 & W^6 & \dots & W^{N-3} \\ \vdots & \vdots & \vdots & \vdots & \vdots \\ 1 & W^{N-1} & W^{N-2} & \dots & W \end{bmatrix} \begin{bmatrix} f[0] \\ f[1] \\ f[2] \\ \vdots \\ f[N-1] \end{bmatrix}$$

where $W = e^{-j\frac{2\pi}{N}}$ and $W = W^{2N} = 1$ (4.16)

A drawback of using equation 4.16 in computing DFT is that matrix multiplications are computationally intensive and the computational load increase with the square of the number of N. Fast Fourier Transform (FFT) is an efficient version of DFT that is employed for speeding up computations by avoiding redundant computations (Cooley *et al*., 1967).

4.5.2 Principal Component Analysis

Principal Component Analysis (PCA) is a technique used for data dimensionality reduction where data is projected onto orthogonal axis (vector components). The axis that carries maximum variance is referred to as principal axis or principal eigen vectors. By projecting raw data onto the first few principal components the main features of the data will be maintained while significantly reducing the dimensionality of the data. Figure 4.8 illustrate the concept behind PCA. PCA is often computed using Singular Value Decomposition (SVD) technique (Baker, 2005).

Singular Value Decomposition

Every M by N Matrix can be decomposed into a product of three unique matrices $U, \sum, V$ as given in equation (4.17):

$$A_{[M,N]} = U_{[M,R]} \sum_{[R,R]} V^T_{[R,N]} \quad (4.17)$$

where $U_{[M,R]}$ is referred as left singular vector, Σ is as diagonal matrix referred as the singular value matrix with its diagonal elements being positive valued numbers arranged in descending order from the first diagonal element to the last. $V_{[R,N]}$ is referred as the right singular vector. V and U are column orthonormal which implies: $U^T U = I$ and $V^T V = I$. Where I an identity matrix and T is the transpose operator.

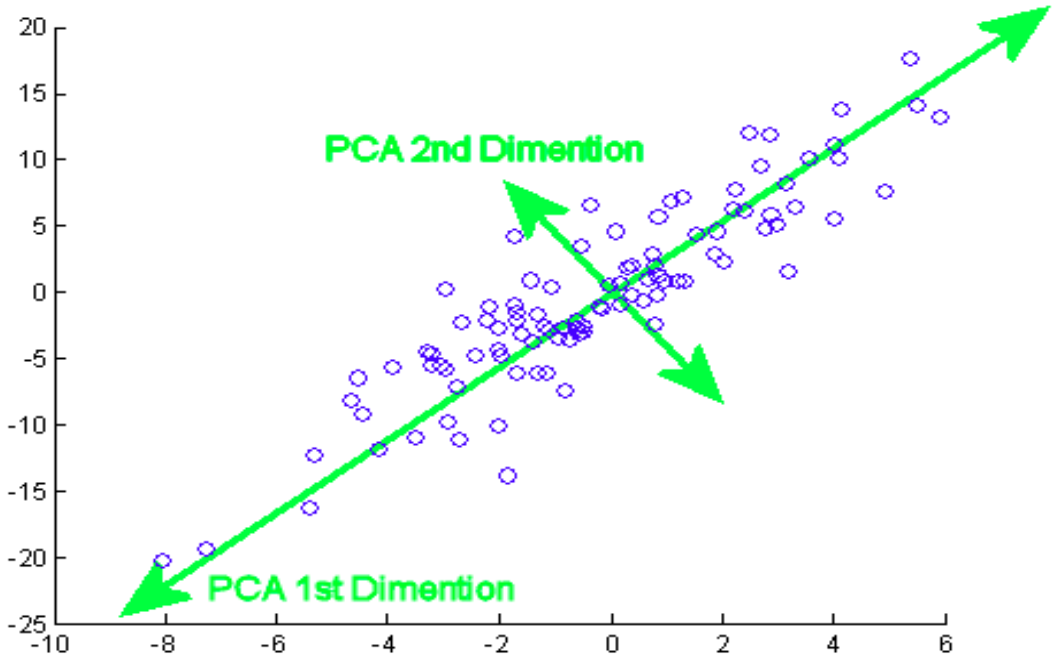

Figure 4.8: Illustration of principal components in Principal Component Analysis - Ref: https://stats.stackexchange.com/questions/2691/making-sense-of-principal-component-analysis-eigenvectors-eigenvalues

The following matrix manipulation procedures gives the relationship between SVD and the eigen value problem, a technique used for computing the principle eigen vectors and eigen values.

$$A_{[M,N]}A_{[M,N]}^{T} = U_{[M,R]}\Sigma_{[R,R]}V_{[R,N]}^{T}V_{[R,N]}\Sigma_{[R,R]}^{T}U_{[M,R]}^{T} = U_{[M,R]}\Sigma_{[R,R]}^{2}U_{[M,R]}^{T} \quad (4.18)$$

Multiplying both sides of Equation 4.18 by $U_{[M,R]}$, we obtain

$$A_{[M,N]}A_{[M,N]}^{T}U_{[M,R]} = U_{[M,R]}\Sigma_{[R,R]}V_{[R,N]}^{T}V_{[R,N]}\Sigma_{[R,R]}^{T}U_{[M,R]}^{T} =$$

$$U_{[M,R]}\Sigma_{[R,R]}^{2}U_{[M,R]}^{T}U_{[M,R]} = \Sigma_{[R,R]}^{2}U_{[M,R]} \quad (4.19)$$

Which is an eigen value problem that can be write as

$$\Gamma\boldsymbol{x} = \lambda\boldsymbol{x} \quad (4.20)$$

where $\Gamma = A_{[M,N]}A_{[M,N]}^{T}$, $\boldsymbol{x} = U_{[M,R]}$ and $\lambda = \Sigma_{[R,R]}^{2}$.

Conceptually, matrices $\Sigma_{[R,R]}^{2}$ and U are computed by solving the eigen problem given in equation 4.20. U matrix gives the eigen vectors which are column orthogonal and $\Sigma_{[R,R]}^{2}$ contains the eigen values.

SVM models have been widely applied in soving machine learning tasks. However, they suffer from some shortcomings including; sensitivity to noisy data and presence of outliers, high computational and memory intensiveness especially for large datasets and limited scalability to increase in data dimensitionality. The drawbacks can however be mitigated by performing data preprocessing techniques such as implementation of data scaling and dimensionality reduction prior to training of the model.

4.6 Sample classification

After suitable features were identified and extracted using PCA as described in the previous subsection, a classifier was applied to differentiate between hemozoin positive and negative samples and also categorize hemozoin samples according to hemozoin concentrations in the case of whole blood samples. Support Vector Machine (SVM) was chosen as the ideal classifier for this task. The reason for choosing SVM was because it can give high classification accuracy even with few training set examples unlike Artificial Neural Networks (ANN) – a complimentary machine learning technique that require huge labeled dataset for training.

4.6.1 Support Vector Machine

Support Vector Machine (SVM) seeks to find decision boundaries in data set that maximizes the separation distance (margin) between data classes. Figure 4.9 illustrate the concept. The figure shows two classes of data (positive and negative samples) separated by a median line (decision function) whose equation is given by;

$$\boldsymbol{w}^T\boldsymbol{x_i} + b = 0 \qquad (4.21)$$

$\boldsymbol{w}$ is a vector that is perpendicular to the decision function. The data points lying along the gutters are referred to as support vectors. $\boldsymbol{x_i}$ is a feature vector an comprises of a n dimensional column vector whose elements are parameters/features that are ideally unique for a given class. The distance between the gutters is referred as the margin. The decision rule of the classifier can be expressed by the following equations.

$$w^T.x_i + b \geq 1 \quad for\ positive\ samples \tag{4.22a}$$

$$w^T.x_i + b \leq -1 \quad for\ negative\ samples \tag{4.22b}$$

$$w^T.x_i + b = 1 \quad for\ samples\ along\ the\ gutters \tag{4.22c}$$

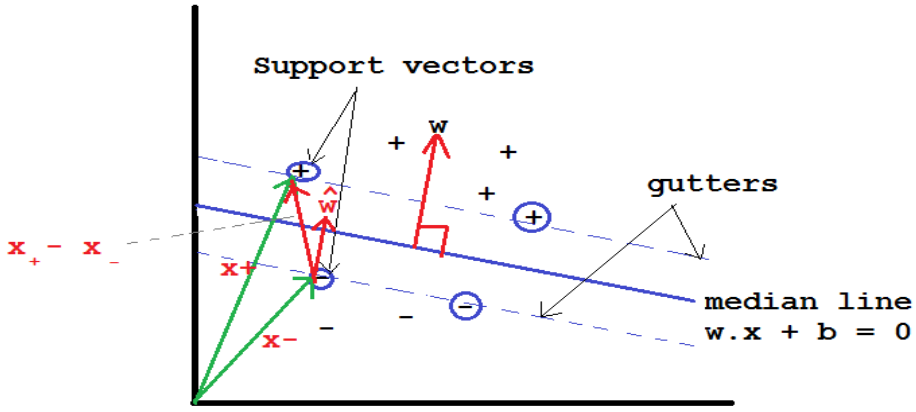

Figure 4.9: Illustration of decision boundary determination in SVM

Superscript T in the equation denotes transpose operation. Lets define an activation function y_i such that

$$y_i = \begin{cases} +1\ for\ posive\ samples \\ -1\ for\ negative\ samples \end{cases} \tag{4.23}$$

Multiplication of the activation function with Equation 4.22 gives

$$y_i(w^T.x_i + b) \geq 1 \quad for\ positive\ and\ negative\ samples \tag{4.24a}$$

$$y_i(w^T.x_i + b) = 1 \quad for\ \ samples\ along\ the\ gutters \tag{4.24b}$$

The width of the margin is give by Equation 4.25, which is the dot product of the difference vector $(\boldsymbol{x}_+ - \boldsymbol{x}_-)$ shown in Figure 4.8 with the unit vector point in the direction of $\boldsymbol{w}$. $\boldsymbol{x}_+$ are the positive samples lying along the gutter while as $\boldsymbol{x}_-$ are the negative samples lying along the gutter.

$$width = (\boldsymbol{x}_+ - \boldsymbol{x}_-) \cdot \frac{\boldsymbol{w}}{\|\boldsymbol{w}\|} \tag{4.25}$$

Simplification of Equation 4.14 gives

$$width = \frac{2\boldsymbol{w}}{\|\boldsymbol{w}\|} \tag{4.26}$$

Maximization of the above function using Lagrange multipliers yields

$$w = \sum \alpha_i y_i x_i \tag{4.27}$$

$$\sum \alpha_i y_i = 0 \tag{4.28}$$

and the Lagrangian that needs to be optimized is given below

$$\mathcal{L} = \sum \alpha_i + \sum_i \sum_j \alpha_i \alpha_j y_i y_j x_i \cdot x_j \tag{4.29}$$

Equation 4.29 is numerically solved to give the values of α_i and α_j which optimizes the Lagrangian. α_i and α_j are the Lagrange multipliers also called supportiveness values and they indicate the contribution of each support vector with regard to the decision function. In the event that data in the two classes is linearly inseparable, non-linear transformations that are functions of the dot

product of input vectors are used instead and this makes it possible to separate the two classes of data by inserting an hyperplane between the data classes. Equation 4.29 then becomes:

$$\mathcal{L} = \sum \alpha_i + \sum_i \sum_j \alpha_i \alpha_j y_i y_j K(x_i \cdot x_j) \quad (4.30)$$

Where K is the non-linear transformation also referred as the kernel. Some of the commonly used kernels are the Radial Basis Function (RBF) given by $e^{-|x_i - x_j|/\sigma}$ and polynomial kernel given by $(x_i \cdot x_j - 1)^n$. Where σ and n are constants.

CHAPTER 5

RESULTS AND DISCUSION

This chapter presents results obtained from implementation of the methodology given in chapter 4. The performance of four variant prototypes of PTIOSM hemozoin sensor namely; the photodiode PTIOSM hemozoin sensor employing optical spectral filtering, the photodiode PTIOSM hemozoin sensor employing computational spectral filtering, the PTIOSM image sensor employing optical spectral filtering, and the PTIOSM image sensor using computational spectral filtering were evaluated. For each setup, validation of the PTIOSM hypothesis as well as determination of the technique's ability in detection of hemozoin in unstained blood samples was evaluated.

5.1 Photodiode PTIOSM hemozoin sensor employing optical spectral filtering

PTIOSM signals of thick blood smear samples were acquired with the EB modulated at 2MHz while the PB intensity was kept constant. After conversion of the acquired PTIOSM signal from time domain to frequency domain and noise filtering of PTIOSM signals, scatter plots for the amplitude spectra belonging to the five *Plasmodium* positive and five *Plasmodium* negative samples were generated. Figure 5.1 shows sample PTIOSM waveforms acquired from the photodiode PTIOSM setup while figure 5.2 gives the plots of the DFT of PTIOSM signals acquired from malaria infected and non infected blood smear samples. From the scatter plots the following observations were made: At some frequency bands of the PTIOSM signal, the *Plasmodium* positive PTIOSM

signals had more spectral energy compared to *Plasmodium* negative PTIOSM signals and therefore it was possible to find a threshold value that differentiated infected samples from the non-infected ones. In the case of the pulsed red light excitation (Figure 5.2 a), 100% classification accuracy of *Plasmodium* positive samples from *Plasmodium* negative samples was possible at frequency band between 1.7 MHz and 1.8 MHz because the signal amplitudes of all infected samples were greater than those of *Plasmodium* negative samples. This means that at this frequency band, the *Plasmodium* parasite detection sensitivity and specificity was 100% (there were no false positives or false negatives). For the PTIOSM signals due to pulsed green light excitation (Figure 5.2b), the best classification accuracy was observed at frequency band between 1.5 MHz and 1.6 MHz. At this frequency band, the signal intensities from all the five *Plasmodium* positive samples were greater than the *Plasmodium* negative signals except for one *Plasmodium* negative sample signal whose amplitude was comparable to those of positive samples. This represents a classification specificity of 100% and sensitivity of 83.3%.

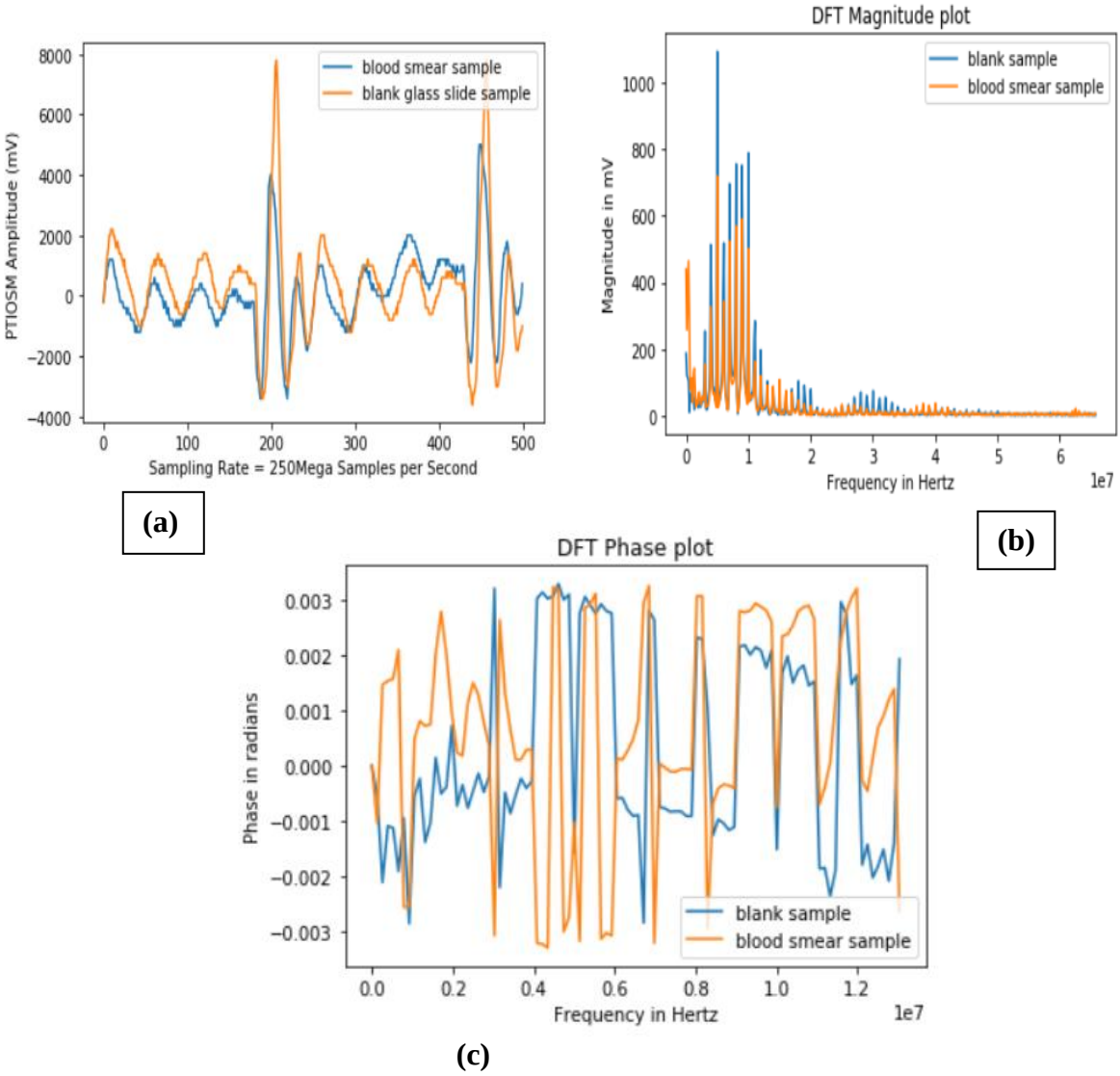

Figure 5.1: Sample PTIOSM Waveforms acquired from the phodiode PTIOSM setup, (a) Oscilloscope waveforms for blood smear and blank glass slide, (b) DFT Magnitude spectra of the sample waveforms (c) Corresponding DFT Phase Spectra

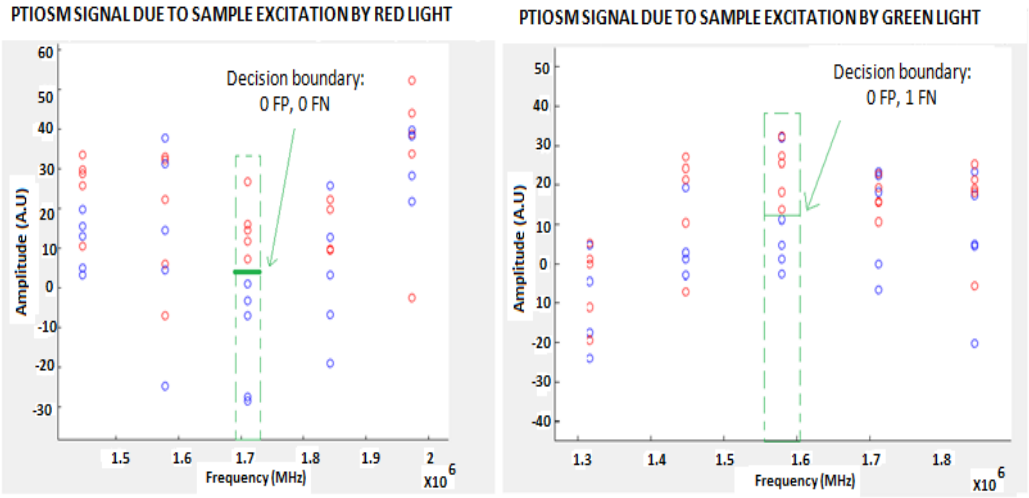

Figure 5.2: Frequency spectra of PTIOSM signal for malaria infected (red circles) and non-infected samples (blue circles). (a) PTIOSM signal due to red light excitation, (b) PTIOSM signal to blue light modulation. FP is false positive samples and FN is false negative samples.

PTIOSM technique ability to correctly classify malaria infected blood smear samples from the non-infected samples can be attributed to two factors; one is the change of hemozoin's refractive index due to absorption of optical energy from the EB which leads to thermal energy raise and subsequently a change in the sample optical properties. The optical absorbers (hemozoin and hemoglobin in this case) act as driven optical oscillators that are pumped by intensity modulated EB. This phenomenon leads to modulation of the PTIOSM signal at frequency band corresponding to it's the resonance frequency of the oscillators. Another possible explanation could be that the excitation beam causes generation of photoacoustic waves, which in turn induces vibration of optical scatterer in the medium leading to modulation of diffuse reflected light from the sample. In this case the chromophores act as a mechanical oscillator whose resonance frequency is dependent on their size

as well as their thermal elastic properties. Variations in the signal intensity from samples having the same infection status (either infected or non-infected) at the resonance frequency can be attributed to variations of the chromophore concentration.

From the observed results, the developed PTIOSM probe has demonstrated excellent capability of malaria diagnosis in blood smear samples. The simple instrumentation involved and its real time operation makes it a suitable candidate for mass screening of the disease in malaria endemic regions. However, further testing using more samples prepared under different conditions (both thin and thick blood smears, stained and non-stained) are required to conclusively determine the techniques sensitivity and specificity. Besides, further experimentation is required to investigate the capability of the probe in quantifying the parasite load (parasitemia) in the samples and the limit of detection of the technique. This work was published and can be found in the following reference (Memeu and Sarroney, 2018). In a previous study by Omucheni *et al.,* (2014) a multispectral microscope was used to image unstained blood smear images. The study reported that using LEDs illumination of wavelengths between 590nm and 700nm it was possible to distinguish malaria infected cells from non-infected cells.

5.1.1 Principal Component Analysis of PTIOSM Signal

PCA is a data dimensionality reduction technique that transforms n dimensional data to m dimensions where m is less than or equal to n. This is achieved by first searching for eigen vectors that maximizes data variance and then projecting the data onto those eigen vectors. The fewer the eigen vector used to project the data, the less the dimensions of the transformed data hence reduction on data size.

Besides dimensionality reduction, data projected onto principal components can reveal hidden structures that can be exploited in classification of different classes of data available. This can be done by visualization of data projected on one, two or three dimensional PCA scatter plots. Higher dimensional clusters can be recognized using computational techniques which measure separation distances from data class mean.

Using PTIOSM signals of whole blood samples mixed with synthentic hemozoin acquired by the photodiode type PTIOSM sensor employing optical spectral filtering, PCA was performed to obtain the eigen vectors and eigen values of the transformed data. Figure 5.3 and Figure 5.4 gives the scree plots of PTIOSM signals for whole blood sample under red and green excitation beams respectively while Figure 5.5 and 5.6 show the whole blood PTIOSM signals projected on the first three principal components.

The objective of performing PCA on PTIOSM signals was to explore the possibility of classifying PTIOSM signals belonging to different classes of samples e.g. hemozoin positive and hemozoin negative blood samples based on the cluster patterns formed. It was observed that hemozoin positive and hemozoin negative PTIOSM signals were distinguishable from the first (PC1) and second (PC2) principal components scatter plots (see Figure 5.5 and Figure 5.6). It was possible to classify samples having different hemozoin concentrations from PC2 and PC3 of the signals acquired following excitation by red light (Figure 5.5(b)). Signals acquired following sample excitation by green light didn’t form distinct

clusters based on their respective hemozoin concentration except for one class of sample (see Figure 5.18(b)). This could be attributed to the fact that hemozoin has a higher optical absorption coefficient in the wavelength band corresponding to red light than in the green region of the visible EM spectrum. Therefore stronger PA signals were induced by red excitation beam.

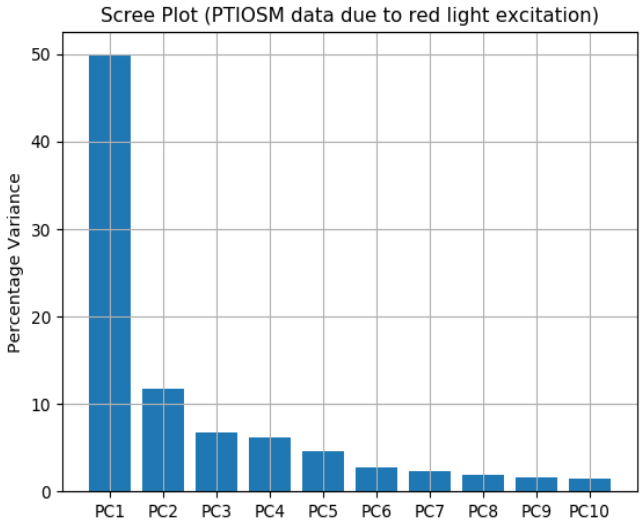

PRINCIPAL COMPONENTS	EIGEN VALUES
1	50
2	11.8
3	6.7
4	6.2
5	4.6
6	2.8
7	2.3
8	1.9
9	1.6
10	1.5

Figure 5.3: Principal Component Analysis scree plot for PTIOSM signal from whole blood samples excited with red light

From the scree plots given in Figure 5.3 and Figure 5.4, it can be seen that the first principal component carries approximately 50% of the signal information. The next five principal components carry about 30% of the remaining signal variance. Collectively, the first ten principal components carry close to 90% of the signal information. This implies that the signal dimensions can be reduced to ten by transforming the raw PTIOSM data to PCA and still maintain significant information about the detected sample features. Omucheni *et al.* (2014) also reported that PCA helped to highlight parasitized regions in microscopic images of unstained blood

smear samples infected by malaria. In a separate study, Schmedes *et al.* (2022) showed that the use of PCA in combination with conditional inference trees had the potential to predict malaria infection status by training the model with molar concentrations of Plasmodium derived antigens obtained from running a blood samples in multi-plexed bead-based assays.

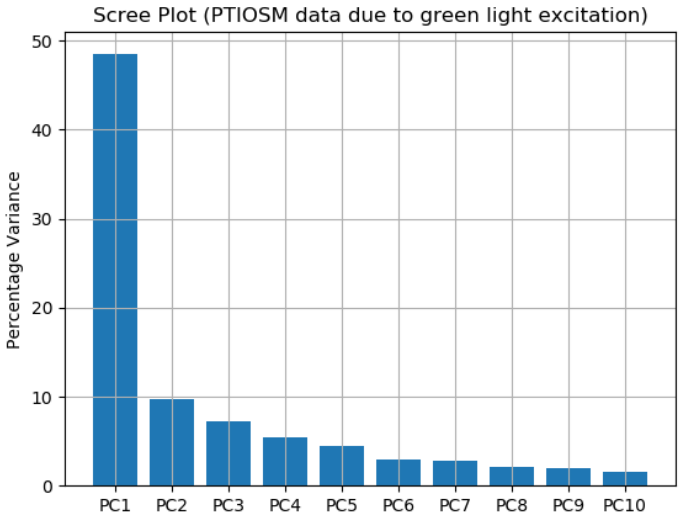

PRINCIPAL COMPONENTS	EIGEN VALUES
1	48.5
2	9.7
3	7.3
4	5.4
5	4.5
6	3
7	2.8
8	2.2
9	2
10	1.6

Figure 5.4: Principal Componen t Analysis scree plot for PTIOSM signal from whole blood samples excited with green light

5.1.2 Clasification of PTIOSM signals using SVM

In order to automate identification of hemozoin positive and hemozoin negative blood samples and categorize different hemozoin concentrations in blood samples, models of SVM were trained and their classification accuracies evaluated. Two SVM models were trained to classify PTIOSM signals into four classes correspoding to hemozoin negative, 0.5g/l hemozoin positive, o.25g/l hemozoin positive and 0.125g/l hemozoin positive blood samples. The training

data for each model was the PCA data from the transformed PTIOSM signals acquired under red and green excitation beams respectively.

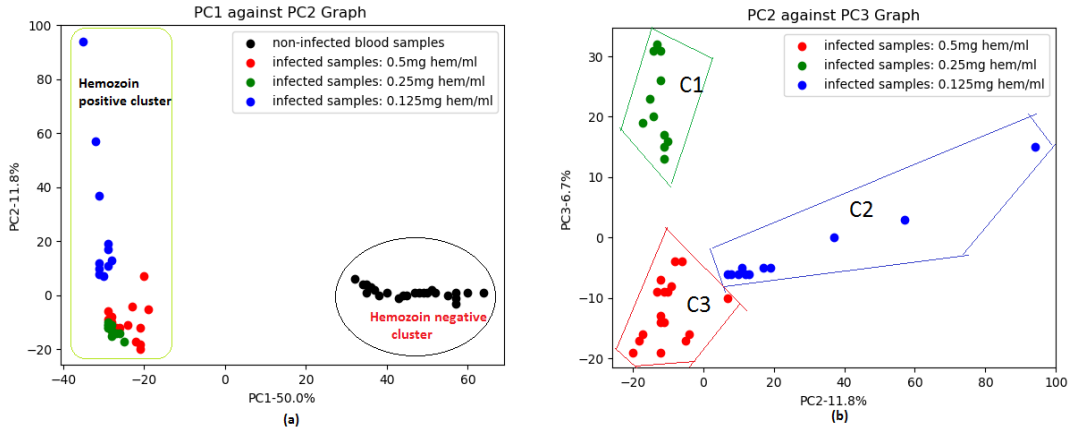

Figure 5.5: Principal Component Analysis projections of PTIOSM data due to red excitation light. (a) PTIOSM signal projected to PC1 and PC2. (b) PTIOSM signal projected to PC2 and PC3.

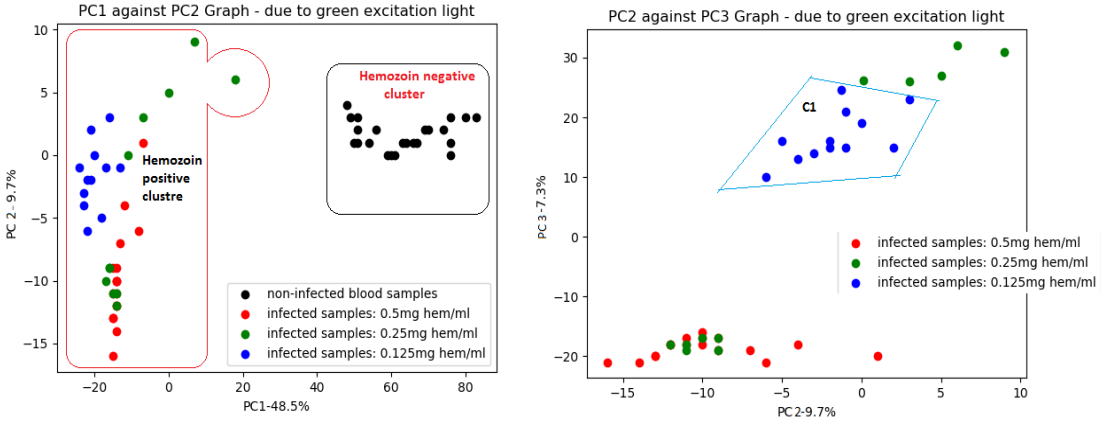

Figure 5.6: Principal Component Analysis projections of PTIOSM data due to green excitation light. (a) PTIOSM signal projected to PC1 and PC2. (b) PTIOSM signal projected to PC2 and PC3.

The feature vectors for training the SVM classifiers were obtained by computation of the dot products of normalized mean centered PTIOSM signals and the first ten PCA eigen vectors. Distinct numerical values corresponding to different sample

classes present in each PTIOSM signal source were used as the target output in the training set. SVM linear kernel provided the best classification accuracy for whole blood samples. Table 5.1 gives parameters and performance of each model trained.

Classification accuracy of 100% was attained for each SVM models trained to classify the four classes of whole blood samples. Whole blood SVM classifiers managed to distinguish hemozoin positive samples from hemozoin negative sample with 100% classification accuracy. In addition the models correctly identified samples having different hemozoin concentration levels. This observation implies that PTIOSM technique and SVM classifier can accurately detect *Plasmodium* infected blood from a patient and determine the parasite load in the blood. It can also be noticed that PTIOSM signals captured under either red or green excitation light were both correctly classified using SVM unlike the case of DFT where PTIOSM signals due to green excitation failed to yield accurate classification results.

5.2 Photodiode PTIOSM hemozoin sensor employing computational spectral filtering

5.2.1 Verification of PTIOSM hypothesis:

A metric referred to as the Modulation Index (MI) defined in Equation 5.1 was used to measure the degree of intensity modulation of the PB when the EB was applied.

$$MI = \frac{PB_{EB}}{PB} \tag{5.1}$$

where; PB_{EB} is the detected intensity of PB when the sample is irradiated by both

the EB and PB while *PB* is the detected intensity of the PB in absence of the EB. Table 5.2 to Table 5.4 gives the values obtained.

The data in the three tables (Table 5.2 to Table 5.4) indicate that different samples when pumped and probed with different optical beam wavelengths yielded different values of modulation index. MI greater than one implies that application of EB (also referred as the pump beam) resulted to enhancement of the detected PB intensity. On the other hand, a value less than one indicate that application of the EB onto the sample resulted to attenuation of detected PB intensity.

Table 5.1: Parameters and performance scores for SVM models used in classification of PTIOSM signals

PTIOSM signal source	**Number of signals used as training set**	**Sample classes present**	**% Acuracy**
Whole blood samples under red excitation light	62	Hemozoin negative, Hemozoin positive (0.5g/l), Hemozoin positive (0.25g/l), Hemozoin positive (0.125g/l)	100%
Whole blood samples under green excitation light	99	Hemozoin negative, Hemozoin positive (0.5g/l), Hemozoin positive (0.25g/l), Hemozoin positive (0.125g/l)	100%

Table 5.2: Probe Blue

Pump Red				Pump Green			
Samples	**M. I**	**Mean**	**SD**	**Samples**	**M. I**	**Mean**	**SD**
+ve 2	126.1	123.6	3.54	+ve 2	125	67.75	80.96
+ve 3	121.1			+ve 3	10.5		
-ve 1	105.6	101.0	6.58	-ve 1	1.42	35.21	47.79
-ve 2	96.3			-ve 2	69		
Blank	2.4			Blank	1.3		

Table 5.3: Probe Green

Pump Blue				Pump Red			
Samples	**M. I**	**Mean**	**SD**	**Samples**	**M. I**	**Mean**	**SD**
+ve 2	0.10	0.19	0.13	+ve 2	0.002	16.00	22.63
+ve 3	0.28			+ve 3	32		
-ve 1	1	157	220.6	-ve 1	1.68	152.34	213.07
-ve 2	313			-ve 2	303		
Blank	0.25			Blank	2.49		

Table 5.4: Probe Red

Pump Blue				Pump Green			
Samples	**M. I**	**Mean**	**SD**	**Samples**	**M. I**	**Mean**	**SD**
+ve 2	134.8	218.2	117.95	+ve 2	134.4	218.2	118.5
+ve 3	301.6			+ve 3	302		
-ve 1	0.21	0.39	0.26	-ve 1	0.40	0.36	0.057
-ve 2	0.57			-ve 2	0.32		
Blank	0.005			Blank	0.003		

Samples comprised of whole blood put on special glass slides containing sample wells with a capacity of 200µL. The slides' well were filled with the samples and covered with the cover slip before signal acquisition. Samples labeled +ve2 and +v3 were confirmed to be malaria positive while samples labeled –ve2 and –v3 were malaria negative. From the recorded results the best performance in classification of different categories of sample signals present was attained when

the sample was probed by blue light and pumped by red right. The values of the MI were distinguishable because the geometric separation distance between mean values for the two classes is greater than the sample variations amongst members of the same class as given by the Standard Deviation (SD) values in the tables. Other combinations of pump probe wavelengths also yielded results that qualify above set criteria but with greater signal variability.

5.3 Image sensor PTIOSM hemozoin setup employing Optical spectral filtering

5.3.1 Verification of PTIOSM Hypothesis

In verification of PTIOSM hypothesis PTIOSM video signals from wet blood smear sample were acquired with and without the Excitation Beam (EB) ON. The video frames were read in sequential order from the raw video clips. After converting the frames to gray scale, mean image intensities were computed per image. The mean intensities formed a time series signal whose FFT was computed. The magnitude and phase of the transformed FD signal were graphed to facilitate visual analysis. Figure 5.6 shows the graph of averaged image intensities in TD for PTIOSM captured images with and without EB. Figure 5.8 and Figure 5.9 give sample magnitude and phase spectra of the FD PTIOSM signals respectively. Table 5.5 gives the mean, standard deviation and range for averaged PTIOSM image intensities with and without the excitation beam. A total of ten samples were analyzed.

Figure 5.7 shows that the intensity of PTIOSM signal acquired when the EB is OFF has got its intensity relatively constant with time whereas the PTIOSM signal acquired when the EB is ON, its intensity fluctuates in time i.e. its intensity is modulated in time. This visual observation is further reinforced by signal metrics

given in Table 5.5 which shows that signal intensity modulation is more pronounce in the case when the EB was ON. Figure 5.8 gives the frequency domain magnitude spectrum of the PTIOSM signal. The figure shows that the magnitude spectra for PTIOSM signal with and without EB are identical. The signals only possess non-zero energy at frequency band 0 Hz. The 0Hz frequency component is due to the detected Probe Beam (PB) light intensity which was kept constant. While the magnitude spectra of the two signals were identical, the phase spectra (as show in Figure 5.9) were different. The modulation of signal intensity in time when EB was applied can be attributed to temporal perturbation of the sample optical properties due to the sample's atomic and molecular dynamics occasioned by the irradiation of the EB beam to the sample.

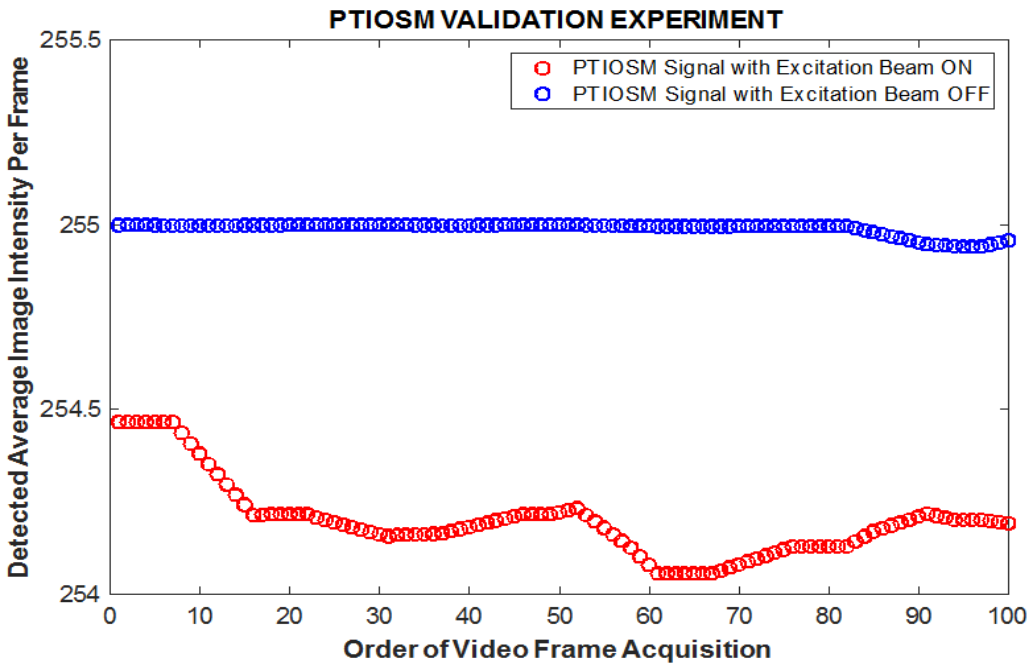

Figure 5.7: Sample time domain PTIOSM signals acquired by the PTIOSM image sensor implementing optical spectral filtering. The blue signal was due to whole blood probed only with the PB while the red signal is due the sample being pumped and probed by the EB and PB simultaneously.

Table 5. 5: Basic statistics for PTIOSM signal of a blood sample captured with an without EB

	MEAN SIGNAL AMPLITUDE	STANDARD DEVIATION	RANGE
ptiosm signal with eb	254.2089	0.1218	0.4087
ptiosm signal without eb	254.9927	0.0169	0.0661

5.3.2 Investigation of PTIOSM image sensor capability in diagnosis of malaria

PTIOSM video signals of sixty blood smear samples were acquired and processed. Forty blood smear samples were confirmed to be malaria positive and twenty were malaria negative using optical microscopy and RDT. The acquired PTIOSM video signals were further clipped into shorter five second versions comprising of 100 frames per video clip. PCA of the first six components of the shorter video clips were computed and the mean of each component evaluated. The means were used as feature vectors for training a SVM classifier and a Logistic Regression classifier for distinguishing malaria infected blood smear samples from non-infected blood smear samples. A total of 4200 feature vector were used in training and testing of the classifiers.

Out of the total 4200 features used, 2000 were from malaria negative samples while 2200 were from malaria positive samples. Table 5.6 shows the first gives five and the last five feature vectors and targets used. The training and testing set data were split into 80% to 20% ratio respectively.

Table 5.7 and Figure 5.10 give the performance of the two classifiers. The linear regression classifier attained an overall accuracy of 64.0% while the SVM classifier attained an accuracy of 70.6%. These values were computed by taking the percentage of total number correct predictions by the classifier to the overall predictions made. Sensitivity and specificity are two other metrics used in evaluating the effectiveness of a medical diagnostic technique. The former gives the probability that the actual outcome of a diagnosis is positive given that the prediction is positive while the later gives the probability of the actual outcome of a diagnosis being negative given the prediction of the technique is negative. For the Logistic regression classifier, the sensitivity and specificity obtained were 64.7% and 63.7% respectively. In the case of SVM classifier 68.4% and 72.9% sensitivity and specificity respectively were achieved. A total of 840 feature vectors were used for testing the two classifiers. Figure 5.9 gives the Receiver Operating Characteristic (ROC) curves for the two classifiers. These curves are generated by comparing the rate of true positives to the rate of false positives. An ideal classifier or diagnostic technique should have the Area Under

the Curve (AUC) of the ROC equal to one. In that case, both the sensitivity and specificity equal 100%. In practice rarely is the AUC of the ROC equal to one. However, a good classifier or disease diagnostic method should have its AUC close to one. In the case of the two PTIOSM classifiers, SMV classifier had AUC equal to 0.707 and logistic regression classifier had its ROC with AUC equal to 0.622.

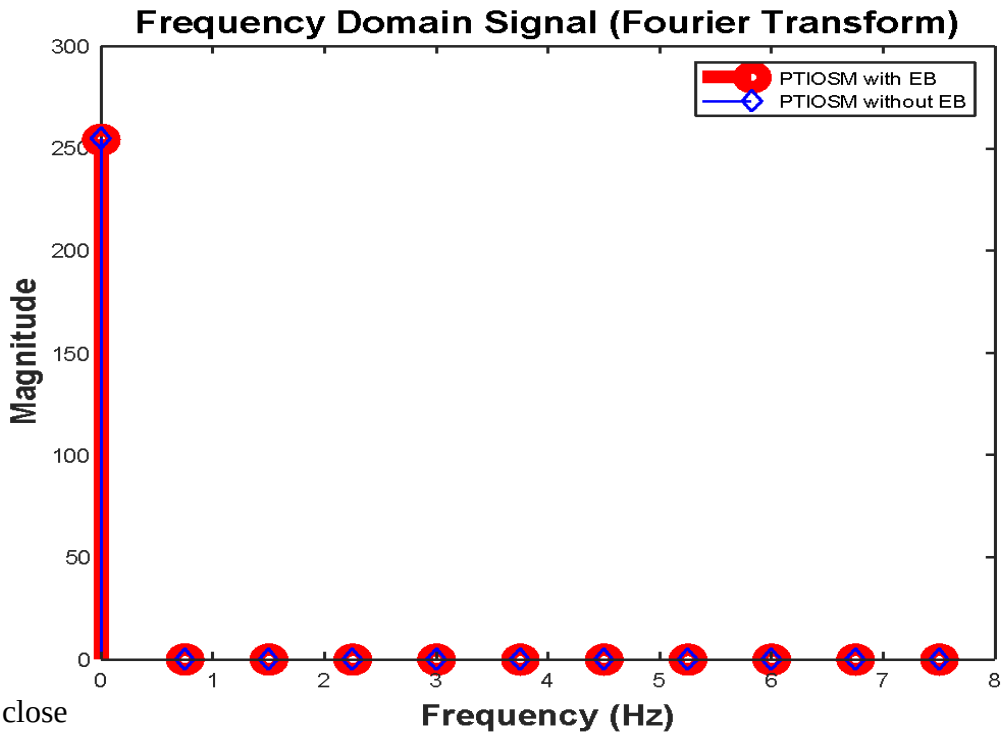

Figure 5.8: Sample frequency domain PTIOSM magnitude spectra computed after raw PTIOSM video was acquired using the PTIOSM image sensor implementing optical spectral filtering. The blue signal was due to whole blood probed only with the PB while the red signal is due the sample being pumped and probed by the EB and PB simultaneously.

A classification accuracy of 70.6% and 64.0% attained by the two classifiers is a modest achievement given that PTIOSM is a frontier topic whose application in malaria diagnostics has not been previously reported. The relatively large size of the dataset used for training and testing the classifiers helped to minimize chances of over-fitting of classifiers' parameters. However, there exists ample room for improvement of the system performance through optimization of both

the hardware design and feature vector selection criteria. Specifically, there is need to explore the optimal PB and EB wavelengths and optical power that would cause maximum modulation of the PB signal during probing of malaria blood samples. The sample volume, blood smear quality, and sample positioning in the PTIOSM sample stage also need to be standardized. The performance of the classifier using other feature vectors besides the principal component images of the acquired PTIOSM video signals ought to be investigated.

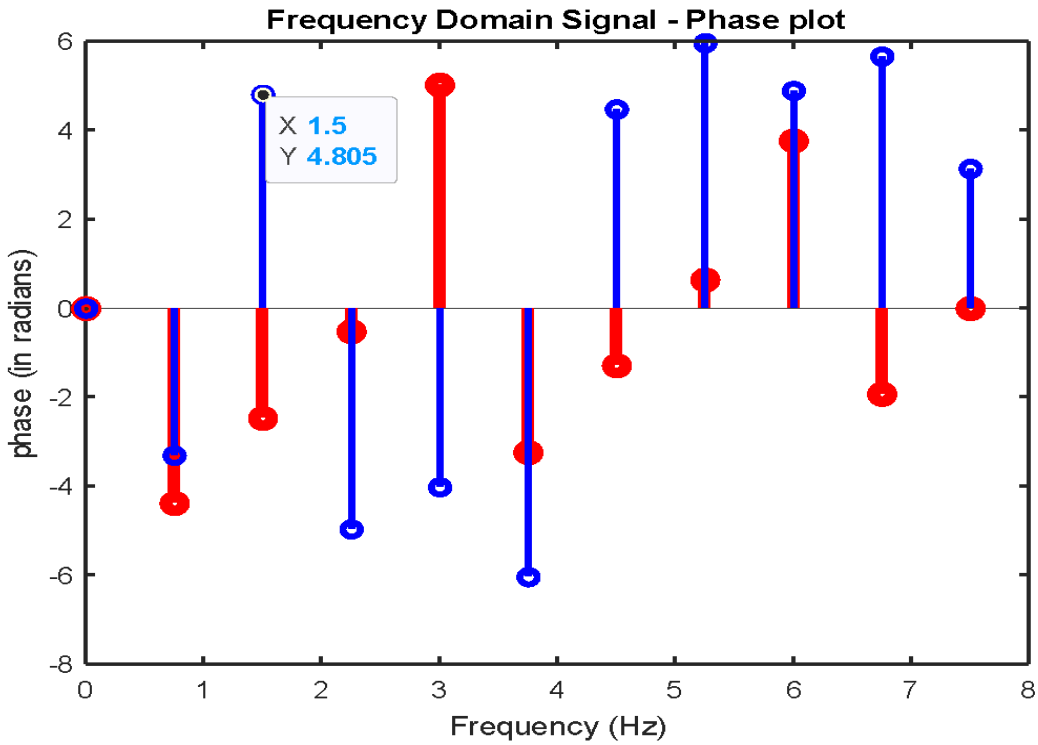

Figure 5.9: Sample frequency domain PTIOSM phase spectra computed after raw PTIOSM video was acquired using the PTIOSM image sensor implementing optical spectral filtering. The blue signal was due to whole blood probed only with the PB while the red signal is due the sample being pumped and probed by the EB and PB simultaneously.

Table 5.6: Sample feature vectors used for training PTIOSM video signal classifiers to perform malaria diagnosis

```
df.head()
```

Python command for displaying the 1st five lows of the dataset

	PC1	PC2	PC3	PC4	PC5	PC6	STATUS
0	-6.410000e-14	-2.770000e-14	-3.350000e-15	1.080000e-13	-4.070000e-15	2.430000e-14	1
1	-3.780000e-14	-1.340000e-14	3.920000e-15	1.080000e-13	-1.520000e-14	2.490000e-14	1
2	-3.870000e-14	-6.870000e-15	-4.300000e-15	1.100000e-13	-3.170000e-14	2.410000e-14	1
3	-3.210000e-14	-1.320000e-14	-3.080000e-15	1.090000e-13	-5.220000e-14	2.650000e-14	1
4	-3.430000e-14	-1.130000e-14	-1.610000e-14	8.900000e-14	-6.660000e-14	2.650000e-14	1

```
[ ] df.tail()
```

Python command for displaying the last five lows of the dataset

	PC1	PC2	PC3	PC4	PC5	PC6	STATUS
4195	-4.180000e-15	1.050000e-14	4.210000e-14	1.970000e-14	-2.620000e-14	2.350000e-14	0
4196	-5.630000e-15	1.770000e-14	3.640000e-14	1.790000e-14	-3.640000e-14	2.030000e-14	0
4197	-6.440000e-15	1.740000e-14	1.960000e-14	-3.540000e-14	3.840000e-14	2.040000e-14	0
4198	-4.980000e-15	2.180000e-14	1.460000e-14	-2.930000e-14	2.730000e-14	2.180000e-14	0
4199	-5.580000e-15	2.150000e-14	6.930000e-15	2.980000e-14	2.340000e-14	2.100000e-14	0

Table 5.7: Performance Metrics of SVM and Logistic Regression Classifier trained to detect malaria infection using PTIOSM video signals

Classifier	Number of True Positives	Number of True Negatives	Number of False Positives	Number of False Negative	Sensitivity (%)	Specificity (%)	Accuracy (%)
SVM	294	299	111	136	68.4	72.9	70.6
Logistic Regression	247	291	167	135	64.7	63.5	64.0

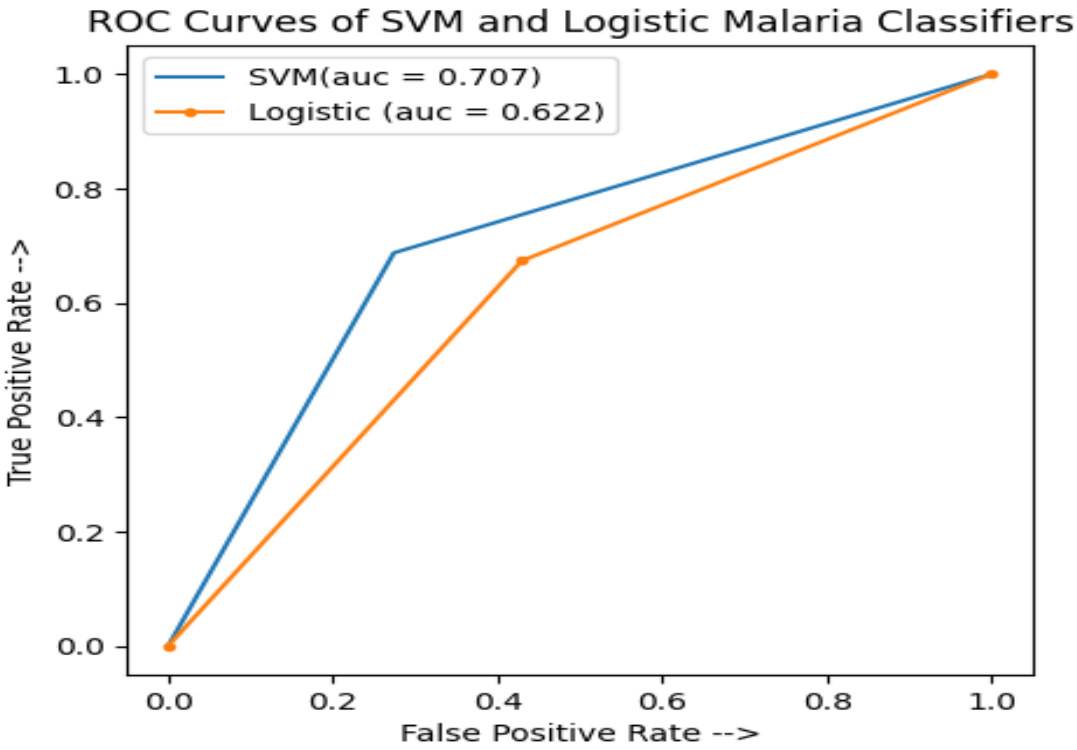

Figure 5.10: Receiver Operating Characteristic (ROC) Curve for SVM and Logistic Regression classifiers

Pervious studies have ultilized SVM in automatic detection of *Plasmodium* parasites in images acquired from malaria blood. Dharpal and Malviya, (2018) reported malaria detection sensitivity and specificity of 97% and 98% respectively after training a SVM binary classifier with textural and color features extracted from malaria blood smear images. The modest SVM detection accuracy reported in the current study indicates that PTIOSM technique holds potential for probing the presence of biomarkers such as hemozoin in the blood and other biological samples.

5.4 Image sensor PTIOSM hemozoin setup employing computational spectral filtering

Unstained thin and thick blood smear samples were loaded in a modified OFM and ten minute videos of the samples captured by the microscope camera with the optical source being PB light

modulated at a frequency of 2Hz. In addition, another set of blood smear videos were captured with the optical source being the modulated PB and a constant intensity EB. Both 625nm (red) and 525nm (green) wavelengths were used as the EB light while 465nm (blue) was used as the PB light. The videos were converted to gray scale and a time axis FFT performed. The FD video frame (image reconstructed at the 2Hz frequency) corresponding to the PB modulation frequency was extracted for visualization and further processing.

Figure 5.11 shows reconstructed 2Hz magnitude spectra images for unstained thick blood smear samples acquired using the modified OFM. The images were reconstructed by performing FFT of the raw microscope video in the time axis and extracting the image spectrum corresponding to the PB modulation frequency. The images were obtained from blood sample of malaria infected subject. Figure 5.11 (a) is the reconstructed PTIOSM image obtained when a thick smear sample was irradiated by PB and red EB light. Figure 5.11 (b) shows image of the same sample under PB and green EB. Figure 5.11 (c) gives a zoomed in view of figure 5.11 (b) which illustrates a feature that resembles the morphology of *Plasmodium* parasite at ring stage. Figure 5.11 (d) is the binary image obtained by manually choosing pixel threshold value that separates the parasite region from the image background.

From MI images shown in Figure 5.11, Plasmodium parasite sites are visible. For instance, images in panel (a) and (b) acquired from sample excitation by red and green EB show Plasmodium parasite at ring stage. The ring structure is clearly visible from the zoomed in image in panel (c) and the binary image in panel (d). The binary image was obtained by choosing a threshold value that separates the image background from the foreground which is the parasite region.

Figure 5.12 is the reconstructed images of the thin blood smear sample obtained from a malaria infected human subject. Figure 5.12 (a) gives the reconstructed image obtained when the sample was illuminated by PB light only. Figure 5.12(b) and (c) show reconstructed images of the same sample under PB + red EB and PB + green EB light respectively. Figure 5.12 (d) and (e) are zoomed images of Figure (a) and (b) showing parasite regions. Figure 5.12 (f) is a binary image obtained by thresholding the extinction coefficient image. Extinction coefficient image was computed by implementing equation 4.9 in the methodology chapter.

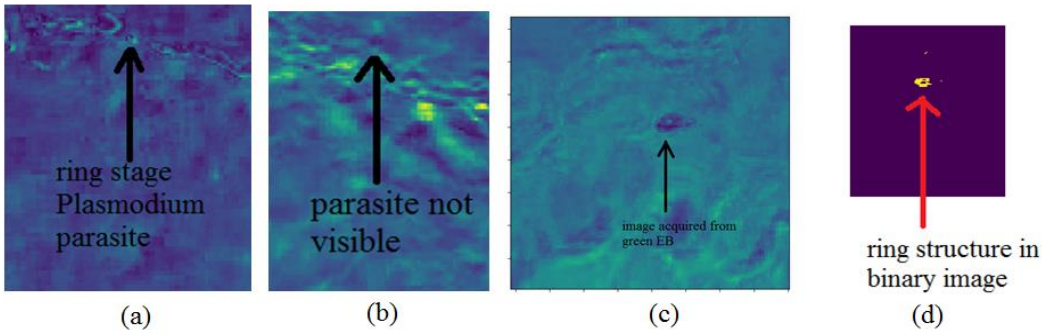

Figure 5.11: reconstructed PTIOSM magnitude images of malaria infected thick blood smear sample. Panel (a) gives the reconstructed PTIOSM image when the sample was under the red EB wavelength, panel (b) is the image of the same sample under green EB, panel (c) is the zoomed in image of panel (a), and panel (d) shows a binary image obtained after pixel value thresholding the image at panel (c).

From Figure 5.12 it can be seen that application of PB and EB enhances the parasite features in the image as can be seen in panel (b) and (c). The images show that the presence of EB visually enhanced the ring structure of the *Plasmodium* parasite. The zoomed image of the PTIOSM image acquired by application of both PB and EB shows both the parasite ring and the two chromatin dot of the parasite. These parasite features are not clear from PB image as can be seen in the zoomed in image of Figure 5.12 (d). Thresholding of the extinction coefficient change ratio image also yielded the parasitized areas in the PTIOSM. Figure 5.13 gives a surface plot image and averaged line plot of the extinction coefficient change ratio image. The figure gives the pixel intensity map or distribution of the extinction coefficient change ratio. It indicates parasite region in the image have got distinct pixel intensity values from areas with non parasitized red blood cells. Specifically, the extinction coefficient change ratio image show that parasite region have significantly higher absolute values in comparison to non-parasitized regions.

Chen *et al*. (2020) reported successful implemtation of Transient Absorption (TA) spectroscopy in imaging β-hematin (a synthetic analog of hemozoin) as well as the natural hemozoin in unstained *Plasmodium* infected erythrocytes. The TA technique involves irradiatiating the sample with two (pump and probe) optical beams. Pump beam light is obtained from a femtosecond pulsed laser while as the probe beam can be sourced from a continous wave laser. The two interacts with the sample and the emergent probe beam is detected and analysed in time domain to elucidate the transient absorption behavior of the sample as result of application of the pump beam. The setup includes bulky and costly pulsed laser and ultrafast signal

acquisition instruments. This makes the technique unsuitable for use in point-of-care centers for malaria screening. PTIOSM imaging technique on the otherhand has demonstrated compared imaging capability as TA imaging but ultilizing very simple instrumentation hence lendering it a low cost alternative for malaria disease diagnosis in resource scarce settings.

5.5 Discussion of the results

In this work, a novel optical pump probe technique for malaria diagnosis termed as PTIOSM malaria sensor was developed and tested. Among the salient features of the technique are; the use of freshly prepared unstained blood smear samples which shortens the diagnostic time, minimal operational skills, simple and compact instrumentation involved in fabrication of the hardware that comprises of use of RGB LED instead of lasers for provision of EB and PB light sources, ability to detect malaria parasites and estimate the parasite load. The technique's ability to be incorporated in optical microscopes and perform PTIOSM microscopy was also demonstrated. The method is expected to find direct application in malaria disease screening. The setup can be optimized to be portable and battery powered to facilitate in-field mass screening of malaria. The PTIOSM probe also has potential for non-invasive screening of malaria if its detection geometry is adjusted from transmission mode to reflection mode. In order to translate the PTIOSM probe from its current proof of concept stage to a clinical gadget used for routine malaria diagnosis, the following three recommendations ought to be considered; One is the need to increase the

technique's diagnostic sensitivity and specificity. This can be one through optimization of the optical wavelengths and power used in the PB and EB with a view of enhancing signal contrast between malaria positive and malaria negative blood samples. Closely connected to the first point is the need to incorporate a technique for ensuring the EB intensity is of uniform intensity. The second recommendation is need for development of a PTIOSM microscope setup with automatic sample scanning feature as well as ability to perform automated image analysis.

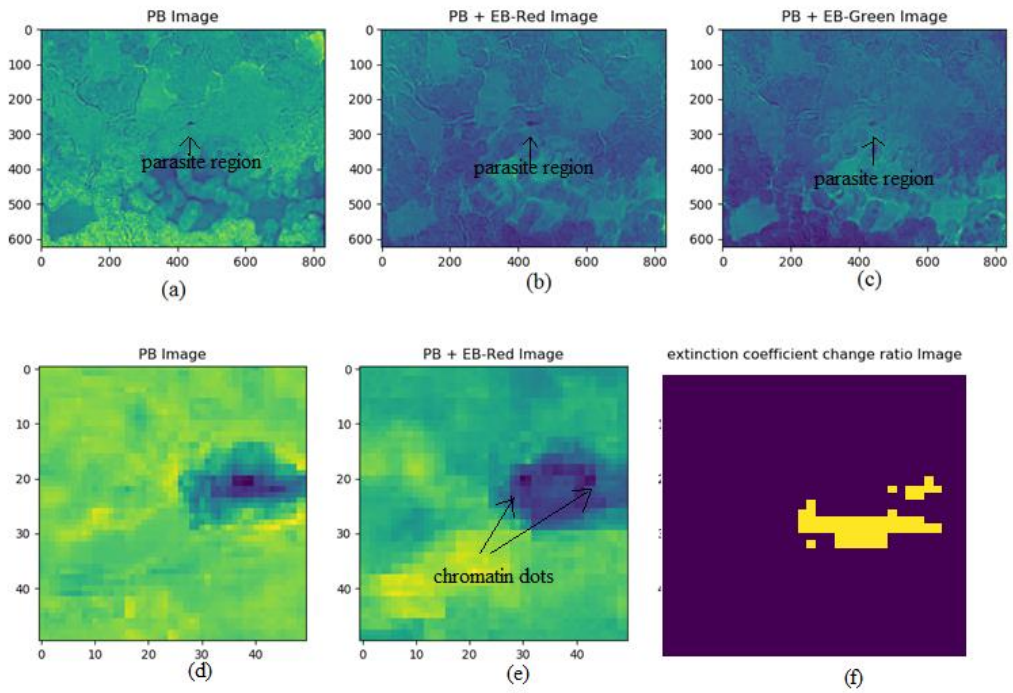

Figure 5.12: Reconstructed frequency domain PTIOSM magnitude images of thin blood smear samples. Panel (a – c) show images acquired under different PB and EB wavelength. Panels (d) and (e) show zoomed in images from panel (a) and (b) respectively. Panel (f) show a binary image obtained from thresholding the extinction coefficient change ratio image.

In order to facilitate non-invasive detection of *Plasmodium* parasites in human subjects, the probe need to be re-designed to change its detection geometry from transmission mode (where the optical sources and optical detector are in opposite sides of the sample) to reflection mode (where the optical source and detector are in the same side with respect to the sample being probed). The probe can then be attached either at the finger tip or the ear lobe for signal acquisition.

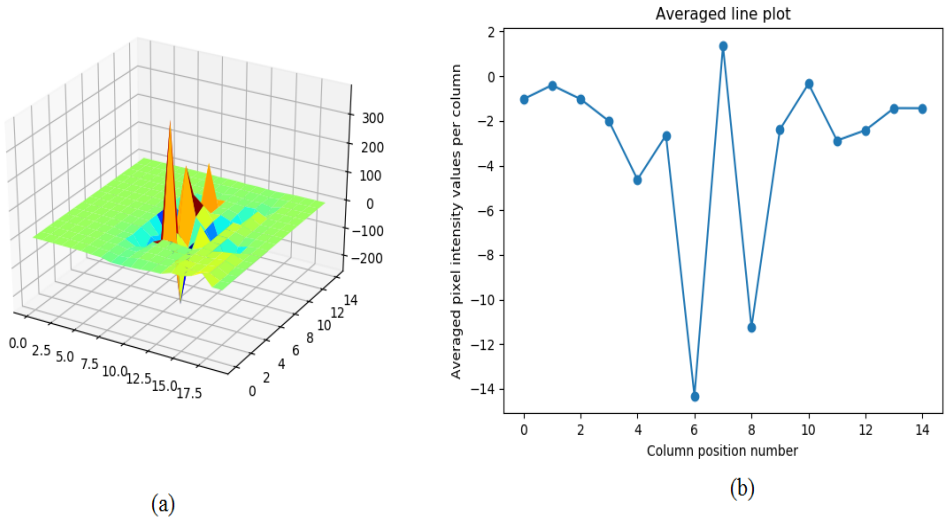

Figure 5.13: Surface plot of the extinction coefficient image. Panel (a) is a 3D surface plot showing the intensity values of different parasite image sites. Panel (b) show a line scan chosen in the middle part of the image.

CHAPTER 6

CONCLUSIONS

This work was aimed at developing a novel optical technique termed as Photothermal Induced Optical Scattering Modulation (PTIOSM) and testing its utility in detection of the presence of hemozoin (an endogenous malaria biomarker) in unstained blood samples. First, an analytical model was developed showing how an optical beam (probe beam) traversing throught a light absorbing sample results in its intensity being modulated due to absorption of a secondary optical beam (the pump beam) by the sample. The model also describes a parameter referred as the extinction coefficient change ratio can distinguish different molecule species present in a light absorbing sample. Extinction coefficient change ration can be experimentally determined by measuring the transmitted intensities of the probe beam when the sample is illuminated by two different pump beam wavelengths (I_2 and I_3) as well as probe beam intensity when no pump beam is applied (I_1) and then implementing the following mathematical expression: $\ln\left(\frac{I_2}{I_1}\right) / \ln\left(\frac{I_3}{I_1}\right)$. Four different versions of PTIOSM prototypes were designed and fabricated to experimentally verify the phenomenon and test the viability of the technique in detection of hemozoin in blood samples. Signals acquired by the four prototypes showed modulation of probe beam intensity upon application of the pump beam. The prototypes also exhibited potential of accurately detecting the presence of hemozoin in blood. The photodiode type PTIOSM probes yielded hemozoin detection accuracy of 100% for samples spiked with synthetic hemozoin. By applying PCA on signals acquired by the probes, it was possible to identify varying levels of hemozoin

concentration present in the samples. Malaria diagnosis from blood smear samples was performed using an image sensor PTIOSM probe. This yielded a detection accurary of 71% with disease detection sensitivity of 68% and specificity of 73%. Mophological features of *Plasmodium* parasites in unstained blood smear images were visualized by computing the extinction coefficient change ratio images.

Following the findings of this study the following two recommendations for future work are made. First, there is need to conduct more elaborate studies comparing simulation results obtained from implementation of PTIOSM model and the experimental values. This can be done by first measuring the change in optical absorption coeffient following application of different pump beam wavelengths. The obtained values could then be substituted in PTIOSM equations to compute the extinction coefficient change ratios. The values can then be compared with the experimental measured values.

Secondary, there is need to explore the possibility of employing PTIOSM technique as a variant of optical spectroscopic technique. The experiment could entail investigating the dependencies of optical extinction change ratio and modation of optical absorption coefficient with changing pump beam wavelengths for different chromophores of known chemical species.

REFERENCES

Allen, T. J., and Beard, P. C. (2007). *Dual wavelength laser diode excitation source for 2D photoacoustic imaging* (A. A. Oraevsky and L. V. Wang, Eds.; p. 64371U). https://doi.org/10.1117/12.698651

Allen, T. J., and Beard, P. C. (2013). *Light emitting diodes as an excitation source for biomedical photoacoustics* (A. A. Oraevsky and L. V. Wang, Eds.; p. 85811F). https://doi.org/10.1117/12.2004471

Baker, K. (2005). Singular value decomposition tutorial. *The Ohio State University*, *24*.

Bannister, L. H., and Sherman, I. W. (2009). *Plasmodium*. In John Wiley and Sons, Ltd (Ed.), *Encyclopedia of Life Sciences*. John Wiley and Sons, Ltd. http://doi.wiley.com/10.1002/9780470015902.a0001970.pub2

Berry, A., Benoit-Vical, F., Fabre, R., Cassaing, S., and Magnaval, J. F. (2008). PCR-based methods to the diagnosis of imported malaria. *Parasite*, *15*(3), 484–488. https://doi.org/10.1051/parasite/2008153484

Cai, C., Carey, K. A., Nedosekin, D. A., Menyaev, Y. A., Sarimollaoglu, M., Galanzha, E. I., Stumhofer, J. S., and Zharov, V. P. (2016a). In vivo photoacoustic flow cytometry for early malaria diagnosis. *Cytometry Part A*, *89*(6), 531–542.

Cai, C., Carey, K. A., Nedosekin, D. A., Menyaev, Y. A., Sarimollaoglu, M., Galanzha, E. I., Stumhofer, J. S., and Zharov, V. P. (2016b). In vivo photoacoustic flow cytometry for early malaria diagnosis: Photoacoustic Flow Cytometry for Malaria Diagnosis. *Cytometry Part A*, *89*(6), 531–542. https://doi.org/10.1002/cyto.a.22854

Chen, Andy J., Kai-Chih Huang, Selina Bopp, Robert Summers, Puting Dong, Yimin Huang, Cheng Zong, Dyann Wirth, and Ji-Xin Cheng. Quantitative imaging of intraerythrocytic hemozoin by transient absorption microscopy, Journal of Biomedical Optics 25, no. 1 (2020): 014507-014507.

Collins, J. T., Knapper, J., Stirling, J., Mduda, J., Mkindi, C., Mayagaya, V., Mwakajinga, G. A., Nyakyi, P. T., Sanga, V. L., and Carbery, D. (2020). Robotic microscopy for everyone: The OpenFlexure microscope. *Biomedical Optics Express*, *11*(5), 2447–2460.

Cooley, J. W., Lewis, P. A., and Welch, P. D. (1967). Historical notes on the fast Fourier transform. *Proceedings of the IEEE*, *55*(10), 1675–1677.

Cox-Singh, J., Davis, T. M., Lee, K.-S., Shamsul, S. S., Matusop, A., Ratnam, S., Rahman, H. A., Conway, D. J., and Singh, B. (2008). Plasmodium knowlesi malaria in humans is widely distributed and potentially life threatening. *Clinical Infectious Diseases*, *46*(2), 165–171.

Daoudi, K., van den Berg, P. J., Rabot, O., Kohl, A., Tisserand, S., Brands, P., and Steenbergen, W. (2014). Handheld probe integrating laser diode and ultrasound transducer array for ultrasound/photoacoustic dual modality imaging. *Optics Express*, *22*(21), 26365. https://doi.org/10.1364/OE.22.026365.

Davidson, M.S., Andradi-Brown, C., Yahiya, S., Chmielewski, J., O'Donnell, A.J., Gurung, P., Jeninga, M.D., Prommana, P., Andrew, D.W., Petter, M. and Uthaipibull, C., 2021. Automated detection and staging of malaria parasites from cytological smears using convolutional neural networks. *Biological imaging*, *1*, p.e2.

Deán-Ben, X. L., and Razansky, D. (2013). Functional optoacoustic human angiography with handheld video rate three dimensional scanner. *Photoacoustics*, *1*(3–4), 68–73. https://doi.org/10.1016/j.pacs.2013.10.002.

Dharpal, S. N. and Malviya, A.V. (2018). Automated Enumeration of Malaria Parasite Using SVM Classifier, IJRTI Volume 3 Issue 10, ISSN: 2456-3315

Dima, A., and Ntziachristos, V. (2012). Non-invasive carotid imaging using optoacoustic tomography. *Optics Express*, *20*(22), 25044–25057.

Escalante, A. A., Barrio, E., and Ayala, F. J. (1995). Evolutionary origin of human and primate malarias: Evidence from the circumsporozoite protein gene. *Molecular Biology and Evolution*, *12*(4), 616–626.

Fan, Y., Mandelis, A., Spirou, G., and Vitkin, A. (2004). Development of a laser photothermoacoustic frequency-swept system for subsurface imaging: Theory and experiment. *The Journal of the Acoustical Society of America*, *116*(6), 3523–3533. https://doi.org/10.1121/1.1819393.

Franko, M. (2001). Recent applications of thermal lens spectrometry in food analysis and environmental research. *Talanta*, *54*(1), 1–13.

Galanzha, E., and Zharov, V. (2013). Circulating Tumor Cell Detection and Capture by Photoacoustic Flow Cytometry in Vivo and ex Vivo. *Cancers*, *5*(4), 1691–1738. https://doi.org/10.3390/cancers5041691.

Garnham, P. C. C. (1966). Malaria parasites and other haemosporidia. *Malaria Parasites and Other Haemosporidia.*

Goldsby, R., Kindt, T., and Osborne, B. (2000). *Kuby Immunology 4th Edition. W. H.*

Jacques, S. L. (2013). Optical properties of biological tissues: A review. *Physics in Medicine and Biology*, *58*(11), R37.

Joel T. Collins, Joe Knapper, Julian Stirling, Joram Mduda, Catherine Mkindi, Valeriana Mayagaya, Grace A. Mwakajinga, Paul T. Nyakyi, Valerian L. Sanga, Dave Carbery, Leah White, Sara Dale, Zhen Jieh Lim, Jeremy J. Baumberg, Pietro Cicuta, Samuel McDermott, Boyko Vodenicharski, and Richard Bowman, "Robotic microscopy for everyone: the OpenFlexure microscope," Biomed. Opt. Express 11, 2447-2460 (2020).

Kantele, A., and Jokiranta, T. S. (2011). Review of Cases With the Emerging Fifth Human Malaria Parasite, Plasmodium knowlesi. *Clinical Infectious Diseases*, *52*(11), 1356–1362. https://doi.org/10.1093/cid/cir180.

Knapper, J., Collins, J. T., Stirling, J., McDermott, S., Wadsworth, W., and Bowman, R. W. (2022). Fast, high-precision autofocus on a motorised microscope: Automating blood sample imaging on the OpenFlexure Microscope. *Journal of Microscopy*, *285*(1), 29-39.

Kolkman, R. G. M., Steenbergen, W., and van Leeuwen, T. G. (2006). In vivo photoacoustic imaging of blood vessels with a pulsed laser diode. *Lasers in Medical Science*, *21*(3), 134–139. https://doi.org/10.1007/s10103-006-0384-z.

Kuniyil Ajith Singh, M., Steenbergen, W., and Manohar, S. (2016). Handheld Probe-Based Dual Mode Ultrasound/Photoacoustics for Biomedical Imaging. In M. Olivo and U. S. Dinish (Eds.), *Frontiers in Biophotonics for Translational Medicine* (Vol. 3, pp. 209–247). Springer Singapore. https://doi.org/10.1007/978-981-287-627-0_7.

Lawrence, C., and Olson, J. A. (1986). Birefringent hemozoin identifies malaria. *American Journal of Clinical Pathology*, *86*(3), 360–363.

Lukianova-Hleb, E., Bezek, S., Szigeti, R., Khodarev, A., Kelley, T., Hurrell, A., Berba, M., Kumar, N., D'Alessandro, U., and Lapotko, D. (2015). Transdermal Diagnosis of Malaria Using Vapor Nanobubbles. *Emerging Infectious Diseases*, *21*(7), 1122–1127. https://doi.org/10.3201/eid2107.150089.

Lukianova-Hleb, E. Y., Campbell, K. M., Constantinou, P. E., Braam, J., Olson, J. S., Ware, R. E., Sullivan, D. J., and Lapotko, D. O. (2014). Hemozoin-generated vapor nanobubbles for transdermal reagent- and needle-free detection of malaria. *Proceedings of the National Academy of Sciences*, *111*(3), 900–905. https://doi.org/10.1073/pnas.1316253111.

Makler, M. T., Palmer, C. J., and Ager, A. L. (1998). A review of practical techniques for the diagnosis of malaria. *Annals of Tropical Medicine and Parasitology*, *92*(4), 419–433.

Maslov, K., and Wang, L. V. (2008). Photoacoustic imaging of biological tissue with intensity-modulated continuous-wave laser. *Journal of Biomedical Optics*, *13*(2), 024006. https://doi.org/10.1117/1.2904965

Memeu, D. M., Kaduki, K. A., Mjomba, A. C. K., Muriuki, N. S., and Gitonga, L. (2013). Detection of plasmodium parasites from images of thin blood smears. *Open Journal of Clinical Diagnostics*, *03*(04), 183–194. https://doi.org/10.4236/ojcd.2013.34034.

Memeu, D. M., and Sarroney, M. A. (2018). *Photo-Thermal Induced Optical Scattering Modulation Sensor for Malaria Diagnosis*.

Mendelow, B. V., Lyons, C., Nhlangothi, P., Tana, M., Munster, M., Wypkema, E., Liebowitz, L., Marshall, L., Scott, S., and Coetzer, T. L. (1999). Automated malaria detection by depolarization of laser light. *British Journal of Haematology*, *104*(3), 499–503.

Newman, D. M., Heptinstall, J., Matelon, R. J., Savage, L., Wears, M. L., Beddow, J., Cox, M., Schallig, H. D. F. H., and Mens, P. F. (2008). A Magneto-Optic Route toward the In Vivo Diagnosis of Malaria: Preliminary Results and Preclinical Trial Data. *Biophysical Journal*, *95*(2), 994–1000. https://doi.org/10.1529/biophysj.107.128140.

Oliveira, M. F., Kycia, S. W., Gomez, A., Kosar, A. J., Bohle, D. S., Hempelmann, E., Menezes, D., Vannier-Santos, M. A., Oliveira, P. L., and Ferreira, S. T. (2005). Structural and morphological characterization of hemozoin produced by *Schistosoma mansoni* and *Rhodnius prolixus*. *FEBS Letters*, *579*(27), 6010–6016. https://doi.org/10.1016/j.febslet.2005.09.035.

Prahl, S. A. (1989). *A Monte Carlo model of light propagation in tissue*. *10305*, 1030509.

Pramanik, M., and Wang, L. V. (2009). Thermoacoustic and photoacoustic sensing of temperature. *Journal of Biomedical Optics*, *14*(5), 054024.

Richards-Kortum, R., and Sevick-Muraca, E. (1996). Quantitative optical spectroscopy for tissue diagnosis. *Annual Review of Physical Chemistry*, *47*(1), 555–606.

Saha, R. K., Karmakar, S., and Roy, M. (2012). Computational Investigation on the Photoacoustics of Malaria Infected Red Blood Cells. *PLoS ONE*, *7*(12), e51774. https://doi.org/10.1371/journal.pone.0051774

Samson, E. B., Goldschmidt, B. S., Whiteside, P. J., Sudduth, A. S., Custer, J. R., Beerntsen, B., and Viator, J. A. (2012). Photoacoustic spectroscopy of β-hematin. *Journal of Optics*, *14*(6), 065302.

Schmedes, S. E., Dimbu, R. P., Steinhardt, L., Lemoine, J. F., Chang, M. A., Plucinski, M., and Rogier, E. (2022). Predicting Plasmodium falciparum infection status in blood using a multiplexed bead-based antigen detection assay and machine learning approaches. *Plos one*, *17*(9), e0275096.

Sell, J. (2012). *Photothermal investigations of solids and fluids*. Elsevier.

Sergey, A. T., and Andreas, M. (2006). Fourier-domain biophotoacoustic subsurface depth selective amplitude and phase imaging of turbid phantoms and biological tissue. *Journal of Biomedical Optics*, *11*(4), 1083–3668. https://doi.org/0.1117/1.2337290

Shapiro, H. M., and Perlmutter, N. G. (2008). Killer applications: Toward affordable rapid cell-based diagnostics for malaria and tuberculosis. *Cytometry Part B: Clinical Cytometry: The Journal of the International Society for Analytical Cytology*, *74*(S1), S152–S164.

Slater, A. F., Swiggard, W. J., Orton, B. R., Flitter, W. D., Goldberg, D. E., Cerami, A., and Henderson, G. B. (1991). An iron-carboxylate bond links the heme units of malaria pigment. *Proceedings of the National Academy of Sciences*, *88*(2), 325–329.

Tuchin, V. V. (2011). *Advanced optical flow cytometry: Methods and disease diagnoses*. John Wiley and Sons.

Tuchin, V. V., and Tuchin, V. (2007). *Tissue optics: Light scattering methods and instruments for medical diagnosis*.

Wang, L., Maslov, K., and Wang, L. V. (2013). Single-cell label-free photoacoustic flowoxigraphy in vivo. *Proceedings of the National Academy of Sciences*, *110*(15), 5759–5764. https://doi.org/10.1073/pnas.1215578110

Wang, L. V., and Hu, S. (2012). Photoacoustic Tomography: In Vivo Imaging from Organelles to Organs. *Science*, *335*(6075), 1458–1462. https://doi.org/10.1126/science.1216210

Wang, L. V., and Wu, H. (2007). *Biomedical Optics: Principles and Imaging*. John Wiley and Sons.

Wang, T., Nandy, S., Salehi, H. S., Kumavor, P. D., and Zhu, Q. (2014). A low-cost photoacoustic microscopy system with a laser diode excitation. *Biomedical Optics Express*, *5*(9), 3053. https://doi.org/10.1364/BOE.5.003053.

Wang, X., Xie, X., Ku, G., Wang, L. V., and Stoica, G. (2006). Noninvasive imaging of hemoglobin concentration and oxygenation in the rat brain using high-resolution photoacoustic tomography. *Journal of Biomedical Optics*, *11*(2), 024015. https://doi.org/10.1117/1.2192804.

Winkler, A. M., Maslov, K., and Wang, L. V. (2013). Towards single molecule detection using photoacoustic microscopy. *SPIE BiOS*, 85811A-85811A. http://proceedings.spiedigitallibrary.org/proceeding.aspx?articleid=1660845.

Wongsrichanalai, C., Barcus, M. J., Muth, S., Sutamihardja, A., and Wernsdorfer, W. H. (2007). A review of malaria diagnostic tools: Microscopy and rapid diagnostic test (RDT). *The American Journal of Tropical Medicine and Hygiene*, *77*(6 Suppl), 119–127.

Word Health Organization. (2003). *The Africa malaria report 2003*. http://ihi.eprints.org/503/.

World Health Organization. (2015). *World Malaria Report 2015*.

Xia, J., Yao, J., and Wang, L. V. (2014). Photoacoustic tomography: Principles and advances. *Electromagnetic Waves (Cambridge, Mass.)*, *147*, 1.

Yang, X., Maurudis, A., Gamelin, J., Aguirre, A., Zhu, Q., and Wang, L. V. (2009). Photoacoustic tomography of small animal brain with a curved array transducer. *Journal of Biomedical Optics*, *14*(5), 054007. https://doi.org/10.1117/1.3227035.

Yao, J., and Wang, L. V. (2014). Sensitivity of photoacoustic microscopy. *Photoacoustics*, *2*(2), 87–101. https://doi.org/10.1016/j.pacs.2014.04.002.

Yu, C.-H. (2014). Application of Parseval's theorem on evaluating some definite integrals. *Turkish Journal of Analysis and Number Theory*, *2*(1), 1–5.

Zhang, H. F., Maslov, K., Stoica, G., and Wang, L. V. (2006). Functional photoacoustic microscopy for high-resolution and noninvasive in vivo imaging. *Nature Biotechnology*, *24*(7), 848–851. https://doi.org/10.1038/nbt1220.

Zhou, Y., Li, G., Zhu, L., Li, C., Cornelius, L. A., and Wang, L. V. (2015). Handheld photoacoustic probe to detect both melanoma depth and volume at high speed *in vivo*. *Journal of Biophotonics*, *8*(11–12), 961–967. https://doi.org/10.1002/jbio.201400143

APPENDICES

Appendix A1: Matlab code for PTIOSM Video Preprocessing

```
% Script performs image preprocessing of photothermal blood images

%Read Video
Vid=VideoReader('C:\Users\DANIEL\Documents\Oscilloscope_2\photothe
rmal\video\24aug2020\whole blood\wholeblood.wmv');

%Take the first hundred frames
f_1_100 = read(vid,[1 100]);

%select the blue channel
f_1_100_blue = f_1_100(:,:,3,:);

%crop sub-images of the blue channel
f_blue = f_1_100_blue(360-25:360+25,640-25:640+25,:,:);

%Display the cropped region
imshow(f_blue(:,:,:,1))

%Reshape the 100 frame video to 2D matrix
X = reshape(f_blue,size(f_blue,1)*size(f_blue,2),100);
X = double(X);

%Compute the principal eigen vectors
coeff = pca(X);

%Mean center the data
X= X - mean(X);

%Project the reshaped data onto the eigen vectors
Itransformed = X*coeff;

%compute mean of PCs
mean_pca_data = mean(Itransformed);

%Transform the projected data to images and display
Ipc1 = reshape(Itransformed(:,1),size(f_blue,1),size(f_blue,2));
figure, imshow(Ipc1,[]);
Ipc2 = reshape(Itransformed(:,2),size(f_blue,1),size(f_blue,2));
Ipc3 = reshape(Itransformed(:,3),size(f_blue,1),size(f_blue,2));
figure, imshow(Ipc2,[]);
figure, imshow(Ipc3,[]);
figure, scatter(mean_pca_data(:,1),mean_pca_data(:,2))
```

Appendix A2: Matlab Code for computing basic statistical metrics for PTIOSM videos

```
function vid_stats = vidstats(url,url2)

% Script performs image preprocessing of photothermal blood images

%Read Video
vid = VideoReader(url);
vid_stats = zeros(15,5);
%pca_mean(:,4)= 6.5;
for xx = 1:100
    %Take the first hundred frames
    f_1_100 = read(vid,[xx 8+xx]);

    %select the blue channel
    f_1_100_blue = f_1_100(:,:,3,:);

    %crop sub-images of the blue channel
    f_blue = f_1_100_blue(360-25:360+25,640-25:640+25,:,:);

    %Display the cropped region
    %imshow(f_blue(:,:,:,1))

    %Reshape the 100 frame video to 2D matrix
    %X = zeros(size(f_blue,1)*size(f_blue,2),100);
    X = reshape(f_blue,size(f_blue,1)*size(f_blue,2),9);
    X = double(X);
     %Compute the mean of the captured frames
    X_mean = mean(X);

    %compute FFT using a separate user defined matlab function
computefft

    [S, Mag1, Phase1, f] = computefft(X_mean); % where Mag1 is the
returned signal magnitudes,
    % Phase1 is the returned signal phase
    %Compute the average of the computed means
    X_average = mean(X_mean);

    %Compute the standard deviation of the computed means
    X_std = std(X_mean);
     %Compute the range in the computed means
    X_max = max(X_mean);
    X_min = min(X_mean);
    X_range = X_max - X_min;
    vid_stats(xx,:) = [X_average,X_std,X_range,
max(Mag1),max(Phase1)];
    display(xx)
end
csvwrite(url2,vid_stats);
```

Appendix A3: Matlab Code for computing Fourier Transform of the PTIOSM signals

```
function [S, Mag1, Phase1, f] = computefft(s_t)
%computefft(s_t,T) is a function to com
%pute fft of a signal
%s_t is the time domain signal
%T is the sampling period
%p1 is the magnitude of the frequency components
%f is the frequencies
fs = 15;
S = fft(s_t);
L= length(s_t);
Mag2 = abs(S)./L;
Mag1 = Mag2(1:L/2+1);
Mag1(2:end-1) = 2*Mag1(2:end-1);
f = fs*(0:(L/2))/L;

Phase2 = angle(S);
Phase1 = Phase2(1:L/2+1);
Phase1(2:end-1) = 2*Phase1(2:end-1);
```

Appendix A4: Python Code for Developing and testing a SVM Malaria Classifier

```
import numpy as np

import matplotlib.pyplot as plt

import pandas as pd

from sklearn.decomposition import PCA

from sklearn import preprocessing
```

Choose Files No file chosen Upload widget is only available when the cell has been executed in

the current browser session. Please rerun this cell to enable.

```
Saving malaria data.csv to malaria data.csv

from google.colab import files

data_to_load = files.upload()

import io

df = pd.read_csv(io.BytesIO(data_to_load['malaria data.csv']))

df.head()

df.tail()

train_x1 = np.asanyarray(df[['PC1']])

train_x2 = np.asanyarray(df[['PC2']])

train_x3 = np.asanyarray(df[['PC3']])

train_x4 = np.asanyarray(df[['PC4']])

train_x5 = np.asanyarray(df[['PC5']])

train_x6 = np.asanyarray(df[['PC6']])


train_y = np.asanyarray(df[['STATUS']])

train_x1.shape

features = np.zeros([4200,6])
```

```
features[:,0] = train_x1.T

features[:,1] = train_x2.T

features[:,2] = train_x3.T

features[:,3] = train_x4.T

features[:,4] = train_x5.T

features[:,5] = train_x6.T

tagets = np.asanyarray(df[['STATUS']])

from sklearn.model_selection import train_test_split

x_train,x_test,y_train,y_test =
train_test_split(features,tagets,test_size = 0.2)

from sklearn.preprocessing import StandardScaler

Sc_x = StandardScaler()

x_train = Sc_x.fit_transform(x_train)

x_test = Sc_x.transform(x_test)

from sklearn.svm import SVC

model = SVC(kernel='rbf')

model.fit(x_train,y_train)

model.score(x_test,y_test)

#from sklearn.preprocessing import StandardScaler
```



```
#Sc_x = StandardScaler()

#x_train = Sc_x.fit_transform(x_train)

#x_test = Sc_x.transform(x_test)

y_pred = model.predict(x_test)

from sklearn.metrics import roc_curve, auc
```

```
fpr, tpr, threshold = roc_curve(y_test,y_pred)

auc = auc(fpr,tpr)

plt.plot(fpr,tpr)

auc

from sklearn.linear_model import LogisticRegression

model_logistic = LogisticRegression()

model_logistic.fit(x_train, y_train)
```

10/8/2020 SVM_MalariaClassifier - Colaboratory

https://colab.research.google.com/drive/1eJ0K5WSmjtOK7dPABfAJImM4F0V8ae_t#printMode=true 4/7

```
#y_pred_logistic = model_logistic.decision_function(x_test)

y_pred_logistic = model_logistic.predict(x_test)

model_logistic.score(x_test,y_test)

logifpr, logitpr, threshold = roc_curve(y_test,y_pred_logistic)

from sklearn.metrics import roc_curve, auc

logiauc = auc(logifpr,logitpr)

logiauc

plt.plot(logifpr,logitpr)

from sklearn.metrics import confusion_matrix

con_mat_logistic = confusion_matrix(y_test,y_pred_logistic)

t f i t i ( t t d)
```

10/8/2020 SVM_MalariaClassifier - Colaboratory

https://colab.research.google.com/drive/1eJ0K5WSmjtOK7dPABfAJImM4F0V8ae_t#printMode=true 5/7

```
con_mat_svm = confusion_matrix(y_test,y_pred)

con_mat_svm

con_mat_logistic

sensitivity_logistic =
con_mat_logistic[0,0]/(con_mat_logistic[0,0]+con_mat_logistic[1,0])
```

```
sensitivity_svm =
con_mat_svm[0,0]/(con_mat_svm[0,0]+con_mat_svm[1,0])

print(sensitivity_logistic)

print(sensitivity_svm)

specificity_logistic =
con_mat_logistic[1,1]/(con_mat_logistic[1,1]+con_mat_logistic[0,1])

specificity_svm =
con_mat_svm[1,1]/(con_mat_svm[1,1]+con_mat_svm[0,1])

print("specificity_logistic")

print(specificity_logistic)

print("specificity_SVM")

print(specificity_svm)

logistic_fpr, logistic_tpr, threshold = roc_curve(y_test,
y_pred_logistic)

auc_logistic = auc(logistic_fpr,logistic_tpr)

svm_fpr,svm_tpr,threshold = roc_curve(y_test,y_pred)

auc_svm = auc(svm_fpr,svm_tpr)

plt.figure(figsize=(5,5), dpi = 100)

plt.plot(svm_fpr,svm_tpr,linestyle = '-',label='SVM(auc = %0.3f)'%
auc_svm)

plt.plot(logistic_fpr,logistic_tpr,marker = '.',label='Logistic (auc
= %0.3f)'% auc_logistic)
```



```
p p ( g _ p , g _ p , , g ( ) _ g )

plt.xlabel('False Positive Rate -->')

plt.ylabel('True Positive Rate -->')

plt.legend()
```

```
plt.title("ROC Curves of SVM and Logistic Malaria Classifiers")

plt.show()

plt.plot(svm_fpr,svm_tpr,linestyle = '-',label='SVM(auc = %0.3f)'%
auc_svm)

plt.plot(logistic_fpr,logistic_tpr,marker = '.',label='Logistic (auc
= %0.3f)'% auc_logistic)

plt.plot(svm_fpr,svm_tpr,'or')

plt.plot(logistic_fpr,logistic_tpr,'or')
```

Appendix A5: Python Code for Developing and testing a SVM Anemia Classifier

```
import numpy as np
import matplotlib.pyplot as plt
import pandas as pd
from sklearn.decomposition import PCA
from sklearn import preprocessing
```

Choose Files No file chosen Upload widget is only available when the cell has been executed in

the current browser session. Please rerun this cell to enable.

```
Saving anemia-status.csv to anemia-status.csv
from google.colab import files
data_to_load = files.upload()
import io
df = pd.read_csv(io.BytesIO(data_to_load['anemia-status.csv']))
```

	PCA1	PCA2	PCA3	HBM	STATUS
0	5.560000e-15	3.490000e-15	6.720000e-15	12.8	1
1	-5.560000e-15	2.850000e-15	3.430000e-15	12.8	1
2	7.650000e-15	-5.650000e-15	4.160000e-15	12.8	1
3	1.720000e-14	-1.210000e-14	2.720000e-15	12.8	1
4	4.610000e-15	-8.870000e-15	2.690000e-15	12.8	1

```
df.head()
train_x1 = np.asanyarray(df[['PCA1']])
train_x2 = np.asanyarray(df[['PCA2']])
train_x3 = np.asanyarray(df[['PCA3']])
```

```
train_y = np.asanyarray(df[['STATUS']])

train_x1.shape

features = np.zeros([135,3])

features[:,0] = train_x1.T

features[:,1] = train_x2.T

features[:,2] = train_x3.T

tagets = np.asanyarray(df[['STATUS']])
```



```
from sklearn.model_selection import train_test_split

x_train,x_test,y_train,y_test =

train_test_split(features,tagets,test_size = 0.2)

from sklearn.svm import SVC

model = SVC(kernel='rbf')

model.fit(x_train,y_train)

model.score(x_test,y_test)
```

Appendix A6: Published papers from this thesis

Open Journal of Biophysics, 2018, 8, 185-193

http://www.scirp.org/journal/ojbiphy

ISSN Online: 2164-5396

ISSN Print: 2164-5388

A.6.1 Photo-Thermal Induced Optical Scattering Modulation Sensor for Malaria Diagnosis

Daniel Maitethia Memeu[1,2], Merenga Abdallah Sarroney[2], Ciira Maina[3]

[1]Department of Physical Sciences, Meru University of Science and Technology, Meru, Kenya

[2]Department of Physics, Kenyatta University, Nairobi, Kenya

[3]Dedan Kimathi University of Technology, Nyeri, Kenya

Email: danielmaitethia@gmail.com

https://doi.org/10.4236/ojbiphy.2018.84014

How to cite this paper: Memeu, D.M., Sarroney, M.A. and Maina, C. (2018) Photo-Thermal Induced Optical Scattering Modulation Sensor for Malaria Diagnosis. *Open Journal of Biophysics*, **8**, 185-193.

Received: April 27, 2018

Accepted: September 10, 2018

Published: September 13, 2018

Abstract

Malaria is one of the leading killer diseases in sub-Saharan Africa. Although the disease is curable, early and accurate diagnosis is key to effective therapy. Existing malaria diagnostic techniques have low detection accuracy especially when the parasite load in the blood is low. In this paper, we report on a sim-ple photo-thermal based technique for detection of the *Plasmodium* parasites' biomarker (hemozoin) in blood smear samples. The technique has demon-strated 100% *Plasmodium* detection sensitivity and specificity from the ten blood smear test samples used.

Keywords

Photothermal Induced Optical Scattering Modulation, Photoacoustic Probing, Hemozoin, Hemoglobin, Probe Beam, Excitation Beam

Introduction

Malaria Background

Malaria is a tropical disease that has been a leading cause of deaths in sub-Saharan Africa with children below five years being the most affected. Ac-cording to World Health Organization (WHO) 2015 malaria report, the disease caused about 0.5 million deaths globally and infected approximately 200 million people during the reported period [1]. The disease is caused by a protozoan pa-rasite of the geneus *Plasmodia*. There are five species of *Plasmodia* that infect humans namely; *Plasmodium falciparum*, *Plasmodium vivax*, *Plasmodium ovale*, *Plasmodium malariae*, and *Plasmodium knowlesi*. The parasites are transmitted from infected to non-infected persons through a bite by female

anopheles mosquito. Once the parasites have been launched into the blood stream, they are transported to the liver for incubation [2]. Upon maturity the parasites are released to the blood stream where they attack red blood cells (erythrocytes), feeding on hemoglobin and depositing a by-product known as hemozoin. Hemozoin is an insoluble iron compound. The compound has been reported to possess nano-rod structure and strongly absorbs optical radiation [3]. Hemozoin therefore can serve as *Plasmodium* parasite biomarker in blood.

Early and accurate diagnosis of the malaria is key to effective treatment of the disease. However existing malaria diagnostic technique such as optical micro-scopy (which is the gold standard method) and *Plasmodium* parasites antigen detection assays also known as Rapid Diagnostic Techniques (RDTs) lack high detection sensitivity and specificity [2], [4]. Both methods are invasive with opt-ical microscopy also being a time consuming process. Therefore, there is an ur-gent need for development of a rapid malaria diagnostic technique with capabil-ity of non-invasive operation.

Limited studies have been reported on development of non-invasive tech-niques for malaria diagnosis [5]-[11]. The trend from the reported literature points towards use of photothermal related techniques for probing hemozoin presence in infected erythrocytes flowing through blood vessels beneath the skin surface. Photoacoustic flow cytometry has been the most preferred option [2],

[9] [10] [11]. This is because photoacoustic detection techniques boast from a number of desirable features which include; high detection sensitivity due to high optical absorption contrast in absorbing molecules. Besides, the emitted acoustic signal is less immune to scattering as and therefore can form high reso-lution images as compared to purely optical imaging technique such as Diffuse Optical Tomography (DOT) [12], [13]. Third, optically bulk tissue can be probed in reflection mode where both the optical source and the detector can be situated on the same side of the probed sample [14] [15] [16] [17]. Other exist-ing photo-thermal based techniques such as thermal lens effect [18] are consi-dered not suitable for *in vivo* probing of hemozoin since they require use of thin transparent samples (small volumes) and forward mode detection (where the optical sources is in the opposite side of the detector with respect to the sample). These requirements render the techniques unsuitable for *in vivo* probing of hu-man tissue—because of its bulkiness and the strong optical scattering involved.

Figure 1 (obtained from reference [19]) **gives** the schematic diagrams of pho-toacoustic flow cytometry and thermal lensing. PBDBEB is the diameter of the probe beam of a thermal lens setup before application of the excitation beam to the sample. PBDAEB is the diameter (divergence) of the probe beam after the application of the excitation beam. Thermal lens effect causes broadening of the probe beam and change of its intensity after the sample has been irradiated by the excitation beam. This is because when the sample absorbs

optical energy from the excitation beam the energy is converted to heat and temporary con-fined within the illuminated region of the absorber. This causes perturbation of

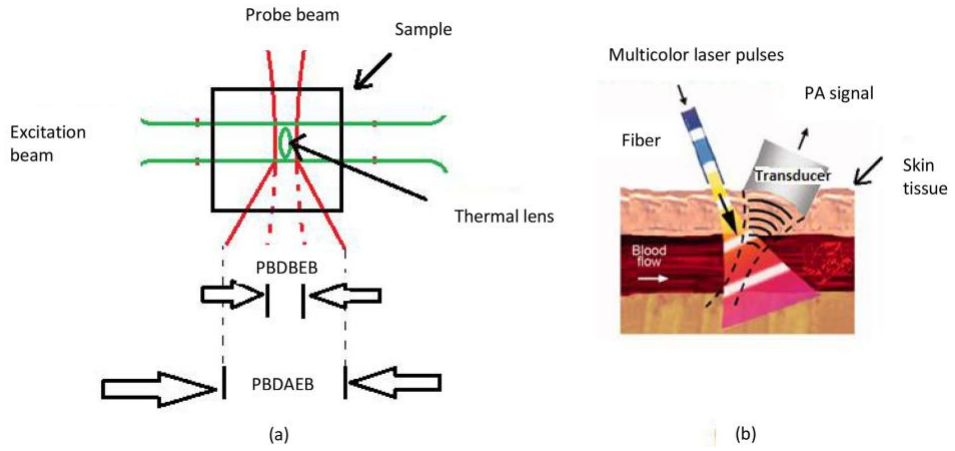

Figure 1. Configurations of thermal lensing and photoacoustic flow cytometry. (a) Perpendicular geometry of thermal lens setup [19], thermal lens effect; (b) photoacoustic flow cytometry, PA flow cytometry.

the absorber's intrinsic optical properties (specifically the refractive index) from the equilibrium (steady) state which in turn causes divergence and change of in-tensity of the probe beam.

The reported photoacoustic based malaria diagnostic technique on the other hand suffers from a number of limitations which has hampered its clinical adop-tion. One major challenge has been the problem of wide inter- and in-tra-variability of detected PA signals. Detected acoustic signals also suffer from low SNR due to acoustic attenuation before the signal reaches the transducer. The conversion efficiency from optical energy to acoustic energy in tissue (wa-ter) is also significantly low due to the low value of Gruneisten parameter for water which is estimated to be 0.2 [20]. This requires use of sophisticated hard-ware to suppress the noise and amplify the detected signal and this makes the setup complex, bulky and expensive.

In this paper, we report development of a novel technique termed as Photo-thermal Induced Optical Scattering Modulation (PTIOSM) for detection of he-mozoin in malaria infected blood. The technique is premised on the fact that photon absorption by chromophores is followed by a relaxation session where the absorber's molecules move from excited state to ground state. If the relaxa-tion process is non-radiative, the absorbed optical energy is released in form of heat. The emitted heat energy takes some time before it diffuses away from where it is deposited (Thermal conferment time). During this phase, the

intrin-sic optical properties such as the absorber's refractive index and its optical ab-sorption coefficient are temporarily modified.

In the case of PTIOSM technique, modulation in the probe beam signal is de-tected in the reflection (backward) mode instead of transmission (forward) mode as is the case for thermal lens deflection. Modulation intensity with respect to optical excitation wavelength is expected to carry information on the compo-sition as well as the concentration on chromophores in the probed sample.

= Materials and Methods

2.1. PTIOSM Set-Up

A common anode, 3 W - 9 W RGB Light Emitting Diode (LED) (product ID 2524, from Adafruit Industries, USA [21]) was used as the optical source for providing both the Probe Beam (PB) and the Excitation Beam (EB). The PB was produced by forward biasing the blue LED segment with a constant 350 mA current to generate blue light whose peak wavelength was 465 nm. The EB beam was produced by driving the red and green LED segments with 1 MHz square pulses having 40 nS pulse width. The input signal for driving the LED segments was from a DDS function generator (KKmoon 40 MHz Function Signal Gene-rator Dual-channel DDS Arbitrary Waveform Pulse Signal Generator 1 Hz - 100 MHz Frequency Meter) that was coupled to a custom made RGB LED driver circuit. **Figure 2** gives the block diagram of the setup. Both the red and green LED segments were overdriven with 2 A forward current during the ON period of the driving waveform in order to produce sufficient optical intensity for gen-eration of PTIOSM signal.

Light from the RGB LED (PB and EB) irradiated samples (stained blood smear slides) and the transmitted light passed through an optical filter (Omega Optical, Inc. 450 nm SP (450 SP) RapidEdge 25 mm Optical Shortpass Filter) that blocked the EB (the red and green pulsed light) but transmitted the probe beam (the blue light) after interacting with the photo-thermally excited sample. A photodiode and trans-impedance amplifier module (OPT101) was used to detect light from the filter and the generated photodiode current was converted to a voltage signal and then pre-amplified using an inbuilt trans-impedance am-plifier in the module. To boost the bandwidth of the detected signal, a 100 ohms resistor was externally connected to the trans-impedance module (between pin 2 and 5 while pin 4 was left unconnected) to provide the negative feedback instead of using the inbuilt 1 MΩ resistor that

offers a limited bandwidth of 12 KHz [22]. The output of the trans-impedance amplifier was coupled to a digital oscil-loscope (OWON SDS1052, 2 channel, 500 MS/s, 10 KB recording length) for di-gitization. The digitized signal was then loaded to a computer for signal processing. Matlab R2015b software was used for processing the acquired PTIOSM signals. **Figure 3** gives the algorithmic steps used for signal processing.

2.2. Signal Pre-Processing

The aim of this stage was to reduce or possibly eliminate the noise riding in the acquired PTIOSM signal. There were two possible main sources of noise in the acquired signals; the radiative pick-up noise from adjacent switching equipment such as the function generator, and the background (stray) light detected by the photodiode. Noise correction was performed by coherently subtracting the PTIOSM signal due to a blank glass slide (also termed as the reference sample) from a PTIOSM signal obtained from a stained blood smear sample. The resul-tant differential signal was free of existing common mode noise.

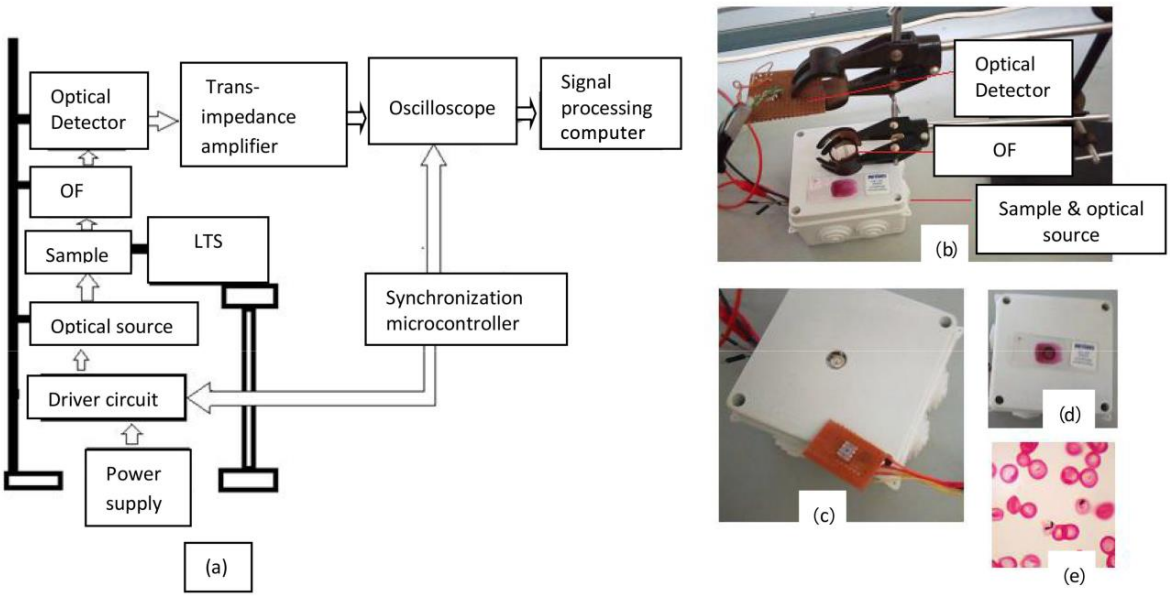

Figure 2. Setup diagram of the PTIOSM probe for malaria diagnosis, (a) setup block diagram: OF (optical Filter), LTS (Linear translational stage); (b) photo of the setup showing optical source, sample, optical filter and photodiode circuit; (c) Optical source and detector; (d) blood smear sample; (e) microscopic view of the sample.

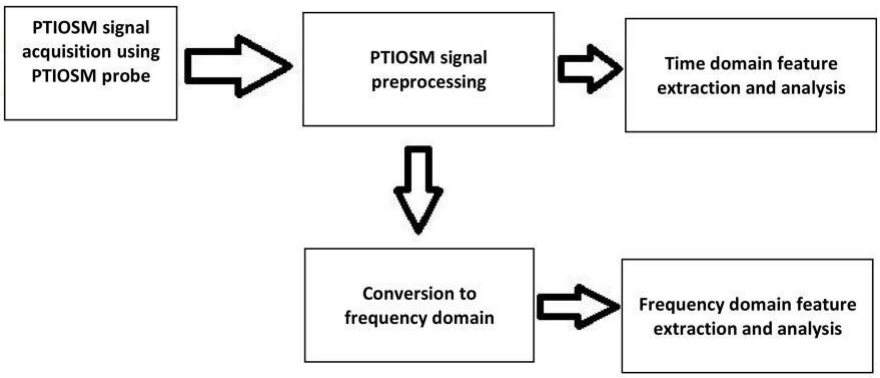

Figure 3. Algorithmic steps for PTIOSM signal processing.

2.3. Frequency Domain Feature Extraction

Fast Fourier Transform (FFT) algorithm implemented in Matlab was used to convert the acquired time domain signals to frequency domain. The amplitude and phase spectrums of the frequency domain signals were plotted in Matlab and visually analyzed with a view of identifying the frequency bands which best differentiated infected samples from non-infected samples based on their signal intensities at different frequency bands.

2.4. Sample Description

Two sets of Geimsa stained blood smear samples were used to test the developed PTIOSM probe. One was *Plasmodium falciparum* infected blood smears samples (acquired from Carolina biological company [23]) and the other was *Plasmo-dium* non-infected blood smear samples locally prepared. In each of the two sets, PTIOSM signals from five slides were acquired, processed and analyzed as de-scribed above.

3. Results

Frequency Domain PTIOSM Signals

After conversion from time domain to frequency domain and noise filtering of PTIOSM signals, scatter plots for the amplitude spectra belonging to the five *Plasmodium* positive and five *Plasmodium* negative samples were made (**Figure 4**)**.** From the scatter plots the following observations were made: At some fre-quency bands of the PTIOSM signal, the *Plasmodium* positive PTIOSM signals had more spectral energy compared to *Plasmodium* negative PTIOSM signals and therefore it was possible to find a threshold value that differentiated infected samples from the non-infected ones. In the case of the pulsed red light excitation (**Figure 4(a)**), 100% classification accuracy of *Plasmodium* positive samples from *Plasmodium* negative samples was possible at frequency band between 1.7 MHz and 1.8 MHz because the signal amplitudes of all infected samples were greater than those of *Plasmodium* negative samples. This means that at this fre-quency band, the *Plasmodium* parasite detection sensitivity and specificity was 100% (there were no false positives or false negatives). For the PTIOSM signals due to pulsed green light excitation (**Figure 4(b)**), the best classification accura-cy was observed at frequency band between 1.5 MHz and 1.6 MHz. At this fre-quency band, the signal intensities from all the five *Plasmodium* positive sam-ples were greater than the *Plasmodium* negative signals except for one *Plasmo-dium* negative sample signal whose amplitude was comparable to those of posi-tive samples. This represents a classification specificity of 100% and sensitivity of 83.3%.

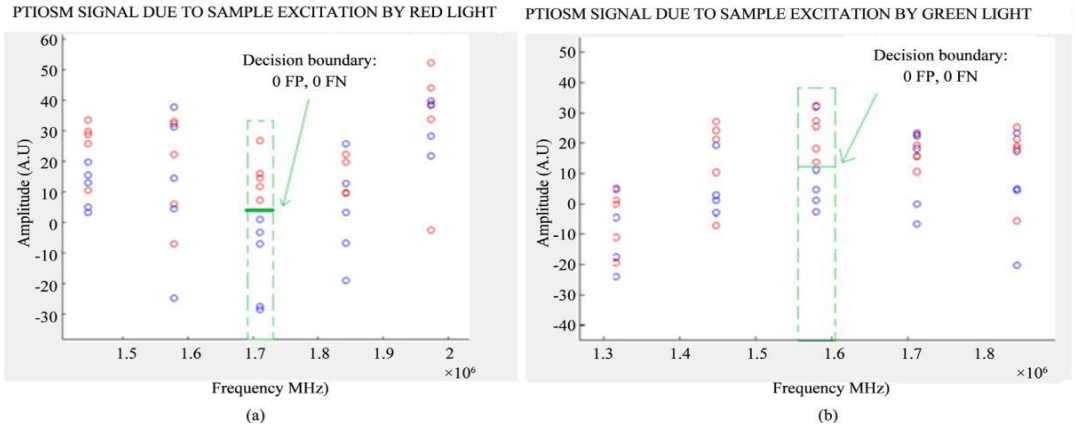

Figure 4. Frequency spectra of PTIOSM signal for malaria infected (red circles) and non-infected samples (blue circles).

(a) PTIOSM signal due to red light excitation; (b) PTIOSM signal to blue light modulation. FP is false positive samples and FN is false negative samples.

et al.

4. Discussion

PTIOSM technique ability to correctly classify malaria infected blood smear samples from the non-infected samples can be attributed to two factors; change of hemozoin's refractive index during optical excitation hence causing a signifi-cant modulation of the PTIOSM signal at frequency band corresponding to its size. Another possible explanation could be that the excitation beam causes gen-eration of photoacoustic waves, which in turn induces vibration of optical scat-terer in the medium leading to modulation of diffuse reflected light from the sample. Variations of signal intensity from samples having the same infection status (either infected or non-infected) can be attributed to two possible factors: the concentration of responsible chromophores (in this case hemozoin and he-moglobin) and the optical excitation intensity.

From the reported results, the developed PTIOSM probe has demonstrated excellent capability of malaria diagnosis in blood smear samples. The simple in-strumentation involved and its real time operation makes it a suitable candidate for mass screening of the disease in malaria endemic regions. However, further testing using more samples prepared under different conditions (both thin and thick blood smears, stained and non-stained) are required to conclusively de-termine the techniques sensitivity and specificity. Besides, further experimenta-tion is required to investigate the capability of the probe in quantifying the para-site load (parasitemia) in the samples and the limit of detection of the technique.

5. Conclusion

A novel, simple photo-thermal based technique (PTIOSM) for detection of *Plasmodium* parasites in infected blood smear samples has been described. A RGB LED was used as the optical source to supply both the PB and the EB. Dif-fusely reflected PB light from the sample was detected by a photodiode, ampli-fied and the signal preprocessed for noise cancellation. Fourier transform was used to convert the signals from time domain to frequency domain and then some specific frequency bands were used to differentiate *Plasmodium* infected samples from non-infected samples based on an empirically determined intensi-ty threshold. The technique yielded 100% detection sensitivity and specificity using red LED light as the excitation beam.

Conflicts of Interest

The authors declare no conflicts of interest regarding the publication of this pa-per.

References

[1] World Health Organization (2015) World Malaria Report 2015.

[2] https://www.cdc.gov/malaria/about/biology/index.html

[3] Samson, E.B., Goldschmidt, B.S., Whiteside, P.J., Sudduth, A.S., Custer, J.R., Beerntsen, B. and Viator, J.A. (2012) Photoacoustic Spectroscopy of β-Hematin.

[4] Makler, M., Palmer, C. and Ager, A. (1998) A Review of Practical Techniques for the Diagnosis of Malaria. *Annals of Tropical Medicine and Parasitology*, **92**, 419-433.

[5] Scholl, P.F., Kongkasuriyachai, D., Demirev, P.A., Feldman, A.B., Lin, J.S., Sullivan, J.D. and Kumar, N. (2004) Rapid Detection of Malaria Infection *in Vivo* by Laser Desorption Mass Spectrometry. *The American Journal of Tropical Medicine and Hygiene*, **71**, 546-51.

[6] Bélisle, J.M., Costantino, S., Leimanis, M.L., Bellemare, M.J., Bohle, D.S., Georges, E. and Wiseman, P.W. (2008) Sensitive Detection of Malaria Infection by Third Harmonic Generation Imaging. *Biophysical Journal*, **94**, L26-L28. https://doi.org/10.1529/biophysj.107.125443

[7] Burnett, J.L., Carns, J.L. and Richards-Kortum, R. (2017) Towards a Needle-Free Diagnosis of Malaria: *In Vivo* Identification and Classification of Red and White Blood Cells Containing Haemozoin. *Malaria Journal*, **16**, 447. https://doi.org/10.1186/s12936-017-2096-1

[8] Saha, R.K., Karmakar, S. and Roy, M. (2012) Computational Investigation on the Photoacoustics of Malaria Infected Red Blood Cells. *PLoS ONE*, **7**, e51774. https://doi.org/10.1371/journal.pone.0051774

[9] Lukianova-Hleb, E.Y., Campbell, K.M., Constantinou, P.E., Braam, J., Olson, J.S., Ware, R.E., Sullivan, D.J. and Lapotko, D.O. (2014) Hemozoin-Generated Vapor Nanobubbles for Transdermal Reagent- and Needle-Free Detection of Malaria. *Proceedings of the National Academy of Sciences*, **111**, 900-905. https://doi.org/10.1073/pnas.1316253111

[10] Cai, C., Carey, K.A., Nedosekin, D.A., Menyaev, Y.A., Sarimollaoglu, M., Galanzha, E.I., Stumhofer, J.S. and Zharov, V.P. (2016) *In Vivo* Photoacoustic Flow Cytometry for Early Malaria Diagnosis. *Cytometry Part A*, **89**, 531-542. https://doi.org/10.1002/cyto.a.22854

[11] Lukianova-Hleb, E., Bezek, S., Szigeti, R., Khodarev, A., Kelley, T., Hurrell, A., Ber-ba, M., Kumar, N., D'Alessandro, U. and Lapotko, D. (2015) Transdermal Diagnosis of Malaria Using Vapor Nanobubbles. *Emerging Infectious Diseases*, **21**, 1122. https://doi.org/10.3201/eid2107.150089

[12] Beard, P. (2011) Biomedical Photoacoustic Imaging. *Interface Focus*, rsfs20110028.

[13] Xia, J., Yao, J. and Wang, L.V. (2014) Photoacoustic Tomography: Principles and Advances. *Progress in Electromagnetics Research*, **147**, 1. https://doi.org/10.2528/PIER14032303

[14] Deán-Ben, X.L. and Razansky, D. (2013) Functional Optoacoustic Human Angio-graphy with Handheld Video Rate Three Dimensional Scanner. *Photoacoustics*, **1**, 68-73. https://doi.org/10.1016/j.pacs.2013.10.002

[15] Zhou, Y., Li, G., Zhu, L., Li, C., Cornelius, L.A. and Wang, L.V. (2015) Handheld Photoacoustic Probe to Detect Both Melanoma Depth and Volume at High Speed *in Vivo*. *Journal of Biophotonics*, **8**, 961-967. https://doi.org/10.1002/jbio.201400143

[16] Kuniyil Ajith Singh, M., Steenbergen, W. and Manohar, S. (2016) Handheld Probe-Based Dual Mode Ultrasound/Photoacoustics for Biomedical Imaging. In: Olivo, M. and Dinish, U.S., Eds., *Frontiers in Biophotonics for Translational Medi-cine*, Vol. 3, Springer, Singapore, 209-247.

[17] Daoudi, K., Van Den Berg, P.J., Rabot, O., Kohl, A., Tisserand, S., Brands, P. and Steenbergen, W. (2014) Handheld Probe Integrating Laser Diode and Ultrasound

18. *Journal of Optics*, **14**, 065302. https://doi.org/10.1088/2040-8978/14/6/065302

Transducer Array for Ultrasound/Photoacoustic Dual Modality Imaging. *Optics Express*, **22**, 26365-26374.

[18] Liu, M. and Franko, M. (2014) Progress in Thermal Lens Spectrometry and Its Ap-plications in Microscale Analytical Devices. *Critical Reviews in Analytical Chemi-stry*, **44**, 328-353.

[19] Canto, F., Couston, L., Magnaldo, A., Broquin, J.-E. and Signoret, P. (2008) Ther-mal Lens Spectroscopy as a "New" Analytical Tool for Actinide Determination in Nuclear Reprocessing Processes.

[20] Wang, L.V. and Wu, H. (2007) Biomedical Optics: Principles and Imaging. John Wiley & Sons, Hoboken.

[21] https://www.adafruit.com/product/2524

[22] http://www.ti.com/lit/ds/symlink/opt101.pdf

[23] https://www.carolina.com/protists-microscope-slides/Plasmodium-falciparum-slide -smear/297190.pr

Open Journal of Clinical Diagnostics, 2021, 11, 59-75

https://www.scirp.org/journal/ojcd

ISSN Online: 2162-5824

ISSN Print: 2162-5816

A.6.2 Review of Photoacoustic Malaria Diagnostic Techniques

Daniel Maitethia Memeu[1,2], Abdallah Merenga Sallorey[2], Ciira Maina[3], Dickson Mwenda Kinyua[1,4]

[1]Department of Physical Sciences, Meru University of Science and Technology, Meru, Kenya

[2]Department of Physics, Kenyatta University, Nairobi, Kenya

[3]Dedan Kimathi University of Technology, Nyeri, Kenya

[4]Department of Pure and Applied Sciences, Kirinyaga University, Kerugoya, Kenya

Email: danielmaitethia@gmail.com

How to cite this paper:
Memeu, D.M., Sallorey, A.M., Maina, C. and Kinyua, D.M. (2021) Review of Photoacoustic Malaria Diagnostic Techniques. *Open Journal of Clinical Diagnostics*, **11**, 59-75.
https://doi.org/10.4236/ojcd.2021.112005

Received: October 6, 2020

Accepted: June 26, 2021

Published: June 29, 2021

1. Introduction

1.1. Background of Malaria Disease

Malaria is a common disease in tropical countries that poses serious public health concerns. It is one of the leading causes of mortality globally. Nearly 0.5 million deaths were attributed to the disease in the year 2015 according to the world malaria report [1]. The majority of these deaths comprise of children less than

five years old from sub-Saharan Africa. Besides, it is estimated that approx-imately 200 million people are infected with the disease and 3.2 billion people are at risk of contracting the disease annually according to the report. This has created a heavy social-economic burden to the affected countries due to huge treatment costs and absenteeism from work and schools [2].

The disease is caused by protozoan parasites of the genus *Plasmodium* which lives in peripheral blood, spleen or liver of humans. The parasites are introduced to the human host through bites by infected mosquitoes—malaria vectors. Once in the bloodstream, the parasites move to the liver for incubation and multipli-cation. They later move back to the bloodstream and attack the Red Blood Cells (RBCs). The parasites feed on the cells' hemoglobin reducing or completely in-hibiting the cells' ability to bind oxygen. Hemoglobin is a complex bio-molecule made of two simpler molecules; the iron compound called heme and a protein molecule globin. The parasite digests globin to meet its nutritional needs but converts heme (which is toxic to the parasite [3]) into a by-product called he-mozoin. Hemozoin, an inert insoluble crystal composed of iron nano-rods [4], is then deposited in parasites' food vacuoles. Presence of hemozoin in RBCs in pe-ripheral blood is, therefore, an indicator of malaria infection. Notably, hemozoin production is also associated with other blood-feeding parasites such as *Schisto-soma mansoni* and *Rhodnius prolixus* [5] [6]. *However*, neither Schistosoma-mansoni nor Rhodniusprolixus resides in peripheral blood.

There are five species of *Plasmodium* parasites that infect humans [7], name-ly; *Plasmodium falciparum, Plasmodium ovale, Plasmodiumvivax, Plasmodium malariae,* and *Plasmodium knowlesi*. *Plasmodium falciparum* is the most fatal while other species cause mild to moderate illnesses. Each of the five species has distinct morphological features which are used for *Plasmodium* parasites species identification during optical microscopy diagnosis.

The parasites undergo three main inter-erythrocyte life stages, namely; the early stage is also known as ring stage, intermediate stage also called trophozoite stage and Mature stage also called schizont stage (the reproductive stage). Upon maturity of the parasites, the infected cells' rapture and the merozoites (offspring of the parasites) are re-leased into the bloodstream where they attack other health erythrocytes and the cycle starts afresh. However, some *Plasmodium* merozoites formed during asex-ual reproduction of the schizonts differentiate to become the sexual form of the parasites (gametocytes) that are taken up by mosquitoes during blood meals and aid in the transmission of the disease [8]. **Figure 1** [9] shows the life cycle of the *Plasmodium* parasite in the human host.

1.2. Malaria Diagnostic Techniques

Malaria diagnosis entails detection of the presence of the *Plasmodium* parasites in the patient blood and determination of the following parameters; species, life stages, and parasitemia estimation—an indicator of disease severity given by ei-ther the number of *Plasmodium* parasites or the number of infected erythrocytes

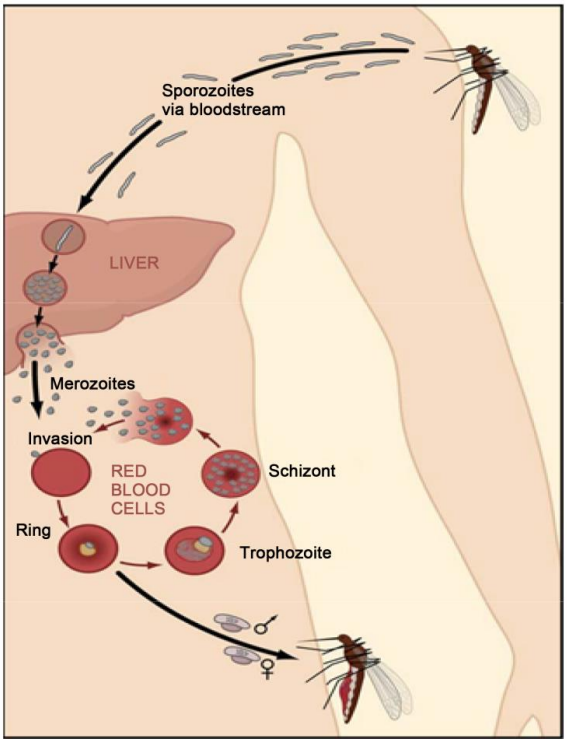

Figure 1. *Plasmodium* life cycle in the human host. Sporozoites are re-leased into the blood by the mosquito, they are delivered to the liver for incubation and multiplication. After multiplication, the merozoites are released into the blood to attach red blood cells. While in the red blood cells they feed on hemoglobin, undergo cell division and eventually make the cell rapture for the merozoite to be released and attach more cells. Some merozoites differentiate to be the sexual form and these are the ones that the mosquito takes during blood meal to perpetuate transmis-sion. The diagram is adopted from ref [9]. per unit volume of blood. A number of malaria diagnostic techniques exist and more are under development. The gold standard method is optical microscopy

[11]. The technique involves examination of stained blood smear samples using a light microscope to aid visualization of *Plasmodium* parasites in eryt-hrocytes. Labeling (staining) of blood smear samples with Giemsa is undertaken prior to examination of the slides. Staining helps to highlight the parasites' pig-ment (hemozoin) and hence makes the parasites conspicuous. This technique is time-consuming and labor-intensive due to the need for sample preparation and the enumeration of detected parasites in the microscope field of view. A single malaria test takes between 30 to 60 minutes. In addition, reliability of the results from this method depends on the experience of the microscope operator.

Other malaria diagnostic methods include; Polymerase Chain Reaction (PCR) based technique [12], *Plasmodium* parasite antigen detection based technique also referred as Rapid Diagnostic Test (RDT) [13] and Fluorescence microsco-py-based techniques [11]. Antigen-based technique is widely used and boasts of a relatively fast detection speed of about fifteen minutes. However, the technique has low parasite detection sensitivity and specificity especially when the parasite load is low in the blood. The test is also relatively expensive with a single test costing about 1US$. In contrast, PCR technique has high detection sensitivity and specificity. It probes and amplifies genetic material of the *Plasmodium* para-sites present in the blood. However, the technique demands the use of sophisti-cated equipments and expensive reagents. Besides, a highly skilled operator is also required to perform the test. The technique is therefore used in research la-boratories and confirmation of malaria tests. Fluorescent based technique relies on staining of blood smears with a fluorescent dye that would highlight the pa-rasite nucleus. A fluorescent microscope is then used to observe the stained blood sample. The technique has also not yet found wide clinical adoption in malaria screening due to high cost of equipment, reagents and demand for highly skilled expertise.

Some of the malaria diagnostic techniques reported by literature as being un-der development include; Third Harmonic Generation (THG) technique [14], Magneto-optic based technique [15], and computer vision assisted optical mi-croscopy technique [16] [17]. Label-free optical microscopy using multispectral imaging and chemometrics techniques has also been explored [18] [19]. Recent-ly, a few publications have reported on the development of Photo-Thermal (PT) and Photo-Acoustic (PA) based techniques for *in vivo* malaria diagnosis [4] [20]

[22] [23]. Preliminary results regarding the techniques' performance are impressive but more work is needed before the method can be clinically accepted for malaria screening.

Generally, the mainstream malaria diagnostic techniques suffer from a num-ber of shortcomings [10] [11] which include low detection sensitivity and speci-ficity, labor and time intensiveness and demand for reagents and sophisticated equipments which are often expensive and inaccessible to people in resource scarce settings where often malaria is endemic. There is therefore an urgent need for development of new and more efficient techniques for malaria diagnosis. The remaining part of this paper explains in detail the principle behind photoacous-tic-based malaria diagnostic technique and the reported progress.

= Photoacoustic Effect and Its Application in Biomedical Imaging and Diagnostics

Photoacoustic effect is a process in which acoustic waves in the Ultrasound (US) frequency range are emitted upon absorption of optical radiation by chromo-phores (light absorbing molecules). The phenomenon was first reported in 1880 by Alexander Graham Bell [24]. Photoacoustic effect involves conversion of theB absorbed optical energy to thermal energy which leads to temperature rise and thermo-elastic expansion in the irradiated region. Consequently, a transient pres-sure wave is generated and propagates through the sample. Reported biomedical applications of the technique include; anatomical and functional imaging of bi-ological tissue [25]-[32], disease diagnostics [33]-[43] as well as guidance and monitoring of therapeutic interventions [44] [45].

Efficient generation of PA signals demands two conditions to be satisfied; thermal and stress confinement [46]. This means that both heat conduction and thermo-elastic expansion are confined within the illuminated tissue region dur-ing optical excitation time span. Generation of PA waves therefore requires use of either Time Domain (TD) techniques (where short optical pulses, typically in nanosecond range are used to

excite the sample) [46] [47] [48] [49] or Frequen-cy Domain (FD) techniques where intensity modulated Continuous Wave (CW) laser light is used to generate ultrasonic pressure waves in tissue [50] [51] [52]

[54]. In the case of FD techniques, either fixed frequency or linearly varying frequency (Chirped) optical signals are used to excite the sample. Use of pulsed optical beam produces stronger PA signals compared to fixed frequency intensi-ty modulated optical excitation [55]. However, Chirped optical excitation com-bined with lock-in detection have been reported to yield PA signals whose Signal to Noise Ratio (SNR) is comparable to that of pulsed excitation [50]. They also have other salient advantages such as; wide dynamic range which implies low energy optical sources can be used and this has a congruent advantage of mini-mizing the risk of tissue damage due to excessive optical exposure, depth tenabili-ty, and capability to use continuous wave diode lasers as opposed to bulky and expensive pulsed lasers. Both TD and chirped FD techniques can be used for tissue depth profilometry as they carry time of flight information.

Intensity of the generated PA waves is a measure of the tissue's optical absorp-tion coefficient μ_a —a parameter which infers the molecular composition and molar concentration of the constituent tissue chromophores (see Equation (1)) as well as the tissues mechanical and thermal properties [56]. To perform quan-titative photoacoustic spectroscopy, the tissue should be excited by multispectral optical radiation (pulsed or intensity modulated) and the acoustic waves induced by each optical wavelength detected by either a focused ultrasonic transducer or transducer arrays placed in close proximity to the sample being probed. The signal is then amplified and processed to compensate for signal attenuation in the medium and the detector response. Spectroscopic inversion of the recovered initial photoacoustic pressure intensity $P_0{}^{\lambda_i}$ (see Equation (2)) is then per-formed to determine sample properties such as optical absorption coefficient spa-tial distribution map, molecular composition, or concentration of chromophores in the sample. Some of the reported literature on these subjects can be found in references [57]-[63].

Photoacoustic imaging and sensing boasts of a number of advantages over other imaging modalities [56]; first is high spatial resolution and sharp image contrast due to low scattering of the generated ultrasonic signal and high optical absorption sensitivity by bio-molecules. Second is the ability to perform mul-ti-scale imaging hence yielding images of varying spatial resolution (from sub-micrometer to centimeter scale) and therefore enabling imaging of cell orga-nelles, cells, tissues and organs of the same

specimen using a single imaging mod-ality. This has the potential to enable simultaneous studies of biological pheno-mena at varying spatial and time scales with minimal intra-subject variability. Since non-ionizing optical radiation is used to excite the tissue, the technique is safe. It is also relatively cheap compared to other medical imaging modalities such as Nuclear Magnetic Resonance Imaging (NMRI) and X-Ray Computed Tomography (X-Ray CT). Recently, Photoacoustic Flow Cytometry (PAFC) has been proposed for detection of Circulating Tumor Cells (CTC) [64] [65] [66] [67]. The technique has also been explored for malaria diagnosis [21] [22] [23].

2.1. Malaria Diagnosis Using Photoacoustics

The major chromophores in malaria infected blood are total hemoglobin (Hbt) and hemozoin [20]. Hbt is the sum of oxy-hemoglobin (HbO_2) and deoxy-he-moglobin (Hb) molecules in the blood. **Figure 2** is an excerpt of the spectral plots of hemozoin (Hz) and Hemoglobin (Hb) extracted from the work of saha *et al.* [16], *and* Cai *et al.* [18]. **Table 1** gives values of the optical absorption coef-ficients and molar concentrations of Hemozoin (Hz) in an infected erythrocyte

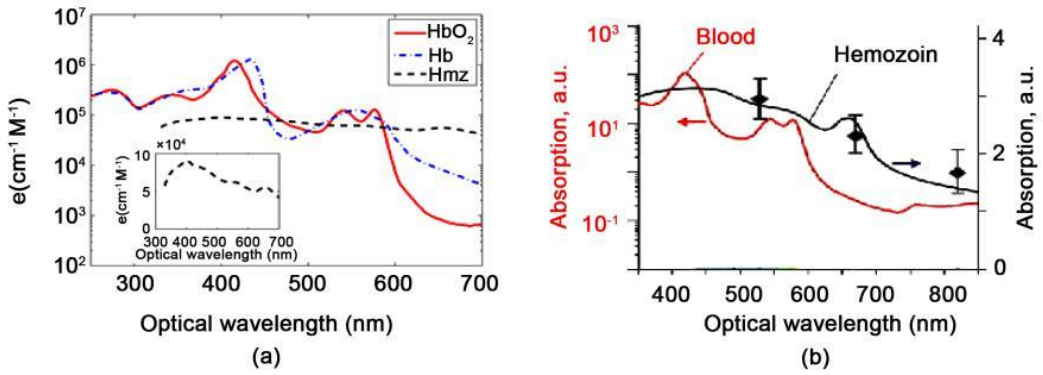

Figure 2. (a) Molar extinction coefficients of oxyhemoglobin, deoxyhemoglobin, and hemozoin [20], the inset is a zoomed up view of the hemozoin spectrum showing its cha-racteristic peaks. (b) 70% oxygenated blood and hemozoin [22].

Table 1. Optical absorption coefficients and molar concentration of hemozoin in both healthy and *Plasmodium* infected erythrocytes. Values of μ_a are extracted from [20]. as extracted from the work of Saha *et al*. [20]. Based on the values of molar con-centration of Hz present in the cell, it is possible to differentiate various stages of infection. Previous studies have demonstrated the possibility of *in vivo* imaging of oxygen saturation and malignant tumor hypoxia [50] [68]-[73], oxygen me-tabolic rate [74], methemoglobin [75] and oxygen release rate in blood vessels and individual erythrocytes using sub-wavelength Optical Resolution Photoac-oustic

Microscope (OR-PAM) [76]. This suggests that a similar approach can be used to detect the presence of other dominant optical absorbers in individual erythrocytes such as hemozoin in case of malaria.

The following is a brief analysis of the problem. Optical absorption coefficient due to a malaria infected erythrocyte can be described by the following equation.

$$\mu_a^{\lambda_i} = \varepsilon_{Hz}^{\lambda_i} [c_{Hz}] + \varepsilon_{tHb}^{\lambda_i} [c_{tHb}]$$

$\varepsilon_i^{\lambda_i}$ is the molar extinction coefficient of the i^{th} chromophore present in the

cell. Both μ_a and ε are wavelength dependent hence the superscript λ_i . $[c_i]$ is the molar concentration of the i^{th} bio-molecule in the cell. The initial pho-toacoustic signal generated due to absorption of an optical pulse of wavelength λ_i is the product of the deposited optical energy $A_e = \mu_a^{\lambda_i} \Phi^{\lambda_i}$ and a factor called gruneisen parameter (Γ). Φ is the local optical fluence distribution in the blood which depends on the intensity of the incident light as well as blood opti-cal properties (mainly, optical absorption and scattering coefficients). In case the chromophore relaxation after photon absorption is not 100% non-radiative, a down scaling factor is included in the product to account for the fraction of photon energy converted to heat energy. Therefore, the initial PA pressure is given by the following equation [63].

$$P_0^{\lambda_i} = \Gamma n_{th} \mu_a^{\lambda_i} \Phi^{\lambda_i} \qquad (2)$$

With the transformed thermal energy density due to non-radiative relaxation of chromophores given by

$H = n_{th} \mu_{a\lambda_i} \Phi_{\lambda_i}$

n_{th} is the fraction of optical energy converted to heat energy ($n_{th} = 1$ for non-fluorescent and non-photoluminescent chromophores). The grueneisen parameter is a thermodynamic quantity which gives the photoacoustic efficiency of the tissue, *i.e.*, the fraction of the thermal energy converted to acoustic waves.

The generated acoustic signal P_o (also referred as initial PA pressure) propa-gates through the tissue and is detected by an ultrasonic transducer placed at the tissue surface, a distance *r* from the target absorber (in this case a skin subsur-

el). The detected acoustic signal, P_d differs from the initial PA

signal due to; acoustic attenuation through the tissue, partial detection geometry of the traducer and the transducer's detection efficiency $\eta(f)$. The transducer output signal, P_d is therefore a product of the initial signal, P_o and a scaling factor, T_d which accounts for the described signal attenuation *i.e.*,

$$P_d(f) = T_d(f) P_o \qquad (4)$$

With

$$T_d(f) = \eta(f) \frac{N_A}{2\sqrt{\quad}} e^{-\alpha_o f^2 l} \qquad (5)$$

where; *NA* is the traducers' numerical aperture, *l* is its focal length and α_o is the tissue attenuation coefficient. Numerical values for the parameters in Equa-tion (4) for some commercially available ultrasonic transducers can be found in reference [77].

2.2. Reported Work

A limited number of studies have so far been carried out regarding *in vivo* photoacoustic diagnosis of malaria. Generally, the principle of *in vivo* Photoacoustic Flow Cytometry (PAFC) [78] has been adopted. The technique entails use of a focused ultrasonic transducer to detect PA signals emitted due to optical excita-tion of the flowing erythrocytes in blood vessels located below the skin surface. The signal peak intensity is monitored in time to keep track of the flowing eryt-hrocytes (infected and non-infected). Healthy erythrocytes produce a nearly constant amplitude signal. Hemozoin – an endogenous malaria biomarker has either higher or lower optical absorption than hemoglobin depending on the optical wavelength used. This implies that the amplitude of *Plasmodium* infected blood would differ from that of healthy blood. The following is a brief review of the few reported literature.

Cai *et al*. [22] proposed an *in vivo* (PAFC) technique for early diagnosis of malaria. They used a focused US transducer for detection of PA signal from flowing erythrocytes irradiated by three pulsed laser lights of wavelengths 532 nm, 671 nm, and 820 nm. The signal was then amplified, digitized and loaded to a PC for processing. The system's spatial resolution was reported to be be-tween 1 - 6 µm. Both *in vitro* and *in vivo* experiments using mice as the animal model were conducted to determine the sensitivity of the device. The authors reported that their technique was 1000 times more sensitive than optical micro-scopy method and could detect an infected erythrocyte 3 hours after inoculation of *Plasmodium* parasites into a healthy mouse compared to 3 days taken before detection using optical microscopy. They observed that when the optical energy used was increased beyond a certain threshold, hemozoin vapor nano-bubble formation occurred in the infected cells and this produced PA signal of in-creased intensity—a process termed as nonlinear photoacoustics. They also used the process to perform real time destruction of infected cells (photo-thermal malaria therapy) while monitoring the efficiency of the therapy. They observed that the PA signal ratio of infected cells to non-infected cells was highest at 671 nm optical excitation wavelength.

Lukianova-Hleb *et al*. (2014) [21] described a picosecond pulsed laser tech-nique for generation and detection of Hemozoin induced Vapor Nano-Bubbles (H-VNB). The authors argued that when hemozoin crystals in infected RBCs absorbs the ultra-short pulsed radiation (having picoseconds range pulse width)

of sufficient energy, nano-volume liquid around the hemozoin crystals is over-heated and vaporized resulting in generation of transient vapor bubbles which undergo explosive expansion and collapsing—a process that is accompanied by emission of high intensity acoustic waves. Both *in vitro* and *in vivo* sets of he-mozoin positive and hemozoin negative samples consisting of blood smears, whole blood and live mice were studied. Laser pulses were shone on samples and the emitted acoustic waves detected by an ultrasonic transducer. The transducer output was coupled to a digital oscilloscope. The detected signal was then ana-lyzed in the time domain. It was found that samples containing hemozoin pro-duced acoustic signals of higher amplitudes than hemozoin negative samples. It was reported that the technique yielded high correlation in differentiating *Plas-modium* parasite life stages and parasitemia estimation in comparison with opt-ical microscopy. The optical wavelength used for excitation of PA signals was 672 nm—an absorption peak for hemozoin. The optical energies per pulse

used for *in vitro* and *in vivo* experiments were 10 μJ and 15 μJ respectively. Lukiano-va-Hleb *et al*. (2015) [23] used the technique for *in vivo* detection of parasites in humans and infected mosquitoes. Similar results were obtained.

In general, photoacoustic based malaria diagnosis boasts of several advantages over other diagnostic methods which includes; use of endogenous contrast agent (hemozoin) for parasite detection as opposed to exogenous contrast agents as is the case in optical microscopy, potential for *in vivo* diagnosis. Use of non-ionizing radiation, which makes it safe, real time monitoring and capability for early de-tection of the disease hence making treatment more effective. In addition, it is possible to use the technique for diagnosis of other blood related disease. How-ever, the reported photoacoustic diagnostic systems suffer from a number of challenges which must be addressed before the technology can be clinically adopted. For example, the technique cannot perform quantitative measurement of chromophore molar concentration in absolute units. In most of the reported work [21] [22] [23], the distinction between healthy and diseased samples is made based on the relative amplitudes values of the induced PA signal between the two sets of samples. The limitation of this approach is wide signal amplitudes variability within subjects of the same class, which makes system calibration dif-ficult. Secondly, the reported PA systems are bulky and expensive due to the demand for high-energy nanosecond pulsed multispectral laser sources, high fre-quency sensitive ultrasonic transducers and lock-in amplifiers. Besides, the use of fluence estimation models for quantitative PA spectroscopy makes the mea-surements time intensive and quasi real time. Their accuracy also depends on how well the tissue geometry is known a priori.

There is a promising trend in addressing these challenges going by the num-ber of publications and research groups working on the problem. Simplification of PA hardware has been attempted by substitution of the bulky and expensive Optical Parametric Oscillator (OPO) tuned laser sources with much smaller and cheap diode laser sources [79] [80] [81] and Light Emitting Diodes (LEDs) [82] that have a wide range of optical wavelengths and are commercially available. Notably, Quantellaser^{TM} has developed a compact high energy multispectral pulsed diode laser module operating in four different wavelengths (808, 915, 940 or 980 nm) in the NIR region customized for PA applications. Its high optical pulse energy (of 1 mJ per emitted wavelength per 80 nS pulse width) is achieved by stacking multiple diode lasers of the same wavelength. Attempts to develop a compact hand held photoacoustic probe for *in vivo* imaging have also been re-ported [83] [84] [85] [86].

Use of chirped FD techniques in photoacoustic spectroscopy applications [50] has the potential of simplifying the instrumentation complexity of the PA systems by enabling use of cheap and portable CW diode lasers as PA optical sources. Moreover, eliminate the need for computationally demanding numeri-cal algorithms for fluence estimation. Development of a sensitive FD photoac-oustic technique for hypoxia monitoring and early cancer detection has been reported [34] [35]. The technique is termed as Wavelength Modulated Differen-tial Photoacoustic Technique (WM-DPAS). The technique uses two optical wa-velengths (680 nm and 808 nm) to monitor variations in oxyhemoglobin con-centration in tissue. One wavelength (680 nm in this case) should have maxi-mum variation in extinction coefficients for oxyhemoglobin and deoxyhemoglo-bin while the other wavelength (808 nm which is the isosbestic wavelength) should ideally have the extinction coefficients coinciding. Two CW laser sources are intensity modulated out of phase (differentially) and their output coupled to the sample for photoacoustic excitation. The emitted PA signal is detected by an ultrasonic transducer. Upon signal preprocessing, the Fourier transform of the signal is performed to obtain both amplitude and phase signals of the differential PA time domain signal. The phase signal is said to be independent of the optical fluence and its variation is only due to variations in the molar concentration of the probed chromophore. Judging from the reported features and performance of WM-DPAS, this technique is likely to be very suitable for *in-vivo* detection of malaria.

Future Prospect

In order to make photoacoustic based malaria diagnostic techniques clinically viable and a method of choice, the technique has to process the following quali-ties; high diagnostic sensitivity and specificity, be fast, affordable, compact and portable. More work is needed in development of efficient PA techniques for detection of endogenous disease biomarkers such as hemozoin. Simplification of the instrumentation in PA systems will also be a significant contribution. As far as malaria diagnostics is concerned, it would be valuable to explore the possibil-ity of using a PA based system to differentiate different species of *Plasmodium* in a malaria patient. This could be done by determining oxygen saturation levels in erythrocytes infected by different *Plasmodium* species. It would also be worth-while to investigate the potential of WM-PAS in non-invasive malaria detection.

4. Conclusion

A review of reported literature on photoacoustic-based malaria diagnostic tech-niques and a discussion of the existing research gap have been presented in this paper. Suggestions for future refinements have also been offered.

Conflicts of Interest

The authors declare no conflicts of interest regarding the publication of this pa-per.

References

[24] World Health Organization (2016) World Malaria Report 2015. World Health Or-ganization, Geneva.

[25] World Health Organization (2003) The Africa Malaria Report 2003. World Health Organization, Geneva.

[26] Kumar, S., Guha, M., Choubey, V., Maity, P. and Bandyopadhyay, U. (2007) Anti-malarial Drugs Inhibiting Hemozoin (β-Hematin) Formation: A Mechanistic Up-date. *Life Sciences*, **80**, 813-828. https://doi.org/10.1016/j.lfs.2006.11.008

[27] Samson, E.B., Goldschmidt, B.S., Whiteside, P.J.D., *et al*. (2012) Photoacoustic Spec-troscopy of β-Hematin. *Journal of Optics*, **14**, 065302. https://doi.org/10.1088/2040-8978/14/6/065302

[28] Oliveira, M.F., Silva, J.R., Dansa-Petretski, M., *et al*. (2000) Hemozoin Formation in the Midgut of the Blood-Sucking Insect Rhodniusprolixus. *FEBS Letters*, **477**, 95-98. https://doi.org/10.1016/S0014-5793(00)01786-5

[29] Oliveira, M.F., Kycia, S.W., Gomez, A., *et al*. (2005) Structural and Morphological Characterization of Hemozoin Produced by Schistosomamansoni and Rhodniuspro-lixus. *FEBS Letters*, **579**, 6010-6016. https://doi.org/10.1016/j.febslet.2005.09.035

[30] White, N.J. (2008) Plasmodium Knowlesi: The Fifth Human Malaria Parasite. *Clin-ical Infectious Diseases*, **46**, 172-173. https://doi.org/10.1086/524889

[31] Ngwa, C.J., Rosa, T. and Pradel, G. (2016) The Biology of Malaria Gametocytes. In-techOpen. https://doi.org/10.5772/65464

[32] Cowman, A.F. and Crabb, B.S. (2006) Invasion of Red Blood Cells by Malaria Para-sites. *Cell*, **124**, 755-766. https://doi.org/10.1016/j.cell.2006.02.006

[33] Wongsrichanalai, C., Barcus, M.J., Muth, S., Sutamihardja, A. and Wernsdorfer, W.H. (2007) A Review of Malaria Diagnostic Tools: Microscopy and Rapid Diagnostic Test (RDT). *American Journal of Tropical Medicine and Hygiene*, **77**, 119-127. https://doi.org/10.4269/ajtmh.2007.77.119

[34] Makler, M.T., Palmer, C.J. and Ager, A.L. (1998) A Review of Practical Techniques for the Diagnosis of Malaria. *Annals of Tropical Medicine and Parasitology*, **92**, 419-434. https://doi.org/10.1080/00034989859401

[35] Johnston, S.P., Pieniazek, N.J., Xayavong, M.V., Slemenda, S.B., Wilkins, P.P. and da Silva, A.J. (2006) PCR as a Confirmatory Technique for Laboratory Diagnosis of Malaria. *Journal of Clinical Microbiology*, **44**, 1087-1089. https://doi.org/10.1128/JCM.44.3.1087-1089.2006

[36] Moody, A. (2002) Rapid Diagnostic Tests for Malaria Parasites. *Clinical Microbiol-ogy Reviews*, **15**, 66-78. https://doi.org/10.1128/CMR.15.1.66-78.2002

[37] Bélisle, J.M., Costantino, S., Leimanis, M.L., *et al*. (2008) Sensitive Detection of Malaria Infection by Third Harmonic Generation Imaging. *Biophysical Journal*, **94**, L26-L28. https://doi.org/10.1529/biophysj.107.125443

[15] Newman, D.M., Heptinstall, J., Matelon, R.J., *et al*. (2008) A Magneto-Optic Route toward the *in Vivo* Diagnosis of Malaria: Preliminary Results and Preclinical Trial Data. *Biophysical Journal*, **95**, 994-1000. https://doi.org/10.1529/biophysj.107.128140

[16] Memeu, D.M., Kaduki, K.A., Mjomba, A., Muriuki, N.S. and Gitonga, L. (2013) De-tection of Plasmodium Parasites from Images of Thin Blood Smears. *Open Journal of Clinical Diagnostics*, **3**, 183-194. https://doi.org/10.4236/ojcd.2013.34034

[17] Gitonga, L., Memeu, D.M., Kaduki, K.A., Kale, M.A.C. and Muriuki, N.S. (2014) Determination of Plasmodium Parasite Life Stages and Species in Images of Thin Blood Smears Using Artificial Neural Network. *Open Journal of Clinical Diagnos-tics*, **4**, 78-88. https://doi.org/10.4236/ojcd.2014.42014

[18] Omucheni, D.L., Kaduki, K.A., Bulimo, W.D. and Angeyo, H.K. (2014) Application of Principal Component Analysis to Multispectral-Multimodal Optical Image Analy-sis for Malaria Diagnostics. *Malaria Journal*, **13**, Article No. 485. https://doi.org/10.1186/1475-2875-13-485

[19] Merdasa, A., Brydegaard, M., Svanberg, S. and Zoueu, J.T. (2013) Staining-Free Malaria Diagnostics by Multispectral and Multimodality Light-Emitting-Diode Mi-croscopy. *Journal of Biomedical Optics*, **18**, 036002. https://doi.org/10.1117/1.JBO.18.3.036002

[20] Saha, R.K., Karmakar, S. and Roy, M. (2012) Computational Investigation on the Photoacoustics of Malaria Infected Red Blood Cells. *PLoS ONE*, **7**, e51774. https://doi.org/10.1371/journal.pone.0051774

[21] Lukianova-Hleb, E.Y., Campbell, K.M., Constantinou, P.E., *et al*. (2014) Hemo-zoin-Generated Vapor Nanobubbles for Transdermal Reagent- and Needle-Free De-tection of Malaria. *Proceedings of the National Academy of Sciences of the United States of America*, **111**, 900-905. https://doi.org/10.1073/pnas.1316253111

[22] Cai, C., Carey, K.A., Nedosekin, D.A., *et al*. (2016) *In Vivo* Photoacoustic Flow Cy-tometry for Early Malaria Diagnosis: Photoacoustic Flow Cytometry for Malaria Di-agnosis. *Cytometry Part A*, **89**, 531-542. https://doi.org/10.1002/cyto.a.22854

[23] Lukianova-Hleb, E., Bezek, S., Szigeti, R., *et al*. (2015) Transdermal Diagnosis of Malaria Using Vapor Nanobubbles. *Emerging Infectious Diseases*, **21**, 1122-1127. https://doi.org/10.3201/eid2107.150089

[24] Bell, A.G. (1880) ART. XXXIV.—On the Production and Reproduction of Sound by Light. *American Journal of Science*, **20**, 305-324. https://doi.org/10.2475/ajs.s3-20.118.305

[25] Zhang, E., Laufer, J. and Beard, P. (2008) Backward-Mode Multiwavelength Pho-toacoustic Scanner Using a Planar Fabry-Perot Polymer Film Ultrasound Sensor for High-Resolution Three-Dimensional Imaging of Biological Tissues. *Applied Optics*, **47**, 561-577. https://doi.org/10.1364/AO.47.000561

[26] Song, L., Maslov, K.I., Bitton, R., Shung, K.K. and Wang, L.V. (2008) Fast 3-D Dark-Field Reflection-Mode Photoacoustic Microscopy *in Vivo* with a 30-MHz Ul-trasound Linear Array. *Journal of Biomedical Optics*, **13**, 054028. https://doi.org/10.1117/1.2976141

[27] Favazza, C.P., Wang, L.V. and Cornelius, L.A. (2011) *In Vivo* Functional Photoac-oustic Microscopy of Cutaneous Microvasculature in Human Skin. *Journal of Bio-medical Optics*, **16**, 026004. https://doi.org/10.1117/1.3536522

[28] Favazza, C.P., Wang, L.V., Jassim, O.W. and Cornelius, L.A. (2011) *In Vivo* Pho-toacoustic Microscopy of Human Cutaneous Microvasculature and a Nevus. *Jour-nal of Biomedical Optics*, **16**, 016015. https://doi.org/10.1117/1.3528661

[29] Silverman, R.H., Kong, F., Chen, Y.C., *et al*. (2010) High-Resolution Photoacoustic Imaging of Ocular Tissues. *Ultrasound in Medicine and Biology*, **36**, 733-742. https://doi.org/10.1016/j.ultrasmedbio.2010.02.006

[30] Hu, S., Rao, B., Maslov, K. and Wang, L.V. (2010) Label-Free Photoacoustic Oph-thalmic Angiography. *Optics Letters*, **35**, 1-3. https://doi.org/10.1364/OL.35.000001

[31] de La Zerda, A., Paulus, Y.M., Teed, R., *et al*. (2010) Photoacoustic Ocular Imaging. *Optics Letters*, **35**, 270-272. https://doi.org/10.1364/OL.35.000270

[32] Zhang, H.F., Puliafito, C.A. and Jiao, S. (2011) Photoacoustic Ophthalmoscopy for *in Vivo* Retinal Imaging: Current Status and Prospects. *Ophthalmic Surgery*, *Lasers and Imaging Retina*, **42**, S106-S115. https://doi.org/10.3928/15428877-20110627-10

[33] Manohar, S., Vaartjes, S.E., van Hespen, J.C.G., *et al*. (2007) Initial Results of *in Vi-vo* Non-Invasive Cancer Imaging in the Human Breast Using Near-Infrared Pho-toacoustics. *Optics Express*, **15**, 12277-12285. https://doi.org/10.1364/OE.15.012277

[34] Oraevsky, A.A., Karabutov, A.A., Solomatin, S.V., *et al*. (2001) Laser Optoacoustic Imaging of Breast Cancer *in Vivo*. *Proceedings Volume* 4256, *Biomedical Optoac-oustics II*, San Jose, 6-16. https://doi.org/10.1117/12.429300

[35] Kruger, R.A., Lam, R.B., Reinecke, D.R., Del Rio, S.P. and Doyle, R.P. (2010) Pho-toacoustic Angiography of the Breast. *Medical Physics*, **37**, 6096-6100. https://doi.org/10.1118/1.3497677

[36] Piras, D., Xia, W., Steenbergen, W., van Leeuwen, T.G. and Manohar, S. (2010) Photoacoustic Imaging of the Breast Using the Twente Photoacoustic Mammos-cope: Present Status and Future Perspectives. *IEEE Journal of Selected Topics in Quantum Electronics*, **16**, 730-739. https://doi.org/10.1109/JSTQE.2009.2034870

[37] Manohar, S., Kharine, A., van Hespen, J.C.G., Steenbergen, W. and van Leeuwen, T.G. (2005) The Twente Photoacoustic Mammoscope: System Overview and Per-formance. *Physics in Medicine & Biology*, **50**, 2543. https://doi.org/10.1088/0031-9155/50/11/007

[38] Zhang, J., Yang, S., Ji, X., Zhou, Q. and Xing, D. (2014) Characterization of Li-pid-Rich Aortic Plaques by Intravascular Photoacoustic Tomography: *Ex Vivo* and *in Vivo* Validation in a Rabbit Atherosclerosis Model with Histologic Correlation. *Journal of the American College of Cardiology*, **64**, 385-390. https://doi.org/10.1016/j.jacc.2014.04.053

[39] Wang, B., Su, J.L., Amirian, J., Litovsky, S.H., Smalling, R. and Emelianov, S. (2010) Detection of Lipid in Atherosclerotic Vessels Using Ultrasound-Guided Spectros-copic Intravascular Photoacoustic Imaging. *Optics Express*, **18**, 4889-4897. https://doi.org/10.1364/OE.18.004889

[40] Jansen, K., van Soest, G. and van der Steen, A.F. (2014) Intravascular Photoacoustic Imaging: A New Tool for Vulnerable Plaque Identification. *Ultrasound in Medicine and Biology*, **40**, 1037-1048. https://doi.org/10.1016/j.ultrasmedbio.2014.01.008

[41] Allen, T.J. and Beard, P.C. (2009) Photoacoustic Characterisation of Vascular Tissue at NIR Wavelengths. *Proceedings Volume* 7177, *Photons plus Ultrasound*: *Imaging and Sensing* 2009, San Jose, 71770A. https://doi.org/10.1117/12.808777

[42] Jansen, K., Wu, M., van der Steen, A.F. and van Soest, G. (2014) Photoacoustic Im-aging of Human Coronary Atherosclerosis in Two Spectral Bands. *Photoacoustics*, **2**, 12-20. https://doi.org/10.1016/j.pacs.2013.11.003

[43] Allen, T.J., Beard, P.C., Hall, A., Dhillon, A.P. and Owen, J.S. (2012) Spectroscopic Photoacoustic Imaging of Lipid-Rich Plaques in the Human Aorta in the 740 to 1400 nm Wavelength Range. *Journal of Biomedical Optics*, **17**, 061209. https://doi.org/10.1117/1.JBO.17.6.061209

[44] Funke, A. (2010) On the Feasibility of Photoacoustic Guidance of High Intensity Focused Ultrasound. Optics [physics.optics]. Université Pierre et Marie Curie, Paris.

[45] Bossy, E., Daoudi, K. and Boccara, A.-C. (2006) Time Reversal of Photoacoustic Waves. *Applied Physics Letters*, **89**, 184108. https://doi.org/10.1063/1.2382732

[46] Xia, J., Yao, J. and Wang, L.V. (2014) Photoacoustic Tomography: Principles and Advances. *Progress in Electromagnetics Research*, **147**, 1-22. https://doi.org/10.2528/PIER14032303

[47] Hu, S. (2010) Optical-Resolution Photoacoustic Microscopy. Washington Universi-ty, St. Louis.

[48] Maslov, K., Zhang, H.F., Hu, S. and Wang, L.V. (2008) Optical-Resolution Pho-toacoustic Microscopy for *in Vivo* Imaging of Single Capillaries. *Optics Letters*, **33**, 929-931. https://doi.org/10.1364/OL.33.000929

[49] Wang, L.V. and Hu, S. (2012) Photoacoustic Tomography: *In Vivo* Imaging from Organelles to Organs. *Science*, **335**, 1458-1462. https://doi.org/10.1126/science.1216210

[50] Fan, Y., Mandelis, A., Spirou, G. and Alex Vitkin, I. (2004) Development of a Laser Photothermoacoustic Frequency-Swept System for Subsurface Imaging: Theory and Experiment. *The Journal of the Acoustical Society of America*, **116**, 3523-3533. https://doi.org/10.1121/1.1819393

[51] Mohajerani, P., Kellnberger, S. and Ntziachristos, V. (2014) Frequency Domain Optoacoustic Tomography Using Amplitude and Phase. *Photoacoustics*, **2**, 111-118. https://doi.org/10.1016/j.pacs.2014.06.002

[52] Maslov, K.I. and Wang, L.V. (2008) Photoacoustic Imaging of Biological Tissue with Intensity-Modulated Continuous-Wave Laser. *Journal of Biomedical Optics*, **13**, 024006. https://doi.org/10.1117/1.2904965

[53] Baddour, N. (2008) Theory and Analysis of Frequency-Domain Photoacoustic To-mography. *The Journal of the Acoustical Society of America*, **123**, 2577-2590. https://doi.org/10.1121/1.2897132

[54] LeBoulluec, P., Liu, H. and Yuan, B. (2013) A Cost-Efficient Frequency-Domain Photoacoustic Imaging System. *American Journal of Physics*, **81**, 712. https://doi.org/10.1119/1.4816242

[55] Yao, J. and Wang, L.V. (2014) Sensitivity of Photoacoustic Microscopy. *Photoac-oustics*, **2**, 87-101. https://doi.org/10.1016/j.pacs.2014.04.002

[56] Beard, P. (2011) Biomedical Photoacoustic Imaging. *Interface Focus*, rsfs20110028. https://doi.org/10.1098/rsfs.2011.0028

[57] Guo, Z., Hu, S. and Wang, L.V. (2010) Calibration-Free Absolute Quantification of Optical Absorption Coefficients Using Acoustic Spectra in 3D Photoacoustic Mi-croscopy of Biological Tissue. *Optics Letters*, **35**, 2067-2069. https://doi.org/10.1364/OL.35.002067

[58] Zhou, Y., Yao, J., Maslov, K.I. and Wang, L.V. (2014) Calibration-Free Absolute Quantification of Particle Concentration by Statistical Analyses of Photoacoustic Signals *in Vivo*. *Journal of Biomedical Optics*, **19**, 037001. https://doi.org/10.1117/1.JBO.19.3.037001

[59] Laufer, J., Elwell, C., Delpy, D. and Beard, P. (2005) Measurements of Absolute Blood Oxygen Saturation Using Pulsed Near-Infrared Photoacoustic Spectroscopy:
Accuracy and Resolution. *Physics in Medicine & Biology*, **50**, 4409-4428.

https://doi.org/10.1088/0031-9155/50/18/011

[60] Laufer, J., Cox, B., Zhang, E. and Beard, P. (2010) Quantitative Determination of Chromophore Concentrations from 2D Photoacoustic Images Using a Nonlinear Model-Based Inversion Scheme. *Applied Optics*, **49**, 1219-1233. https://doi.org/10.1364/AO.49.001219

[61] Bauer, A.Q., Nothdurft, R.E., Erpelding, T.N., Wang, L.V. and Culver, J.P. (2011) Quantitative Photoacoustic Imaging: Correcting for Heterogeneous Light Fluence Distributions Using Diffuse Optical Tomography. *Journal of Biomedical Optics*, **16**, 096016. https://doi.org/10.1117/1.3626212

[62] Laufer, J., Delpy, D., Elwell, C. and Beard, P. (2007) Quantitative Spatially Resolved Measurement of Tissue Chromophore Concentrations Using Photoacoustic Spec-troscopy: Application to the Measurement of Blood Oxygenation and Haemoglobin Concentration. *Physics in Medicine & Biology*, **52**, 141-168. https://doi.org/10.1088/0031-9155/52/1/010

[63] Cox, B.T., Laufer, J.G., Beard, P.C. and Arridge, S.R. (2012) Quantitative Spectros-copic Photoacoustic Imaging: A Review. *Journal of Biomedical Optics*, **17**, Article No. 061202. https://doi.org/10.1117/1.JBO.17.6.061202

[64] Galanzha, E.I., Shashkov, E.V., Kelly, T., Kim, J.-W., Yang, L. and Zharov, V.P. (2009) *In Vivo* Magnetic Enrichment and Multiplex Photoacoustic Detection of Cir-culating Tumour Cells. *Nature Nanotechnology*, **4**, 855-860. https://doi.org/10.1038/nnano.2009.333

[65] Galanzha, E.I., Shashkov, E.V., Spring, P.M., Suen, J.Y. and Zharov, V.P. (2009) *In Vivo*, Noninvasive, Label-Free Detection and Eradication of Circulating Metastatic Melanoma Cells Using Two-Color Photoacoustic Flow Cytometry with a Diode La-ser. *Cancer Research*, **69**, 7926-7934. https://doi.org/10.1158/0008-5472.CAN-08-4900

[66] Zharov, V.P., Galanzha, E.I., Shashkov, E.V., Khlebtsov, N.G. and Tuchin, V.V. (2006) *In Vivo* Photoacoustic Flow Cytometry for Monitoring of Circulating Single Cancer Cells and Contrast Agents. *Optics Letters*, **31**, 3623-3625. https://doi.org/10.1364/OL.31.003623

[67] Galanzha, E.I., Kim, J. and Zharov, V.P. (2009) Nanotechnology-Based Molecular Photoacoustic and Photothermal Flow Cytometry Platform for *In-Vivo* Detection and Killing of Circulating Cancer Stem Cells. *Journal of Biophotonics*, **2**, 725-735. https://doi.org/10.1002/jbio.200910078

[68] Sergey, A.T. and Andreas, M. (2006) Fourier-Domain Biophotoacoustic Subsurface Depth Selective Amplitude and Phase Imaging of Turbid Phantoms and Biological Tissue. *Journal of Biomedical Optics*, **11**, 1083-3668. https://doi.org/10.1117/1.2337290

[69] Edem, D., Bahman, L., Choi, S.S., Andreas, M., Wei, S. and Liu, F.-F. (2017) Quan-titative Phase-Filtered Wavelength-Modulated Differential Photoacoustic Radar Tumor Hypoxia Imaging toward Early Cancer Detection. *Journal of Biophotonics*, **10**, 1134-1142. https://doi.org/10.1002/jbio.201600168

[70] Sung, S. (Sean), Mandelis, A., Xinxin, G., Bahman, L., Stephan, K. and Vasilis, N. (2015) Wavelength-Modulated Differential Photoacoustic Spectroscopy (WM-DPAS) for Noninvasive Early Cancer Detection and Tissue Hypoxia Monitoring. *Journal of Biophotonics*, **9**, 388-395. https://doi.org/10.1002/jbio.201670040

[71] Laufer, J., Zhang, E. and Beard, P. (2007) Quantitative *in-Vivo* Measurements of Blood Oxygen Saturation Using Multiwavelength Photoacoustic Imaging. *Proceed- ings Volume* 6437, *Photons Plus Ultrasound: Imaging and Sensing* 2007: *The Eighth Conference on Biomedical Thermoacoustics*, *Optoacoustics*, *and Acousto-Optics*, San Jose, 64371Z. http://proceedings.spiedigitallibrary.org/proceeding.aspx?articleid=1296725 https://doi.org/10.1117/12.700297

[72] Wang, X., Xie, X., Ku, G., Wang, L.V. and Stoica, G. (2006) Noninvasive Imaging of Hemoglobin Concentration and Oxygenation in the Rat Brain Using High-Resolution Photoacoustic Tomography. *Journal of Biomedical Optics*, **11**, 024015. https://doi.org/10.1117/1.2192804

[73] Zhang, H.F., Maslov, K., Sivaramakrishnan, M., Stoica, G. and Wang, L.V. (2007) Imaging of Hemoglobin Oxygen Saturation Variations in Single Vessels *in Vivo* Using Photoacoustic Microscopy. *Applied Physics Letters*, **90**, Article No. 053901. https://doi.org/10.1063/1.2435697

[74] Song, W., Wei, Q., Liu, W., *et al*. (2015) A Combined Method to Quantify the Re-tinal Metabolic Rate of Oxygen Using Photoacoustic Ophthalmoscopy and Optical Coherence Tomography. *Scientific Reports*, **4**, Article No. 6525. https://doi.org/10.1038/srep06525

[75] Tang, M., Zhou, Y., Zhang, R. and Wang, L.V. (2015) Noninvasive Photoacoustic Microscopy of Methemoglobin *in Vivo*. *Journal of Biomedical Optics*, **20**, Article No. 036007. https://doi.org/10.1117/1.JBO.20.3.036007

[76] Wang, L., Maslov, K. and Wang, L.V. (2013) Single-Cell Label-Free Photoacoustic Flowoxigraphy *in Vivo*. *Proceedings of the National Academy of Sciences of the United States of America*, **110**, 5759-5764. https://doi.org/10.1073/pnas.1215578110

[77] Winkler, A.M., Maslov, K. and Wang, L.V. (2013) Towards Single Molecule Detec-tion Using Photoacoustic Microscopy. *Proceedings Volume* 8581, *Photons plus Ul-trasound*: *Imaging and Sensing* 2013, San Francisco, 85811A. http://proceedings.spiedigitallibrary.org/proceeding.aspx?articleid=1660845

[78] Tuchin, V.V. (2011) Advanced Optical Flow Cytometry: Methods and Disease Di-agnoses. John Wiley & Sons, Hoboken. https://doi.org/10.1002/9783527634286

[79] Wang, T., Nandy, S., Salehi, H.S., Kumavor, P.D. and Zhu, Q. (2014) A Low-Cost Photoacoustic Microscopy System with a Laser Diode Excitation. *Biomedical Optics Express*, **5**, 3053-5058. https://doi.org/10.1364/BOE.5.003053

[80] Allen, T.J. and Beard, P.C. (2007) Dual Wavelength Laser Diode Excitation Source for 2D Photoacoustic Imaging. *Proceedings Volume* 6437, *Photons plus Ultrasound*: *Imaging and Sensing* 2007: *The Eighth Conference on Biomedical Thermoacoustics*, *Optoacoustics*, *and Acousto-Optics*, San Jose, 64371U. https://doi.org/10.1117/12.698651

[81] Kolkman, R.G.M., Steenbergen, W. and van Leeuwen, T.G. (2006) *In Vivo* Photoac-oustic Imaging of Blood Vessels with a Pulsed Laser Diode. *Lasers in Medical Science*, **21**, 134-139. https://doi.org/10.1007/s10103-006-0384-z

[82] Allen, T.J. and Beard, P.C. (2013) Light Emitting Diodes as an Excitation Source for Biomedical Photoacoustics. *Proceedings Volume* 8581, *Photons plus Ultrasound*: *Im-aging and Sensing* 2013, San Francisco, 85811F. https://doi.org/10.1117/12.2004471

[83] Deán-Ben, X.L. and Razansky, D. (2013) Functional Optoacoustic Human Angio-graphy with Handheld Video Rate Three Dimensional Scanner. *Photoacoustics*, **1**, 68-73. https://doi.org/10.1016/j.pacs.2013.10.002

[84] Zhou, Y., Li, G., Zhu, L., Li, C., Cornelius, L.A. and Wang, L.V. (2015) Handheld Photoacoustic Probe to Detect Both Melanoma Depth and Volume at High Speed *in Vivo*. *Journal of Biophotonics*, **8**, 961-967. https://doi.org/10.1002/jbio.201400143

[85] Singh, M.K.A., Steenbergen, W. and Manohar, S. (2016) Handheld Probe-Based Dual Mode Ultrasound/Photoacoustics for Biomedical Imaging. In: Olivo, M. and Dinish, U., Eds., *Frontiers in Biophotonics for Translational Medicine*, Vol. 3, Sprin-ger, Singapore, 209-247. https://doi.org/10.1007/978-981-287-627-0_7

[86] Daoudi, K., van den Berg, P.J., Rabot, O., *et al*. (2014) Handheld Probe Integrating Laser Diode and Ultrasound Transducer Array for Ultrasound/Photoacoustic Dual Modality Imaging. *Optics Express*, **22**, 26365. https://doi.org/10.1364/OE.22.026365

Scientific Research Publishing

Open Journal of Clinical Diagnostics, 2021, 11, 59-75

https://www.scirp.org/journal/ojcd

ISSN Online: 2162-5824

ISSN Print: 2162-5816

Review of Photoacoustic Malaria Diagnostic Techniques

Daniel Maitethia Memeu[1,2], Abdallah Merenga Sallorey[2], Ciira Maina[3], Dickson Mwenda Kinyua[1,4]

[1]Department of Physical Sciences, Meru University of Science and Technology, Meru, Kenya

[2]Department of Physics, Kenyatta University, Nairobi, Kenya

[3]Dedan Kimathi University of Technology, Nyeri, Kenya

[4]Department of Pure and Applied Sciences, Kirinyaga University, Kerugoya, Kenya

Email: danielmaitethia@gmail.com

How to cite this paper: Memeu, D.M., Sallorey, A.M., Maina, C. and Kinyua, D.M. (2021) Review of Photoacoustic Malaria Diagnostic Techniques. *Open Journal of Clinical Diagnostics*, **11**, 59-75. https://doi.org/10.4236/ojcd.2021.112005

Received: October 6, 2020

Accepted: June 26, 2021

Published: June 29, 2021

Abstract

Malaria is one of the leading causes of mortality and morbidity in developing countries. Accurate and complete diagnosis is key for effective treatment of the disease. However, mainstream malaria diagnostic techniques suffer from a number of shortcomings. There is therefore an urgent need for develop-ment of new and more efficient techniques for malaria diagnosis. *In vivo* Photoacoustic spectroscopy is an emerging technique, which has great poten-tial of delivering a nearly ideal method for early diagnosis of the disease. The technique promises to be highly sensitive and specific. In this paper, a de-scription of photoacoustic malaria sensing is given. This is followed by a re-view of photoacoustic-based malaria diagnostic techniques and suggestions for future improvements.

Keywords

Plasmodium parasites, In Vivo, Chromophores, Hemoglobin, Hemozoin, Spectroscopic Inversion, Time Domain and Frequency Domain Photoacoustics

1. Introduction

1.1. Background of Malaria Disease

Malaria is a common disease in tropical countries that poses serious public health concerns. It is one of the leading causes of mortality globally. Nearly 0.5 million deaths were attributed to the disease in the year 2015 according to the world malaria report [1]. The majority of these deaths comprise of children less than five years old from sub-Saharan Africa. Besides, it is estimated that approx-imately 200 million people are infected with the disease and 3.2 billion people are at risk of contracting the disease annually according to the report. This has created a heavy social-economic burden to the affected countries due to huge treatment costs and absenteeism from work and schools [2].

The disease is caused by protozoan parasites of the genus *Plasmodium* which lives in peripheral blood, spleen or liver of humans. The parasites are introduced to the human host through bites by infected mosquitoes—malaria vectors. Once in the bloodstream, the parasites move to the liver for incubation and multipli-cation. They later move back to the bloodstream and attack the Red Blood Cells (RBCs). The parasites feed on the cells' hemoglobin reducing or completely in-hibiting the cells' ability to bind oxygen.

Hemoglobin is a complex bio-molecule made of two simpler molecules; the iron compound called heme and a protein molecule globin. The parasite digests globin to meet its nutritional needs but converts heme (which is toxic to the parasite [3]) into a by-product called he-mozoin. Hemozoin, an inert insoluble crystal composed of iron nano-rods [4], is then deposited in parasites' food vacuoles. Presence of hemozoin in RBCs in pe-ripheral blood is, therefore, an indicator of malaria infection. Notably, hemozoin production is also associated with other blood-feeding parasites such as *Schisto-soma mansoni* and *Rhodnius prolixus* [5] [6]. *However,* neither Schistosoma-mansoni nor Rhodniusprolixus resides in peripheral blood.

There are five species of *Plasmodium* parasites that infect humans [7], name-ly; *Plasmodium falciparum*, *Plasmodium ovale*, *Plasmodiumvivax*, *Plasmodium malariae*, and *Plasmodium knowlesi*. *Plasmodium falciparum* is the most fatal while other species cause mild to moderate illnesses. Each of the five species has distinct morphological features which are used for *Plasmodium* parasites species identification during optical microscopy diagnosis. The parasites undergo three main inter-erythrocyte life stages, namely; the early stage is also known as ring stage, intermediate stage also called trophozoite stage and Mature stage also called schizont stage (the reproductive stage). Upon maturity of the parasites, the infected cells' rapture and the merozoites (offspring of the parasites) are re-leased into the bloodstream where they attack other health erythrocytes and the cycle starts afresh. However, some *Plasmodium* merozoites formed during asex-ual reproduction of the schizonts differentiate to become the sexual form of the parasites (gametocytes) that are taken up by mosquitoes during blood meals and aid in the transmission of the disease [8]. **Figure 1** [9] shows the life cycle of the *Plasmodium* parasite in the human host.

1.2. Malaria Diagnostic Techniques

Malaria diagnosis entails detection of the presence of the *Plasmodium* parasites in the patient blood and determination of the following parameters; species, life stages, and parasitemia estimation—an indicator of disease severity given by ei-ther the number of *Plasmodium* parasites or the number of infected erythrocytes

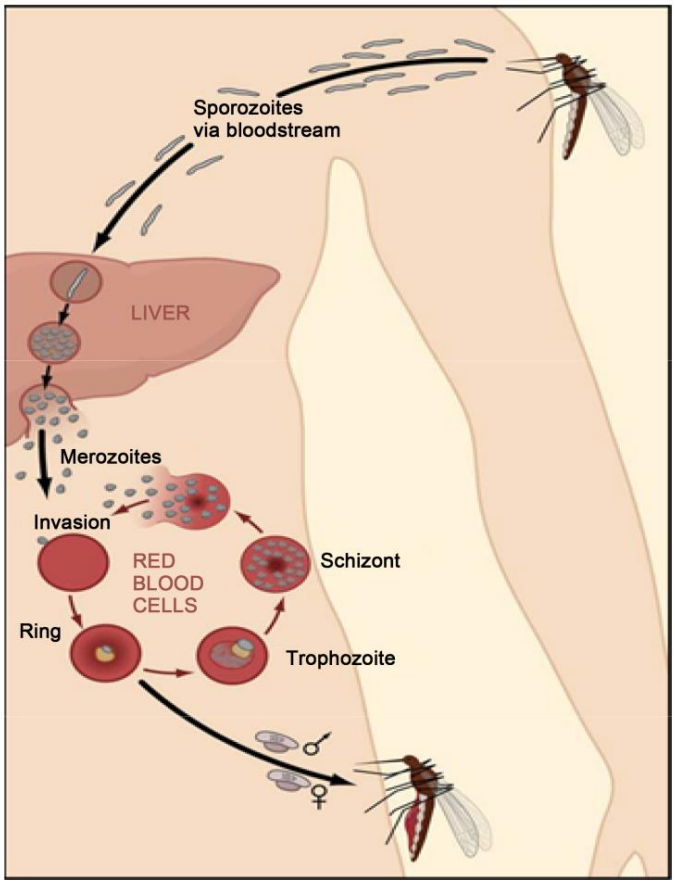

Figure 1. *Plasmodium* life cycle in the human host. Sporozoites are re-leased into the blood by the mosquito, they are delivered to the liver for incubation and multiplication. After multiplication, the merozoites are released into the blood to attach red blood cells. While in the red blood cells they feed on hemoglobin, undergo cell division and eventually make the cell rapture for the merozoite to be released and attach more cells. Some merozoites differentiate to be the sexual form and these are the ones that the mosquito takes during blood meal to perpetuate transmis-sion. The diagram is adopted from ref [9].per unit volume of blood. A number of malaria diagnostic techniques exist and more are under development. The gold standard method is optical microscopy

[11]. The technique involves examination of stained blood smear samples using a light microscope to aid visualization of *Plasmodium* parasites in eryt-hrocytes. Labeling (staining) of blood smear samples with Giemsa is undertaken prior to examination of the slides. Staining helps to highlight the parasites' pig-ment (hemozoin) and hence makes the parasites conspicuous. This technique is time-consuming and labor-intensive due to the need for sample preparation and the enumeration of detected parasites in the microscope field of view. A single malaria test takes between 30 to 60 minutes. In addition, reliability of the results from this method depends on the experience of the microscope operator.

Other malaria diagnostic methods include; Polymerase Chain Reaction (PCR) based technique [12], *Plasmodium* parasite antigen detection based technique also referred as Rapid Diagnostic Test (RDT) [13] and Fluorescence microsco-py-based techniques [11]. Antigen-based technique is widely used and boasts of a relatively fast detection speed of about fifteen minutes. However, the technique has low parasite detection sensitivity and specificity especially when the parasite load is low in the blood. The test is also relatively expensive with a single test costing about 1US$. In contrast, PCR technique has high detection sensitivity and specificity. It probes and amplifies genetic material of the *Plasmodium* para-sites present in the blood. However, the technique demands the use of sophisti-cated equipments and expensive reagents. Besides, a highly skilled operator is also required to perform the test. The technique is therefore used in research la-boratories and confirmation of malaria tests. Fluorescent based technique relies on staining of blood smears with a fluorescent dye that would highlight the pa-rasite nucleus. A fluorescent microscope is then used to observe the stained blood sample. The technique has also not yet found wide clinical adoption in malaria screening due to high cost of equipment, reagents and demand for highly skilled expertise.

Some of the malaria diagnostic techniques reported by literature as being un-der development include; Third Harmonic Generation (THG) technique [14], Magneto-optic based technique [15], and computer vision assisted optical mi-croscopy technique [16] [17]. Label-free optical microscopy using multispectral imaging and chemometrics techniques has also been explored [18] [19]. Recent-ly, a few publications have reported on the development of Photo-Thermal (PT) and Photo-Acoustic (PA) based techniques for *in vivo* malaria diagnosis [4] [20]

[22] [23]. Preliminary results regarding the techniques' performance are impressive but more work is needed before the method can be clinically accepted for malaria screening.

Generally, the mainstream malaria diagnostic techniques suffer from a num-ber of shortcomings [10] [11] which include low detection sensitivity and speci-ficity, labor and time intensiveness and demand for reagents and sophisticated equipments which are often expensive and inaccessible to people in resource scarce settings where often malaria is endemic. There is therefore an urgent need for development of new and more efficient techniques for malaria diagnosis. The remaining part of this paper explains in detail the principle behind photoacous-tic-based malaria diagnostic technique and the reported progress.

= Photoacoustic Effect and Its Application in Biomedical Imaging and Diagnostics

Photoacoustic effect is a process in which acoustic waves in the Ultrasound (US) frequency range are emitted upon absorption of optical radiation by chromo-phores (light absorbing molecules). The phenomenon was first reported in 1880 by Alexander Graham Bell [24]. Photoacoustic effect involves conversion of the absorbed optical energy to thermal energy which leads to temperature rise and thermo-elastic expansion in the irradiated region. Consequently, a transient pres-sure wave is generated and propagates through the sample. Reported biomedical applications of the technique include; anatomical and functional imaging of bi-ological tissue [25]-[32], disease diagnostics [33]-[43] as well as guidance and monitoring of therapeutic interventions [44] [45].

Efficient generation of PA signals demands two conditions to be satisfied; thermal and stress confinement [46]. This means that both heat conduction and thermo-elastic expansion are confined within the illuminated tissue region dur-ing optical excitation time span. Generation of PA waves therefore requires use of either Time Domain (TD) techniques (where short optical pulses, typically in nanosecond range are used to excite the sample) [46] [47] [48] [49] or Frequen-cy Domain (FD) techniques where intensity modulated Continuous Wave (CW) laser light is used to generate ultrasonic pressure waves in tissue [50] [51] [52]

[54]. In the case of FD techniques, either fixed frequency or linearly varying frequency (Chirped) optical signals are used to excite the sample. Use of pulsed optical beam produces stronger PA signals compared to fixed frequency intensi-ty modulated optical excitation [55]. However, Chirped optical excitation com-bined with lock-in detection have been reported to yield PA signals whose Signal to Noise Ratio (SNR) is comparable to that of pulsed excitation [50]. They also have other salient advantages such as; wide dynamic range which implies low energy optical sources can be used and this has a congruent advantage of mini-mizing the risk of tissue damage due to excessive optical exposure, depth tenabili-ty, and capability to use continuous wave diode lasers as opposed to bulky and expensive pulsed lasers. Both TD and chirped FD techniques can be used for tissue depth profilometry as they carry time of flight information.

Intensity of the generated PA waves is a measure of the tissue's optical absorp-tion coefficient μ_a —a parameter which infers the molecular composition and molar concentration of the constituent tissue chromophores (see Equation (1)) as well as the tissues mechanical and thermal properties [56]. To perform quan-titative photoacoustic

spectroscopy, the tissue should be excited by multispectral optical radiation (pulsed or intensity modulated) and the acoustic waves induced by each optical wavelength detected by either a focused ultrasonic transducer or transducer arrays placed in close proximity to the sample being probed. The signal is then amplified and processed to compensate for signal attenuation in the medium and the detector response. Spectroscopic inversion of the recovered initial photoacoustic pressure intensity $P_0^{\lambda_i}$ (see Equation (2)) is then per-formed to determine sample properties such as optical absorption coefficient spa-tial distribution map, molecular composition, or concentration of chromophores in the sample. Some of the reported literature on these subjects can be found in references [57]-[63].

Photoacoustic imaging and sensing boasts of a number of advantages over other imaging modalities [56]; first is high spatial resolution and sharp image contrast due to low scattering of the generated ultrasonic signal and high optical absorption sensitivity by bio-molecules. Second is the ability to perform mul-ti-scale imaging hence yielding images of varying spatial resolution (from sub-micrometer to centimeter scale) and therefore enabling imaging of cell orga-nelles, cells, tissues and organs of the same specimen using a single imaging mod-ality. This has the potential to enable simultaneous studies of biological pheno-mena at varying spatial and time scales with minimal intra-subject variability. Since non-ionizing optical radiation is used to excite the tissue, the technique is safe. It is also relatively cheap compared to other medical imaging modalities such as Nuclear Magnetic Resonance Imaging (NMRI) and X-Ray Computed Tomography (X-Ray CT). Recently, Photoacoustic Flow Cytometry (PAFC) has been proposed for detection of Circulating Tumor Cells (CTC) [64] [65] [66] [67]. The technique has also been explored for malaria diagnosis [21] [22] [23].

2.1. Malaria Diagnosis Using Photoacoustics

The major chromophores in malaria infected blood are total hemoglobin (Hbt) and hemozoin [20]. Hbt is the sum of oxy-hemoglobin (HbO_2) and deoxy-he-moglobin (Hb) molecules in the blood. **Figure 2** is an excerpt of the spectral plots of hemozoin (Hz) and Hemoglobin (Hb) extracted from the work of saha *et al.* [16], *and* Cai *et al.* [18]. **Table 1** gives values of the optical absorption coef-ficients and molar concentrations of Hemozoin (Hz) in an infected erythrocyte

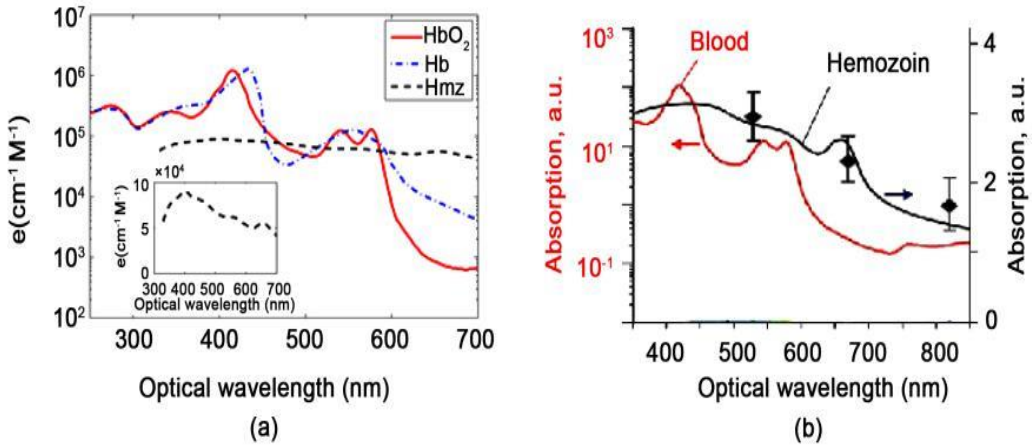

Figure 2. (a) Molar extinction coefficients of oxyhemoglobin, deoxyhemoglobin, and hemozoin [20], the inset is a zoomed up view of the hemozoin spectrum showing its cha-racteristic peaks. (b) 70% oxygenated blood and hemozoin [22].

Table 1. Optical absorption coefficients and molar concentration of hemozoin in both healthy and *Plasmodium* infected erythrocytes. Values of μ_a are extracted from [20].

	Optical Absorption Coefficients μ_a (cm^{-1})		**Hemozoin Molar concentration (*M*)**
	λ = 434 nm	**λ = 700 nm**	
Healthy erythrocyte	6351.59	20.47	0
Ring stage infected erythrocyte	6075.31	40.22	5.3×10^{-13}
Trophozoite infected erythrocyte	4239.99	171.41	6.2×10^{-12}
Schizont infected erythrocyte	2858.57	270.15	1.7×10^{-11}

as extracted from the work of Saha *et al*. [20]. Based on the values of molar con-centration of Hz present in the cell, it is possible to differentiate various stages of infection. Previous studies have demonstrated the possibility of *in vivo* imaging of oxygen saturation and malignant tumor hypoxia [50] [68]-[73], oxygen me-tabolic rate

[74], methemoglobin [75] and oxygen release rate in blood vessels and individual erythrocytes using sub-wavelength Optical Resolution Photoac-oustic Microscope (OR-PAM) [76]. This suggests that a similar approach can be used to detect the presence of other dominant optical absorbers in individual erythrocytes such as hemozoin in case of malaria.

The following is a brief analysis of the problem. Optical absorption coefficient due to a malaria infected erythrocyte can be described by the following equation.

$$\mu_a^{\lambda i} = \varepsilon_{Hz}^{\lambda i} [c_{Hz}] + \varepsilon_{tHb}^{\lambda i} [c_{tHb}] \quad (1)$$

$\varepsilon_i^{\lambda_i}$ is the molar extinction coefficient of the i^{th} chromophore present in the cell. Both μ_a and ε are wavelength dependent hence the superscript λ_i . $[c_i]$ is the molar concentration of the i^{th} bio-molecule in the cell. The initial pho-toacoustic signal generated due to absorption of an optical pulse of wavelength λ_i is the product of the deposited optical energy $A_e = \mu_a^{\lambda_i} \Phi^{\lambda_i}$ and a factor called gruneisen parameter (Γ). Φ is the local optical fluence distribution in the blood which depends on the intensity of the incident light as well as blood opti-cal properties (mainly, optical absorption and scattering coefficients). In case the chromophore relaxation after photon absorption is not 100% non-radiative, a down scaling factor is included in the product to account for the fraction of photon energy converted to heat energy. Therefore, the initial PA pressure is given by the following equation [63].

$$P_0^{\lambda i} = \Gamma n_{th} \mu_a^{\lambda i} \Phi^{\lambda i} \quad (2)$$

W i th the transformed thermal energy density due to non-radiative relaxation of chromophores given by

$H = n_{th} \mu_{a\lambda i} \Phi_{\lambda i}$

n_{th} is the fraction of optical energy converted to heat energy ($n_{th} = 1$ for non-fluorescent and non-photoluminescent chromophores). The grueneisen parameter is a thermodynamic quantity which gives the photoacoustic efficiency of the tissue, *i.e*., the fraction of the thermal energy converted to acoustic waves.

The generated acoustic signal P_o (also referred as initial PA pressure) propa-gates through the tissue and is detected by an ultrasonic transducer placed at the tissue surface, a distance r from the target absorber (in this case a skin subsur- face blood vessel). The detected acoustic signal, P_d differs from the initial PA signal due to; acoustic attenuation through the tissue, partial detection geometry of the traducer and the transducer's detection efficiency η (f) . The transducer output signal, P_d is therefore a product of the initial signal, P_o and a scaling fac tor, T_d which accounts for the described signal attenuation *i.e*.,

$$P_d(f) = T_d(f)\,P_o \qquad (4)$$

With where; *NA* is the traducers' numerical aperture, l is its focal length and α_o is the tissue attenuation coefficient. Numerical values for the parameters in Equa-tion (4) for some commercially available ultrasonic transducers can be found in reference [77].

2.2. Reported Work

A limited number of studies have so far been carried out regarding *in vivo* pho-toacoustic diagnosis of malaria. Generally, the principle of *in vivo* Photoacoustic Flow Cytometry (PAFC) [78] has been adopted. The technique entails use of a focused ultrasonic transducer to detect PA signals emitted due to optical excita-tion of the flowing erythrocytes in blood vessels located below the skin surface. The signal peak intensity is monitored in time to keep track of the flowing eryt-hrocytes (infected and non-infected). Healthy erythrocytes produce a nearly constant amplitude signal. Hemozoin – an endogenous malaria biomarker has either higher or lower optical absorption than hemoglobin depending on the optical wavelength used. This implies that the amplitude of *Plasmodium* infected blood would differ from that of healthy blood. The following is a brief review of the few reported literature.

Cai *et al*. [22] proposed an *in vivo* (PAFC) technique for early diagnosis of malaria. They used a focused US transducer for detection of PA signal from flowing erythrocytes irradiated by three pulsed laser lights of wavelengths 532 nm, 671 nm, and 820 nm. The signal was then amplified, digitized and loaded to a PC for processing.

The system's spatial resolution was reported to be be-tween 1 - 6 μm. Both *in vitro* and *in vivo* experiments using mice as the animal model were conducted to determine the sensitivity of the device. The authors reported that their technique was 1000 times more sensitive than optical micro-scopy method and could detect an infected erythrocyte 3 hours after inoculation of *Plasmodium* parasites into a healthy mouse compared to 3 days taken before detection using optical microscopy. They observed that when the optical energy used was increased beyond a certain threshold, hemozoin vapor nano-bubble formation occurred in the infected cells and this produced PA signal of in-creased intensity—a process termed as nonlinear photoacoustics. They also used the process to perform real time destruction of infected cells (photo-thermal malaria therapy) while monitoring the efficiency of the therapy. They observed that the PA signal ratio of infected cells to non-infected cells was highest at 671 nm optical excitation wavelength.

Lukianova-Hleb *et al*. (2014) [21] described a picosecond pulsed laser tech-nique for generation and detection of Hemozoin induced Vapor Nano-Bubbles (H-VNB). The authors argued that when hemozoin crystals in infected RBCs absorbs the ultra-short pulsed radiation (having picoseconds range pulse width) of sufficient energy, nano-volume liquid around the hemozoin crystals is over-heated and vaporized resulting in generation of transient vapor bubbles which undergo explosive expansion and collapsing—a process that is accompanied by emission of high intensity acoustic waves. Both *in vitro* and *in vivo* sets of he-mozoin positive and hemozoin negative samples consisting of blood smears, whole blood and live mice were studied. Laser pulses were shone on samples and the emitted acoustic waves detected by an ultrasonic transducer. The transducer output was coupled to a digital oscilloscope. The detected signal was then ana-lyzed in the time domain. It was found that samples containing hemozoin pro-duced acoustic signals of higher amplitudes than hemozoin negative samples. It was reported that the technique yielded high correlation in differentiating *Plas-modium* parasite life stages and parasitemia estimation in comparison with opt-ical microscopy. The optical wavelength used for excitation of PA signals was 672 nm—an absorption peak for hemozoin. The optical energies per pulse used for *in vitro* and *in vivo* experiments were 10 μJ and 15 μJ respectively. Lukiano-va-Hleb *et al*. (2015) [23] used the technique for *in vivo* detection of parasites in humans and infected mosquitoes. Similar results were obtained.

In general, photoacoustic based malaria diagnosis boasts of several advantages over other diagnostic methods which includes; use of endogenous contrast agent (hemozoin) for parasite detection as opposed to exogenous contrast agents as is the case in optical

microscopy, potential for *in vivo* diagnosis. Use of non-ionizing radiation, which makes it safe, real time monitoring and capability for early de-tection of the disease hence making treatment more effective. In addition, it is possible to use the technique for diagnosis of other blood related disease. How-ever, the reported photoacoustic diagnostic systems suffer from a number of challenges which must be addressed before the technology can be clinically adopted. For example, the technique cannot perform quantitative measurement of chromophore molar concentration in absolute units. In most of the reported work [21] [22] [23], the distinction between healthy and diseased samples is made based on the relative amplitudes values of the induced PA signal between the two sets of samples. The limitation of this approach is wide signal amplitudes variability within subjects of the same class, which makes system calibration dif-ficult. Secondly, the reported PA systems are bulky and expensive due to the demand for high-energy nanosecond pulsed multispectral laser sources, high frequency sensitive ultrasonic transducers and lock-in amplifiers. Besides, the use of fluence estimation models for quantitative PA spectroscopy makes the mea-surements time intensive and quasi real time. Their accuracy also depends on how well the tissue geometry is known a priori.

There is a promising trend in addressing these challenges going by the num-ber of publications and research groups working on the problem. Simplification of PA hardware has been attempted by substitution of the bulky and expensive Optical Parametric Oscillator (OPO) tuned laser sources with much smaller and cheap diode laser sources [79] [80] [81] and Light Emitting Diodes (LEDs) [82] that have a wide range of optical wavelengths and are commercially available. Notably, Quantellaser^{TM} has developed a compact high energy multispectral pulsed diode laser module operating in four different wavelengths (808, 915, 940 or 980 nm) in the NIR region customized for PA applications. Its high optical pulse energy (of 1 mJ per emitted wavelength per 80 nS pulse width) is achieved by stacking multiple diode lasers of the same wavelength. Attempts to develop a compact hand held photoacoustic probe for *in vivo* imaging have also been re-ported [83] [84] [85] [86].

Use of chirped FD techniques in photoacoustic spectroscopy applications [50] has the potential of simplifying the instrumentation complexity of the PA systems by enabling use of cheap and portable CW diode lasers as PA optical sources. Moreover, eliminate the need for computationally demanding numeri-cal algorithms for fluence estimation. Development of a sensitive FD photoac-oustic technique for hypoxia monitoring and early cancer detection has been reported [34] [35]. The technique is termed as Wavelength Modulated Differen-tial Photoacoustic Technique (WM-DPAS). The technique uses two optical wa-velengths (680 nm and 808 nm) to monitor variations in

oxyhemoglobin con-centration in tissue. One wavelength (680 nm in this case) should have maxi-mum variation in extinction coefficients for oxyhemoglobin and deoxyhemoglo-bin while the other wavelength (808 nm which is the isosbestic wavelength) should ideally have the extinction coefficients coinciding. Two CW laser sources are intensity modulated out of phase (differentially) and their output coupled to the sample for photoacoustic excitation. The emitted PA signal is detected by an ultrasonic transducer. Upon signal preprocessing, the Fourier transform of the signal is performed to obtain both amplitude and phase signals of the differential PA time domain signal. The phase signal is said to be independent of the optical fluence and its variation is only due to variations in the molar concentration of the probed chromophore. Judging from the reported features and performance of WM-DPAS, this technique is likely to be very suitable for *in-vivo* detection of malaria.

[4] Future Prospect

In order to make photoacoustic based malaria diagnostic techniques clinically viable and a method of choice, the technique has to process the following quali-ties; high diagnostic sensitivity and specificity, be fast, affordable, compact and portable. More work is needed in development of efficient PA techniques for detection of endogenous disease biomarkers such as hemozoin. Simplification of the instrumentation in PA systems will also be a significant contribution. As far as malaria diagnostics is concerned, it would be valuable to explore the possibil-ity of using a PA based system to differentiate different species of *Plasmodium* in a malaria patient. This could be done by determining oxygen saturation levels in erythrocytes infected by different *Plasmodium* species. It would also be worth-while to investigate the potential of WM-PAS in non-invasive malaria detection.

4. Conclusion

A review of reported literature on photoacoustic-based malaria diagnostic tech-niques and a discussion of the existing research gap have been presented in this paper. Suggestions for future refinements have also been offered.

Conflicts of Interest

The authors declare no conflicts of interest regarding the publication of this pa-per.

References

[38] World Health Organization (2016) World Malaria Report 2015. World Health Or-ganization, Geneva.

[39] World Health Organization (2003) The Africa Malaria Report 2003. World Health Organization, Geneva.

[40] Kumar, S., Guha, M., Choubey, V., Maity, P. and Bandyopadhyay, U. (2007) Anti-malarial Drugs Inhibiting Hemozoin (β-Hematin) Formation: A Mechanistic Up-date. *Life Sciences*, **80**, 813-828. https://doi.org/10.1016/j.lfs.2006.11.008

[41] Samson, E.B., Goldschmidt, B.S., Whiteside, P.J.D., *et al*. (2012) Photoacoustic Spec-troscopy of β-Hematin. *Journal of Optics*, **14**, 065302. https://doi.org/10.1088/2040-8978/14/6/065302

[42] Oliveira, M.F., Silva, J.R., Dansa-Petretski, M., *et al*. (2000) Hemozoin Formation in the Midgut of the Blood-Sucking Insect Rhodniusprolixus. *FEBS Letters*, **477**, 95-98. https://doi.org/10.1016/S0014-5793(00)01786-5

[43] Oliveira, M.F., Kycia, S.W., Gomez, A., *et al*. (2005) Structural and Morphological Characterization of Hemozoin Produced by Schistosomamansoni and Rhodniuspro-lixus. *FEBS Letters*, **579**, 6010-6016. https://doi.org/10.1016/j.febslet.2005.09.035

[44] White, N.J. (2008) Plasmodium Knowlesi: The Fifth Human Malaria Parasite. *Clin-ical Infectious Diseases*, **46**, 172-173. https://doi.org/10.1086/524889

[45] Ngwa, C.J., Rosa, T. and Pradel, G. (2016) The Biology of Malaria Gametocytes. In-techOpen. https://doi.org/10.5772/65464

[46] Cowman, A.F. and Crabb, B.S. (2006) Invasion of Red Blood Cells by Malaria Para-sites. *Cell*, **124**, 755-766. https://doi.org/10.1016/j.cell.2006.02.006

[47] Wongsrichanalai, C., Barcus, M.J., Muth, S., Sutamihardja, A. and Wernsdorfer, W.H. (2007) A Review of Malaria Diagnostic Tools: Microscopy and Rapid Diagnostic Test (RDT). *American Journal of Tropical Medicine and Hygiene*, **77**, 119-127. https://doi.org/10.4269/ajtmh.2007.77.119

[48] Makler, M.T., Palmer, C.J. and Ager, A.L. (1998) A Review of Practical Techniques for the Diagnosis of Malaria. *Annals of Tropical Medicine and Parasitology*, **92**, 419-434. https://doi.org/10.1080/00034989859401

[49] Johnston, S.P., Pieniazek, N.J., Xayavong, M.V., Slemenda, S.B., Wilkins, P.P. and da Silva, A.J. (2006) PCR as a Confirmatory Technique for Laboratory Diagnosis of Malaria. *Journal of Clinical Microbiology*, **44**, 1087-1089. https://doi.org/10.1128/JCM.44.3.1087-1089.2006

[50] Moody, A. (2002) Rapid Diagnostic Tests for Malaria Parasites. *Clinical Microbiol-ogy Reviews*, **15**, 66-78. https://doi.org/10.1128/CMR.15.1.66-78.2002

[51] Bélisle, J.M., Costantino, S., Leimanis, M.L., *et al*. (2008) Sensitive Detection of Ma-

laria Infection by Third Harmonic Generation Imaging. *Biophysical Journal*, **94**, L26-L28. https://doi.org/10.1529/biophysj.107.125443

[29] Newman, D.M., Heptinstall, J., Matelon, R.J., *et al*. (2008) A Magneto-Optic Route toward the *in Vivo* Diagnosis of Malaria: Preliminary Results and Preclinical Trial Data. *Biophysical Journal*, **95**, 994-1000. https://doi.org/10.1529/biophysj.107.128140

[30] Memeu, D.M., Kaduki, K.A., Mjomba, A., Muriuki, N.S. and Gitonga, L. (2013) De-tection of Plasmodium Parasites from Images of Thin Blood Smears. *Open Journal of Clinical Diagnostics*, **3**, 183-194. https://doi.org/10.4236/ojcd.2013.34034

[31] Gitonga, L., Memeu, D.M., Kaduki, K.A., Kale, M.A.C. and Muriuki, N.S. (2014) Determination of Plasmodium Parasite Life Stages and Species in Images of Thin Blood Smears Using Artificial Neural Network. *Open Journal of Clinical Diagnos-tics*, **4**, 78-88. https://doi.org/10.4236/ojcd.2014.42014

[32] Omucheni, D.L., Kaduki, K.A., Bulimo, W.D. and Angeyo, H.K. (2014) Application of Principal Component Analysis to Multispectral-Multimodal Optical Image Analy-sis for Malaria Diagnostics. *Malaria Journal*, **13**, Article No. 485. https://doi.org/10.1186/1475-2875-13-485

[33] Merdasa, A., Brydegaard, M., Svanberg, S. and Zoueu, J.T. (2013) Staining-Free Malaria Diagnostics by Multispectral and Multimodality Light-Emitting-Diode Mi-croscopy. *Journal of Biomedical Optics*, **18**, 036002. https://doi.org/10.1117/1.JBO.18.3.036002

[34] Saha, R.K., Karmakar, S. and Roy, M. (2012) Computational Investigation on the Photoacoustics of Malaria Infected Red Blood Cells. *PLoS ONE*, **7**, e51774. https://doi.org/10.1371/journal.pone.0051774

[35] Lukianova-Hleb, E.Y., Campbell, K.M., Constantinou, P.E., *et al*. (2014) Hemo-zoin-Generated Vapor Nanobubbles for Transdermal Reagent- and Needle-Free De-tection of Malaria. *Proceedings of the National Academy of Sciences of the United States of America*, **111**, 900-905. https://doi.org/10.1073/pnas.1316253111

[36] Cai, C., Carey, K.A., Nedosekin, D.A., *et al*. (2016) *In Vivo* Photoacoustic Flow Cy-tometry for Early Malaria Diagnosis: Photoacoustic Flow Cytometry for Malaria Di-agnosis. *Cytometry Part A*, **89**, 531-542. https://doi.org/10.1002/cyto.a.22854

[37] Lukianova-Hleb, E., Bezek, S., Szigeti, R., *et al*. (2015) Transdermal Diagnosis of Malaria Using Vapor Nanobubbles. *Emerging Infectious Diseases*, **21**, 1122-1127. https://doi.org/10.3201/eid2107.150089

[38] Bell, A.G. (1880) ART. XXXIV.—On the Production and Reproduction of Sound by Light. *American Journal of Science*, **20**, 305-324. https://doi.org/10.2475/ajs.s3-20.118.305

[39] Zhang, E., Laufer, J. and Beard, P. (2008) Backward-Mode Multiwavelength Pho-toacoustic Scanner Using a Planar Fabry-Perot Polymer Film Ultrasound Sensor for High-Resolution Three-Dimensional Imaging of Biological Tissues. *Applied Optics*, **47**, 561-577. https://doi.org/10.1364/AO.47.000561

[40] Song, L., Maslov, K.I., Bitton, R., Shung, K.K. and Wang, L.V. (2008) Fast 3-D Dark-Field Reflection-Mode Photoacoustic Microscopy *in Vivo* with a 30-MHz Ul-trasound Linear Array. *Journal of Biomedical Optics*, **13**, 054028. https://doi.org/10.1117/1.2976141

[41] Favazza, C.P., Wang, L.V. and Cornelius, L.A. (2011) *In Vivo* Functional Photoac-oustic Microscopy of Cutaneous Microvasculature in Human Skin. *Journal of Bio-medical Optics*, **16**, 026004. https://doi.org/10.1117/1.3536522

[42] Favazza, C.P., Wang, L.V., Jassim, O.W. and Cornelius, L.A. (2011) *In Vivo* Pho- toacoustic Microscopy of Human Cutaneous Microvasculature and a Nevus. *Jour-nal of Biomedical Optics*, **16**, 016015. https://doi.org/10.1117/1.3528661

[44] Silverman, R.H., Kong, F., Chen, Y.C., *et al*. (2010) High-Resolution Photoacoustic Imaging of Ocular Tissues. *Ultrasound in Medicine and Biology*, **36**, 733-742. https://doi.org/10.1016/j.ultrasmedbio.2010.02.006

[45] Hu, S., Rao, B., Maslov, K. and Wang, L.V. (2010) Label-Free Photoacoustic Oph-thalmic Angiography. *Optics Letters*, **35**, 1-3. https://doi.org/10.1364/OL.35.000001

[46] de La Zerda, A., Paulus, Y.M., Teed, R., *et al*. (2010) Photoacoustic Ocular Imaging. *Optics Letters*, **35**, 270-272. https://doi.org/10.1364/OL.35.000270

[47] Zhang, H.F., Puliafito, C.A. and Jiao, S. (2011) Photoacoustic Ophthalmoscopy for *in Vivo* Retinal Imaging: Current Status and Prospects. *Ophthalmic Surgery, Lasers and Imaging Retina*, **42**, S106-S115. https://doi.org/10.3928/15428877-20110627-10

[48] Manohar, S., Vaartjes, S.E., van Hespen, J.C.G., *et al*. (2007) Initial Results of *in Vi-vo* Non-Invasive Cancer Imaging in the Human Breast Using Near-Infrared Pho-toacoustics. *Optics Express*, **15**, 12277-12285. https://doi.org/10.1364/OE.15.012277

[49] Oraevsky, A.A., Karabutov, A.A., Solomatin, S.V., *et al*. (2001) Laser Optoacoustic Imaging of Breast Cancer *in Vivo*. *Proceedings Volume* 4256, *Biomedical Optoac-oustics II*, San Jose, 6-16. https://doi.org/10.1117/12.429300

[50] Kruger, R.A., Lam, R.B., Reinecke, D.R., Del Rio, S.P. and Doyle, R.P. (2010) Pho-toacoustic Angiography of the Breast. *Medical Physics*, **37**, 6096-6100. https://doi.org/10.1118/1.3497677

[51] Piras, D., Xia, W., Steenbergen, W., van Leeuwen, T.G. and Manohar, S. (2010) Photoacoustic Imaging of the Breast Using the Twente Photoacoustic Mammos-cope: Present Status and Future Perspectives. *IEEE Journal of Selected Topics in Quantum Electronics*, **16**, 730-739. https://doi.org/10.1109/JSTQE.2009.2034870

[52] Manohar, S., Kharine, A., van Hespen, J.C.G., Steenbergen, W. and van Leeuwen, T.G. (2005) The Twente Photoacoustic Mammoscope: System Overview and Per-formance. *Physics in Medicine & Biology*, **50**, 2543. https://doi.org/10.1088/0031-9155/50/11/007

[53] Zhang, J., Yang, S., Ji, X., Zhou, Q. and Xing, D. (2014) Characterization of Li-pid-Rich Aortic Plaques by Intravascular Photoacoustic Tomography: *Ex Vivo* and *in Vivo* Validation in a Rabbit Atherosclerosis Model with Histologic Correlation. *Journal of the American College of Cardiology*, **64**, 385-390. https://doi.org/10.1016/j.jacc.2014.04.053

[54] Wang, B., Su, J.L., Amirian, J., Litovsky, S.H., Smalling, R. and Emelianov, S. (2010) Detection of Lipid in Atherosclerotic Vessels Using Ultrasound-Guided Spectros-copic Intravascular Photoacoustic Imaging. *Optics Express*, **18**, 4889-4897. https://doi.org/10.1364/OE.18.004889

[55] Jansen, K., van Soest, G. and van der Steen, A.F. (2014) Intravascular Photoacoustic Imaging: A New Tool for Vulnerable Plaque Identification. *Ultrasound in Medicine and Biology*, **40**, 1037-1048. https://doi.org/10.1016/j.ultrasmedbio.2014.01.008

[56] Allen, T.J. and Beard, P.C. (2009) Photoacoustic Characterisation of Vascular Tissue at NIR Wavelengths. *Proceedings Volume* 7177, *Photons plus Ultrasound*: *Imaging and Sensing* 2009, San Jose, 71770A. https://doi.org/10.1117/12.808777

[57] Jansen, K., Wu, M., van der Steen, A.F. and van Soest, G. (2014) Photoacoustic Im-aging of Human Coronary Atherosclerosis in Two Spectral Bands. *Photoacoustics*, **2**, 12-20. https://doi.org/10.1016/j.pacs.2013.11.003

[58] Allen, T.J., Beard, P.C., Hall, A., Dhillon, A.P. and Owen, J.S. (2012) Spectroscopic Photoacoustic Imaging of Lipid-Rich Plaques in the Human Aorta in the 740 to 1400 nm Wavelength Range. *Journal of Biomedical Optics*, **17**, 061209. https://doi.org/10.1117/1.JBO.17.6.061209

[60] Funke, A. (2010) On the Feasibility of Photoacoustic Guidance of High Intensity Focused Ultrasound. Optics [physics.optics]. Université Pierre et Marie Curie, Paris.

[61] Bossy, E., Daoudi, K. and Boccara, A.-C. (2006) Time Reversal of Photoacoustic Waves. *Applied Physics Letters*, **89**, 184108. https://doi.org/10.1063/1.2382732

[62] Xia, J., Yao, J. and Wang, L.V. (2014) Photoacoustic Tomography: Principles and Advances. *Progress in Electromagnetics Research*, **147**, 1-22. https://doi.org/10.2528/PIER14032303

[63] Hu, S. (2010) Optical-Resolution Photoacoustic Microscopy. Washington Universi-ty, St. Louis.

[64] Maslov, K., Zhang, H.F., Hu, S. and Wang, L.V. (2008) Optical-Resolution Pho-toacoustic Microscopy for *in Vivo* Imaging of Single Capillaries. *Optics Letters*, **33**, 929-931. https://doi.org/10.1364/OL.33.000929

[65] Wang, L.V. and Hu, S. (2012) Photoacoustic Tomography: *In Vivo* Imaging from Organelles to Organs. *Science*, **335**, 1458-1462. https://doi.org/10.1126/science.1216210

[66] Fan, Y., Mandelis, A., Spirou, G. and Alex Vitkin, I. (2004) Development of a Laser Photothermoacoustic Frequency-Swept System for Subsurface Imaging: Theory and Experiment. *The Journal of the Acoustical Society of America*, **116**, 3523-3533. https://doi.org/10.1121/1.1819393

[67] Mohajerani, P., Kellnberger, S. and Ntziachristos, V. (2014) Frequency Domain Optoacoustic Tomography Using Amplitude and Phase. *Photoacoustics*, **2**, 111-118. https://doi.org/10.1016/j.pacs.2014.06.002

[68] Maslov, K.I. and Wang, L.V. (2008) Photoacoustic Imaging of Biological Tissue with Intensity-Modulated Continuous-Wave Laser. *Journal of Biomedical Optics*, **13**, 024006. https://doi.org/10.1117/1.2904965

[69] Baddour, N. (2008) Theory and Analysis of Frequency-Domain Photoacoustic To-mography. *The Journal of the Acoustical Society of America*, **123**, 2577-2590. https://doi.org/10.1121/1.2897132

[70] LeBoulluec, P., Liu, H. and Yuan, B. (2013) A Cost-Efficient Frequency-Domain Photoacoustic Imaging System. *American Journal of Physics*, **81**, 712. https://doi.org/10.1119/1.4816242

[71] Yao, J. and Wang, L.V. (2014) Sensitivity of Photoacoustic Microscopy. *Photoac-oustics*, **2**, 87-101. https://doi.org/10.1016/j.pacs.2014.04.002

[72] Beard, P. (2011) Biomedical Photoacoustic Imaging. *Interface Focus*, rsfs20110028. https://doi.org/10.1098/rsfs.2011.0028

[73] Guo, Z., Hu, S. and Wang, L.V. (2010) Calibration-Free Absolute Quantification of Optical Absorption Coefficients Using Acoustic Spectra in 3D Photoacoustic Mi-croscopy of Biological Tissue. *Optics Letters*, **35**, 2067-2069. https://doi.org/10.1364/OL.35.002067

[74] Zhou, Y., Yao, J., Maslov, K.I. and Wang, L.V. (2014) Calibration-Free Absolute Quantification of Particle Concentration by Statistical Analyses of Photoacoustic Signals *in Vivo*. *Journal of Biomedical Optics*, **19**, 037001. https://doi.org/10.1117/1.JBO.19.3.037001

[75] Laufer, J., Elwell, C., Delpy, D. and Beard, P. (2005) Measurements of Absolute Blood Oxygen Saturation Using Pulsed Near-Infrared Photoacoustic Spectroscopy:Accuracy and Resolution. *Physics in Medicine & Biology*, **50**, 4409-4428.https://doi.org/10.1088/0031-9155/50/18/011

[72] Laufer, J., Cox, B., Zhang, E. and Beard, P. (2010) Quantitative Determination of Chromophore Concentrations from 2D Photoacoustic Images Using a Nonlinear Model-Based Inversion Scheme. *Applied Optics*, **49**, 1219-1233. https://doi.org/10.1364/AO.49.001219

[73] Bauer, A.Q., Nothdurft, R.E., Erpelding, T.N., Wang, L.V. and Culver, J.P. (2011) Quantitative Photoacoustic Imaging: Correcting for Heterogeneous Light Fluence Distributions Using Diffuse Optical Tomography. *Journal of Biomedical Optics*, **16**, 096016. https://doi.org/10.1117/1.3626212

[74] Laufer, J., Delpy, D., Elwell, C. and Beard, P. (2007) Quantitative Spatially Resolved Measurement of Tissue Chromophore Concentrations Using Photoacoustic Spec-troscopy: Application to the Measurement of Blood Oxygenation and Haemoglobin Concentration. *Physics in Medicine & Biology*, **52**, 141-168. https://doi.org/10.1088/0031-9155/52/1/010

[75] Cox, B.T., Laufer, J.G., Beard, P.C. and Arridge, S.R. (2012) Quantitative Spectros-copic Photoacoustic Imaging: A Review. *Journal of Biomedical Optics*, **17**, Article No. 061202. https://doi.org/10.1117/1.JBO.17.6.061202

[76] Galanzha, E.I., Shashkov, E.V., Kelly, T., Kim, J.-W., Yang, L. and Zharov, V.P. (2009) *In Vivo* Magnetic Enrichment and Multiplex Photoacoustic Detection of Cir-culating Tumour Cells. *Nature Nanotechnology*, **4**, 855-860. https://doi.org/10.1038/nnano.2009.333

[77] Galanzha, E.I., Shashkov, E.V., Spring, P.M., Suen, J.Y. and Zharov, V.P. (2009) *In Vivo*, Noninvasive, Label-Free Detection and Eradication of Circulating Metastatic Melanoma Cells Using Two-Color Photoacoustic Flow Cytometry with a Diode La-ser. *Cancer Research*, **69**, 7926-7934. https://doi.org/10.1158/0008-5472.CAN-08-4900

[78] Zharov, V.P., Galanzha, E.I., Shashkov, E.V., Khlebtsov, N.G. and Tuchin, V.V. (2006) *In Vivo* Photoacoustic Flow Cytometry for Monitoring of Circulating Single Cancer Cells and Contrast Agents. *Optics Letters*, **31**, 3623-3625. https://doi.org/10.1364/OL.31.003623

[79] Galanzha, E.I., Kim, J. and Zharov, V.P. (2009) Nanotechnology-Based Molecular Photoacoustic and Photothermal Flow Cytometry Platform for *In-Vivo* Detection and Killing of Circulating Cancer Stem Cells. *Journal of Biophotonics*, **2**, 725-735. https://doi.org/10.1002/jbio.200910078

[80] Sergey, A.T. and Andreas, M. (2006) Fourier-Domain Biophotoacoustic Subsurface Depth Selective Amplitude and Phase Imaging of Turbid Phantoms and Biological Tissue. *Journal of Biomedical Optics*, **11**, 1083-3668. https://doi.org/10.1117/1.2337290

[81] Edem, D., Bahman, L., Choi, S.S., Andreas, M., Wei, S. and Liu, F.-F. (2017) Quan-titative Phase-Filtered Wavelength-Modulated Differential Photoacoustic Radar Tumor Hypoxia Imaging toward Early Cancer Detection. *Journal of Biophotonics*, **10**, 1134-1142. https://doi.org/10.1002/jbio.201600168

[82] Sung, S. (Sean), Mandelis, A., Xinxin, G., Bahman, L., Stephan, K. and Vasilis, N. (2015) Wavelength-Modulated Differential Photoacoustic Spectroscopy (WM-DPAS) for Noninvasive Early Cancer Detection and Tissue Hypoxia Monitoring. *Journal of Biophotonics*, **9**, 388-395. https://doi.org/10.1002/jbio.201670040

[83] Laufer, J., Zhang, E. and Beard, P. (2007) Quantitative *in-Vivo* Measurements of Blood Oxygen Saturation Using Multiwavelength Photoacoustic Imaging. *Proceed- ings Volume* 6437, *Photons Plus Ultrasound: Imaging and Sensing* 2007: *The Eighth Conference on Biomedical Thermoacoustics*, *Optoacoustics*, *and Acousto-Optics*, San Jose, 64371Z. http://proceedings.spiedigitallibrary.org/proceeding.aspx?articleid=1296725https://doi.org/10.1117/12.700297

[85] Wang, X., Xie, X., Ku, G., Wang, L.V. and Stoica, G. (2006) Noninvasive Imaging of Hemoglobin Concentration and Oxygenation in the Rat Brain Using High-Resolution Photoacoustic Tomography. *Journal of Biomedical Optics*, **11**, 024015. https://doi.org/10.1117/1.2192804

[86] Zhang, H.F., Maslov, K., Sivaramakrishnan, M., Stoica, G. and Wang, L.V. (2007) Imaging of Hemoglobin Oxygen Saturation Variations in Single Vessels *in Vivo* Using Photoacoustic Microscopy. *Applied Physics Letters*, **90**, Article No. 053901. https://doi.org/10.1063/1.2435697

[87] Song, W., Wei, Q., Liu, W., *et al*. (2015) A Combined Method to Quantify the Re-tinal Metabolic Rate of Oxygen Using Photoacoustic Ophthalmoscopy and Optical Coherence Tomography. *Scientific Reports*, **4**, Article No. 6525. https://doi.org/10.1038/srep06525

[88] Tang, M., Zhou, Y., Zhang, R. and Wang, L.V. (2015) Noninvasive Photoacoustic Microscopy of Methemoglobin *in Vivo*. *Journal of Biomedical Optics*, **20**, Article No. 036007. https://doi.org/10.1117/1.JBO.20.3.036007

[89] Wang, L., Maslov, K. and Wang, L.V. (2013) Single-Cell Label-Free Photoacoustic Flowoxigraphy *in Vivo*. *Proceedings of the National Academy of Sciences of the United States of America*, **110**, 5759-5764. https://doi.org/10.1073/pnas.1215578110

[90] Winkler, A.M., Maslov, K. and Wang, L.V. (2013) Towards Single Molecule Detec-tion Using Photoacoustic Microscopy. *Proceedings Volume* 8581, *Photons plus Ul-trasound*: *Imaging and Sensing* 2013, San Francisco, 85811A. http://proceedings.spiedigitallibrary.org/proceeding.aspx?articleid=1660845

[91] Tuchin, V.V. (2011) Advanced Optical Flow Cytometry: Methods and Disease Di-agnoses. John Wiley & Sons, Hoboken. https://doi.org/10.1002/9783527634286

[92] Wang, T., Nandy, S., Salehi, H.S., Kumavor, P.D. and Zhu, Q. (2014) A Low-Cost Photoacoustic Microscopy System with a Laser Diode Excitation. *Biomedical Optics Express*, **5**, 3053-5058. https://doi.org/10.1364/BOE.5.003053

[93] Allen, T.J. and Beard, P.C. (2007) Dual Wavelength Laser Diode Excitation Source for 2D Photoacoustic Imaging. *Proceedings Volume* 6437, *Photons plus Ultrasound*: *Imaging and Sensing* 2007: *The Eighth Conference on Biomedical Thermoacoustics, Optoacoustics, and Acousto-Optics*, San Jose, 64371U. https://doi.org/10.1117/12.698651

[94] Kolkman, R.G.M., Steenbergen, W. and van Leeuwen, T.G. (2006) *In Vivo* Photoac-oustic Imaging of Blood Vessels with a Pulsed Laser Diode. *Lasers in Medical Science*, **21**, 134-139. https://doi.org/10.1007/s10103-006-0384-z

[95] Allen, T.J. and Beard, P.C. (2013) Light Emitting Diodes as an Excitation Source for Biomedical Photoacoustics. *Proceedings Volume* 8581, *Photons plus Ultrasound*: *Im-aging and Sensing* 2013, San Francisco, 85811F. https://doi.org/10.1117/12.2004471

[96] Deán-Ben, X.L. and Razansky, D. (2013) Functional Optoacoustic Human Angio-graphy with Handheld Video Rate Three Dimensional Scanner. *Photoacoustics*, **1**, 68-73. https://doi.org/10.1016/j.pacs.2013.10.002

[97] Zhou, Y., Li, G., Zhu, L., Li, C., Cornelius, L.A. and Wang, L.V. (2015) Handheld Photoacoustic Probe to Detect Both Melanoma Depth and Volume at High Speed *in Vivo*. *Journal of Biophotonics*, **8**, 961-967. https://doi.org/10.1002/jbio.201400143

[87] Singh, M.K.A., Steenbergen, W. and Manohar, S. (2016) Handheld Probe-Based Dual Mode Ultrasound/Photoacoustics for Biomedical Imaging. In: Olivo, M. and Dinish, U., Eds., *Frontiers in Biophotonics for Translational Medicine*, Vol. 3, Sprin-ger, Singapore, 209-247. https://doi.org/10.1007/978-981-287-627-0_7

[88] Daoudi, K., van den Berg, P.J., Rabot, O., *et al*. (2014) Handheld Probe Integrating Laser Diode and Ultrasound Transducer Array for Ultrasound/Photoacoustic Dual Modality Imaging. *Optics Express*, **22**, 26365. https://doi.org/10.1364/OE.22.026365

Appendix B1: Nacosti Research Permit

REPUBLIC OF KENYA

NATIONAL COMMISSION FOR SCIENCE,TECHNOLOGY & INNOVATION

Ref No: **794799**

Date of Issue: **25/July/2023**

RESEARCH LICENSE

This is to Certify that Mr,, DANIEL Maitethia MEMEU of Kenyatta University, has been licensed to conduct research as per the provision of the Science, Technology and Innovation Act, 2013 (Rev.2014) in Meru on the topic: PHOTOACOUSTIC MODULATED OPTICAL SCATTERING TECHNIQUE FOR MALARIA DIAGNOSIS for the period ending ; 25/July/2024.

License No: **NACOSTI/P/23/27988**

794799

Applicant Identification Number

Director General
NATIONAL COMMISSION FOR SCIENCE,TECHNOLOGY & INNOVATION

Verification QR Code

NOTE: This is a computer generated License. To verify the authenticity of this document, Scan the QR Code using QR scanner application.

See overleaf for conditions

Legal Notice No. 108: The Science, Technology and Innovation (Research Licensing) Regulations, 2014

The National Commission for Science, Technology and Innovation, hereafter referred to as the Commission, was the established under the Science, Technology and Innovation Act 2013 (Revised 2014) herein after referred to as the Act. The objective of the Commission shall be to regulate and assure quality in the science, technology and innovation sector and advise the Government in matters related thereto.

CONDITIONS OF THE RESEARCH LICENSE

1. The License is granted subject to provisions of the Constitution of Kenya, the Science, Technology and Innovation Act, and other relevant laws, policies and regulations. Accordingly, the licensee shall adhere to such procedures, standards, code of ethics and guidelines as may be prescribed by regulations made under the Act, or prescribed by provisions of international treaties of which Kenya is a signatory to
2. The research and its related activities as well as outcomes shall be beneficial to the country and shall not in any way;

i. Endanger national security
ii. Adversely affect the lives of Kenyans
iii. Be in contravention of Kenya's international obligations including Biological Weapons Convention (BWC), Comprehensive Nuclear-Test-Ban Treaty Organization (CTBTO), Chemical, Biological, Radiological and Nuclear (CBRN).
iv. Result in exploitation of intellectual property rights of communities in Kenya
v. Adversely affect the environment
vi. Adversely affect the rights of communities
vii. Endanger public safety and national cohesion
viii. Plagiarize someone else's work

3. The License is valid for the proposed research, location and specified period.
4. The license any rights thereunder are non-transferable
5. The Commission reserves the right to cancel the research at any time during the research period if in the opinion of the Commission the research is not implemented in conformity with the provisions of the Act or any other written law.
6. The Licensee shall inform the relevant County Director of Education, County Commissioner and County Governor before commencement of the research.
7. Excavation, filming, movement, and collection of specimens are subject to further necessary clearance from relevant Government Agencies.
8. The License does not give authority to transfer research materials.
9. The Commission may monitor and evaluate the licensed research project for the purpose of assessing and evaluating compliance with the conditions of the License.
10. The Licensee shall submit one hard copy, and upload a soft copy of their final report (thesis) onto a platform designated by the Commission within one year of completion of the research.
11. The Commission reserves the right to modify the conditions of the License including cancellation without prior notice.
12. Research, findings and information regarding research systems shall be stored or disseminated, utilized or applied in such a manner as may be prescribed by the Commission from time to time.
13. The Licensee shall disclose to the Commission, the relevant Institutional Scientific and Ethical Review Committee, and the relevant national agencies any inventions and discoveries that are of National strategic importance.
14. The Commission shall have powers to acquire from any person the right in, or to, any scientific innovation, invention or patent of strategic importance to the country.
15. Relevant Institutional Scientific and Ethical Review Committee shall monitor and evaluate the research periodically, and make a report of its findings to the Commission for necessary action.

National Commission for Science, Technology and Innovation(NACOSTI),
Off Waiyaki Way, Upper Kabete,
P. O. Box 30623 - 00100 Nairobi, KENYA Telephone: 020 4007000, 0713788787, 0735404245
E-mail: dg@nacosti.go.ke Website: www.nacosti.go.ke

Appendix B2: Ethical Review Approval

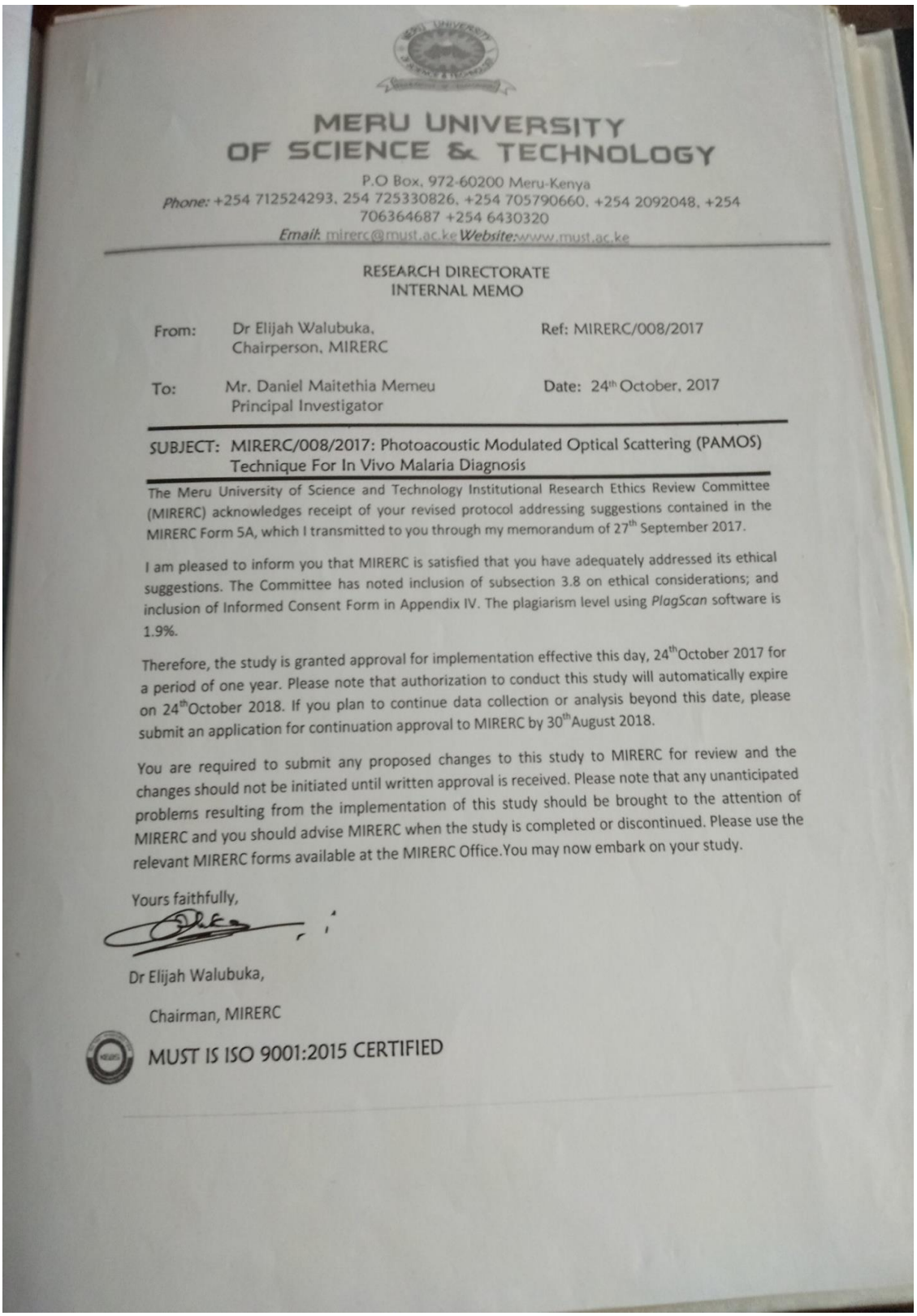

MERU UNIVERSITY
OF SCIENCE & TECHNOLOGY

P.O Box, 972-60200 Meru-Kenya
Phone: +254 712524293, 254 725330826, +254 705790660, +254 2092048, +254 706364687 +254 6430320
Email: mirerc@must.ac.ke *Website:* www.must.ac.ke

RESEARCH DIRECTORATE
INTERNAL MEMO

From: Dr Elijah Walubuka, Chairperson, MIRERC — Ref: MIRERC/008/2017

To: Mr. Daniel Maitethia Memeu, Principal Investigator — Date: 24th October, 2017

SUBJECT: MIRERC/008/2017: Photoacoustic Modulated Optical Scattering (PAMOS) Technique For In Vivo Malaria Diagnosis

The Meru University of Science and Technology Institutional Research Ethics Review Committee (MIRERC) acknowledges receipt of your revised protocol addressing suggestions contained in the MIRERC Form 5A, which I transmitted to you through my memorandum of 27th September 2017.

I am pleased to inform you that MIRERC is satisfied that you have adequately addressed its ethical suggestions. The Committee has noted inclusion of subsection 3.8 on ethical considerations; and inclusion of Informed Consent Form in Appendix IV. The plagiarism level using *PlagScan* software is 1.9%.

Therefore, the study is granted approval for implementation effective this day, 24th October 2017 for a period of one year. Please note that authorization to conduct this study will automatically expire on 24th October 2018. If you plan to continue data collection or analysis beyond this date, please submit an application for continuation approval to MIRERC by 30th August 2018.

You are required to submit any proposed changes to this study to MIRERC for review and the changes should not be initiated until written approval is received. Please note that any unanticipated problems resulting from the implementation of this study should be brought to the attention of MIRERC and you should advise MIRERC when the study is completed or discontinued. Please use the relevant MIRERC forms available at the MIRERC Office.You may now embark on your study.

Yours faithfully,

Dr Elijah Walubuka,

Chairman, MIRERC

MUST IS ISO 9001:2015 CERTIFIED

Appendix B3 Research Approval

KENYATTA UNIVERSITY
GRADUATE SCHOOL

E-mail: kubps@yahoo.com
dean-graduate@ku.ac.ke
Website: www.ku.ac.ke

P.O. Box 43844, 00100
NAIROBI, KENYA
Tel. 810901 Ext. 57530

Internal Memo

FROM: Dean, Graduate School

DATE: 31st October, 2017

TO: Mr. Memeu D. Maitethia
C/o Department of Physics
KENYATTA UNIVERSITY

REF: I84/32278/15

SUBJECT: APPROVAL OF RESEARCH PROPOSAL

This is to inform you that the Graduate School Board at its meeting 18th October, 2017 approved your Ph.D. Research Proposal entitled **"Photocoustic Modulated Optical Scattering Technique for Malaria Diagnosis".**

You may now proceed with your Data collection, subject to clearance with the Director General, National Commission for Science, Technology & Innovation.

As you embark on your data collection, please note that you will be required to submit to Graduate School completed supervision Tracking Forms per semester. The form has been developed to replace the progress Report Forms. The Supervision Tracking Forms are available at the University's Website under Graduate School webpage downloads.

By copy of this letter, the Registrar (Academic) is hereby requested to grant you substantive registration for your Ph.D. studies.

Thank you.

REUBEN MURIUKI
FOR: DEAN, GRADUATE SCHOOL

c.c. Chairman, Department of Physics

Supervisors:

1. Dr. Abdallah M. Sarroney
   C/o Department of Physics
   KENYATTA UNIVERSITY
2. Dr. Ciira Maina
   Department of Electrical & Electronic Engineering
   Dedan Kimathi University
   C/o Department of Physics
   KENYATTA UNIVERSITY

RM/cao

Appendix B4 Reseach Authorization

KENYATTA UNIVERSITY
GRADUATE SCHOOL

E-mail: kubps@yahoo.com
dean-graduate@ku.ac.ke
Website: www.ku.ac.ke

P.O. Box 43844, 00100
NAIROBI, KENYA
Tel. 8710901 Ext. 57530

Our Ref: I84/32278/15 **Date:** 31st October, 2017

The Director General,
National Commission for Science, Technology & Innovation,
P.O. Box 30623-00100,
NAIROBI

Dear Sir/Madam,

RE: RESEARCH AUTHORIZATION FOR MR.MEMEU D. MAITETHIA - REG. NO. I84/32278/15

I write to introduce Mr. Memeu who is a Postgraduate Student of this University. He is registered for a Ph.D. degree programme in the **Department of Physics in the School of Pure & Applied Sciences.**

Mr. Memeu intends to conduct research for Ph.D. thesis entitled, **"Photocoustic Modulated Optical Scattering Technique for Malaria Diagnosis".**

Any assistance given will be highly appreciated.

Yours faithfully,

MRS. LUCY N. MBAABU
FOR: DEAN, GRADUATE SCHOOL

RM/cao